

EFFECTS OF PARTICLE SIZE CLASSIFICATION ON
✓ GYPSUM SIZE DISTRIBUTION IN SIMULATED
STACK-GAS SCRUBBING LIQUORS

E9791
1982
4
Cop. 2

by
Dee Earl Vaden

A Thesis Submitted to the Faculty of the
DEPARTMENT OF CHEMICAL ENGINEERING
In Partial Fulfillment of the Requirements
For the Degree of
MASTER OF SCIENCE
In the Graduate College
THE UNIVERSITY OF ARIZONA

1982

STATEMENT BY AUTHOR

This thesis has been submitted in partial fulfillment of requirements for an advanced degree at The University of Arizona and is deposited in the University Library to be made available to borrowers under rules of the Library.

Brief quotations from this thesis are allowable without special permission, provided that accurate acknowledgment of source is made. Requests for permission for extended quotation from or reproduction of this manuscript in whole or in part may be granted by the head of the major department or the Dean of the Graduate College when in his judgment the proposed use of the material is in the interests of scholarship. In all other instances, however, permission must be obtained from the author.

SIGNED: See Carl Vaden

APPROVAL BY THESIS DIRECTOR

This thesis has been approved on the date shown below:

A. D. Randolph
A. D. RANDOLPH
Professor of Chemical Engineering

12/17/81
Date

*Dedicated to my parents
Who helped make this all possible.*

ACKNOWLEDGMENTS

The author wishes to thank his advisor, Dr. Alan D. Randolph, for his guidance and encouragement throughout this project. Acknowledgment is also given to Dick VanReeth for his craftsmanship in the College of Mines machine shop and Don Pettit for his glass-blowing expertise. Thanks are also given to Dr. Paul Zerella for his crystallization knowledge and help.

The author is indebted to the Electric Power Research Institute, Inc. (EPRI) for financial support under contract RP-1031-3. The following legal notice is required by EPRI.

This work was prepared by The University of Arizona as an account of work sponsored by EPRI. Neither EPRI, members of EPRI, nor The University of Arizona, nor any person acting on behalf of either:

- a. Makes any warranty or representation, express or implied, with respect to the accuracy, completeness, or usefulness of the information contained in this report, or that the use of any information, apparatus, method, or process disclosed in this report may not infringe on privately owned rights.
- b. Assumes any liabilities with respect to the use of, or for damages resulting from the use of, any

information, apparatus, method, or process disclosed
in this report.

TABLE OF CONTENTS

	Page
LIST OF ILLUSTRATIONS	ix
LIST OF TABLES	xi
ABSTRACT	xii
INTRODUCTION	1
Coal Beneficiation	1
Fluidized-Bed Combustion	3
Flue Gas Desulfurization	4
Objectives of the Present Study	10
APPARATUS	14
Measuring Devices	17
Particle Data Inc. Celloscope®	
Particle Counter	17
Leeds & Northrup Microtrac	
Particle Size Monitor	19
Allen-Bradley Sonic Sifter	23
Calibration of Equipment	23
Pumps	23
Stirrers	23
Temperatures	25
pH	25
PDI Particle Counter	25
Microtrac	26
Allen-Bradley Sonic Sifter	26
Solution Make-Up	26
Experimental Set-Up	28
Start-Up	28
Sampling	31
PDI	31
Microtrac	32
Sonic Sifter	33
Shut-Down	34

TABLE OF CONTENTS -- Continued

	Page
Analysis of Data	35
PDI Data	36
Microtrac Data	36
Sonic Sifter Data	40
THEORY	44
Nucleation	44
Growth	47
Accelerated Fines Removal	49
Population Balance	49
System Design	51
Computer Simulation	55
PRESENTATION OF EXPERIMENTAL RESULTS	57
Crystallizer Runs	60
Results	62
Graphs	63
Run 26	63
Run 27	64
Run 28	67
Run 29	72
Runs 31 Through 33	74
DISCUSSION OF RESULTS	91
Disagreement between Computer and Experimental Results	91
Scale	92
Kinetics	92
Dynamics	93
Parameter Changes	94
Comparison of Runs	95
Run 26	95
Run 27	98
Run 28	100
Run 29	101
Runs 31 Through 33	103
Run 31	104
Run 32	106
Run 33	108
Conclusions	110

TABLE OF CONTENTS -- Continued

	Page
Unrelieved Supersaturation	111
Conclusions	116
Crystal Habit Modifier	117
Conclusions	122
Crystal Appearance	124
Conclusions	130
SUMMARY	132
CONCLUSIONS	134
NOMENCLATURE	137
APPENDIX A: MARK V COMPUTER SIMULATION EQUATIONS	141
APPENDIX B: DATA ANALYZING METHODS	149
Estimation of Fines Crystal Size Distribution	150
Microtrac Data	151
Growth Rate	151
APPENDIX C: ALLEN-BRADLEY SONIC SIFTER DATA	152
APPENDIX D: CONVERTED SONIC SIFTER DATA	158
APPENDIX E: LIST OF REFERENCES	160
LIST OF REFERENCES	162

LIST OF ILLUSTRATIONS

Figure		Page
1.	Flow diagram of typical scrubber	7
2.	Flow diagram of Chiyoda Thoroughbred-121 flue gas scrubbing system	9
3.	Schematic of double-drawoff crystallizer with accelerated fines removal	12
4.	Schematic of apparatus	15
5.	Orifice tube and vicinity	18
6.	PDI printout	20
7.	Microtrac printout	21
8.	PDI printout used in data analysis	37
9.	Microtrac printout used in data analysis	38
10.	Plot of $\ln n$ versus L_{avg} using Microtrac and sieve data	43
11.	Crystallizer configuration comparison	52
12.	Configurations simulated by Mark I	54
13.	Plot of Microtrac and sieve data from run 26	66
14.	Plot of Microtrac and sieve data from run 27	69
15.	Plot of Microtrac and sieve data from run 28	71
16.	Plot of sieve data from run 29 with extrapolated fines CSD	75

LIST OF ILLUSTRATIONS -- Continued

Figure		Page
17.	Plot of Microtrac and sieve data from run 32	78
18.	Plot of Microtrac and sieve data from run 31	81
19.	Plot of Microtrac and sieve data from run 33	82
20.	Plot of sieve data from run 34 with extrapolated fines CSD	83
21.	Experimental versus computer nucleation rate	84
22.	Experimental versus calculated nucleation rate	85
23.	Experimental versus computer growth rate . . .	86
24.	Experimental versus computer slurry density . .	87
25.	Experimental versus computer mean size	88
26.	Apparatus used for citric acid experiments . .	118
27.	Crystals grown in low citric acid concentrations (0 ppm to 20 ppm)	119
28.	Crystals grown in high citric acid concentrations (50 ppm to 250 ppm)	120
29.	Crystals grown with and without additive . . .	121
30.	Citric acid breakdown versus pH	123
31.	SEM photographs of gypsum crystals	125
32.	Dual magnification SEM photographs of gypsum crystals	126
33.	Optical microscope photographs of gypsum crystals	127

LIST OF TABLES

Table		Page
1.	Typical Allen-Bradley sieve results	24
2.	Sieve data conversion	41
3.	Mark I results	53
4.	Experimental results	58
5.	Range of variables (DDO runs only)	60
6.	Summary of run conditions	61
7.	Results of runs 26 and 34	65
8.	Results of runs 26, 27, and 34	68
9.	Results of runs 26 and 28	70
10.	Results of runs 29 and 34	73
11.	Results of runs 32 and 34	77
12.	Results of runs 31, 33, and 34	79
13.	Results of runs 26 and 34	96
14.	Results of runs 27 and 34	99
15.	Results of runs 26, 27, 29, and 34	102
16.	Results of runs 31 and 34	105
17.	Results of runs 32 and 34	107
18.	Results of runs 33 and 34	109
19.	Results of computer runs	112

ABSTRACT

The purpose of this study was to test the effects of particle size classification on the crystal size distribution of gypsum in simulated stack-gas scrubbing liquors using a bench-scale double-drawoff (DDO) crystallizer. Various DDO crystallizer conditions were tested experimentally and analyzed with a computer simulation program (Mark V CSD simulator using predetermined growth and nucleation kinetics) to observe the effects of parameter changes on the growth rate, nucleation rate, slurry density, and mass mean size. The effects of the additive citric acid on the crystal habit of gypsum were also studied.

Results show that the double-drawoff crystallizer configuration produced larger crystals and reduced crystallizer fouling compared to the MSMPR crystallizer configuration. Experimental and computer results agree, proving that the predetermined kinetics are a valid gypsum crystallization model and that computer simulation could be used to design a crystallizer that improves crystal size with minimum fouling. Citric acid produced a "potato-like" equant crystal habit, creating a gypsum product with good dewatering and filtering properties. The crystal habit change depended on citric acid concentration and crystallizer pH.

INTRODUCTION

Efficient and reliable coal desulfurization techniques are essential in order to further shift U.S. production of electric power to coal-fired plants. Such a shift is important due to the recent price increase of imported crude, which makes conversion to coal-fired plants attractive, except for the need to install expensive desulfurization equipment.

There are three ways to meet sulfur dioxide (SO₂) emission standards of direct-fired coal power plants:

1. Coal beneficiation.
2. Fluidized-bed combustion.
3. Flue gas desulfurization.

These methods will be discussed and compared on the basis of their technical merits and relative cost for SO₂ removal from coal-fired power plants.

Coal Beneficiation

Cleaning coal prior to combustion has several advantages over flue gas desulfurization and fluidized-bed combustion. Removal of sulfur, ash, and nonvolatile material means less bulk material sent to the plant, thus reducing

transportation costs. Plant equipment will not be fouled with depositing ash and scale. This will decrease downtime and maintenance costs while increasing plant efficiency. Less sulfur in the flue gas will result in reduced operating costs and flue gas desulfurization equipment that might still be necessary. Ideally, coal cleaning would allow burning in a power plant without further emissions removal, but this is not presently the case.

The methods of cleaning coal will be described after a discussion of how sulfur is contained in coal.

Coal contains sulfur in two forms, pyritic and organic. Pyritic sulfur has sulfur bonded with iron to form pyrites. Pyritic sulfur and coal have different physical properties that physical cleaning methods take advantage of to separate pyritic sulfur from coal. In the case of organic sulfur the sulfur molecules are bonded directly to the organic ring structure of coal. Chemical cleaning methods are needed to break these sulfur bonds in order to remove organic sulfur from coal.

Coal usually has more pyritic sulfur than organic sulfur. Therefore, physical cleaning methods such as froth flotation, selective oil agglomeration, high-grade magnetic separation, and dynamic segregation will remove a major portion of the total sulfur in coal. Leaching, chlorinolysis,

pyrolysis, hydrodesulfurization, and gas phase oxidation are chemical coal-cleaning methods that are in the development stage. Commercial scale-up of chemical techniques is presently uneconomical. Thus physical cleaning of pyritic sulfur in coal is the least expensive and the most developed coal beneficiation technology available today.

Because of the poor economics of organic sulfur removal, physical coal cleaning must be coupled with flue gas desulfurization in order to meet sulfur dioxide emission standards. Development of both coal cleaning prior to combustion and flue gas desulfurization will continue in order to produce a reliable process that meets pollution standards.

Fluidized-Bed Combustion

The process of fluidized-bed combustion consists of feeding finely divided coal to a bed of coal and ash particles. Air is passed through the bed at a rate sufficient to fluidize it and to effect combustion of the coal. Heat exchanger tubes are located in the bed to take advantage of the heat generated in the bed.

Compared to conventional pulverized coal boilers, fluidized-bed combustors have the following potential advantages:

1. Better heat transfer, thus requiring less steam tubing and potentially reducing capital costs.

2. Lower combustion temperatures which would reduce tube fouling and corrosion.
3. High or variable ash content coal can be used; thus costs of feed preparation are lower.
4. Coal-crushing costs can be reduced because fine grinding to pulverized fuel sizes would be unnecessary.
5. Limestone can be added to the fluidized bed to trap the sulfur released during combustion (as CaSO_4 , reporting with the ash), thus eliminating external sulfur dioxide removal equipment.

Research studies (Skinner, 1971) have shown that the addition of finely ground limestone to the feed of a fluidized-bed combustor resulted in retention of 99% of the sulfur in a coal of 2% sulfur content. These studies also concluded that increased efficiency of desulfurization necessitated the use of finely ground limestone. Unless this drawback is eliminated, this process might not be economical.

Flue Gas Desulfurization

Flue gas desulfurization (FGD) systems are designed to remove sulfur dioxide (SO_2) from combustion flue gases. Several processes have been investigated and/or are in use. Regenerative processes are second-generation FGD systems

that regenerate the absorption solution and produce a by-product such as sulfur, gypsum, or sulfuric acid. These products can be either stored or sold on the commercial market. Regenerative systems are economically unattractive for FGD installations except when use is justified by site-specific conditions, such as restrictions against dumping or a nearby plant that uses sulfuric acid.

A study conducted by Electric Power Research Institute (EPRI) on the economics of options for coal utilization (Waters and Whitaker, 1977, p. 8) resulted in the following ranking:

1. Direct-fired low sulfur coal
2. Direct-firing of higher-sulfur coal with limestone scrubbing.
3. Direct-fired steam plants employing regenerative scrubbers, advanced gasifiers, and fluidized-bed combustors.

The above list shows that limestone scrubbing of direct-fired higher-sulfur coal is the second most attractive process. The demand for coal will increase the use of higher-sulfur coal, making limestone scrubbing the immediate choice for flue gas desulfurization.

The following sentence is from an EPRI journal (Waters and Whitaker, 1977, p. 8): "So far, the only positive emission control option with which the industry has had significant operating experience and which is capable of

meeting new-source performance standards is lime/limestone scrubbing."

In conclusion, of the three possible ways of meeting sulfur dioxide emission standards with direct-firing of coal--coal beneficiation, fluidized-bed combustion, and flue gas desulfurization--it appears that limestone stack gas scrubbing is the most economically attractive process. Physical coal cleaning is economically feasible, but cannot solely meet SO_2 emission standards. A secondary system, such as stack gas scrubbing, must be used in addition to physical coal cleaning to meet pollution control levels because of organically-bound sulfur that is not removed by physical techniques.

Research will be concentrated on the limestone stack gas scrubber to increase its efficiency and reliability until another process with better qualifications is invented.

Limestone (rather than lime) stack gas scrubbers are most commonly used by industry for FGD. This process absorbs sulfur dioxide into a limestone slurry where it reacts to form calcium sulfite or, if excess air is supplied, calcium sulfate. The product is disposed of as land-fill material. Figure 1 shows a schematic for a typical stack gas scrubber.

A current problem in industry is disposal of the gypsum product. Presently the crystal size is relatively

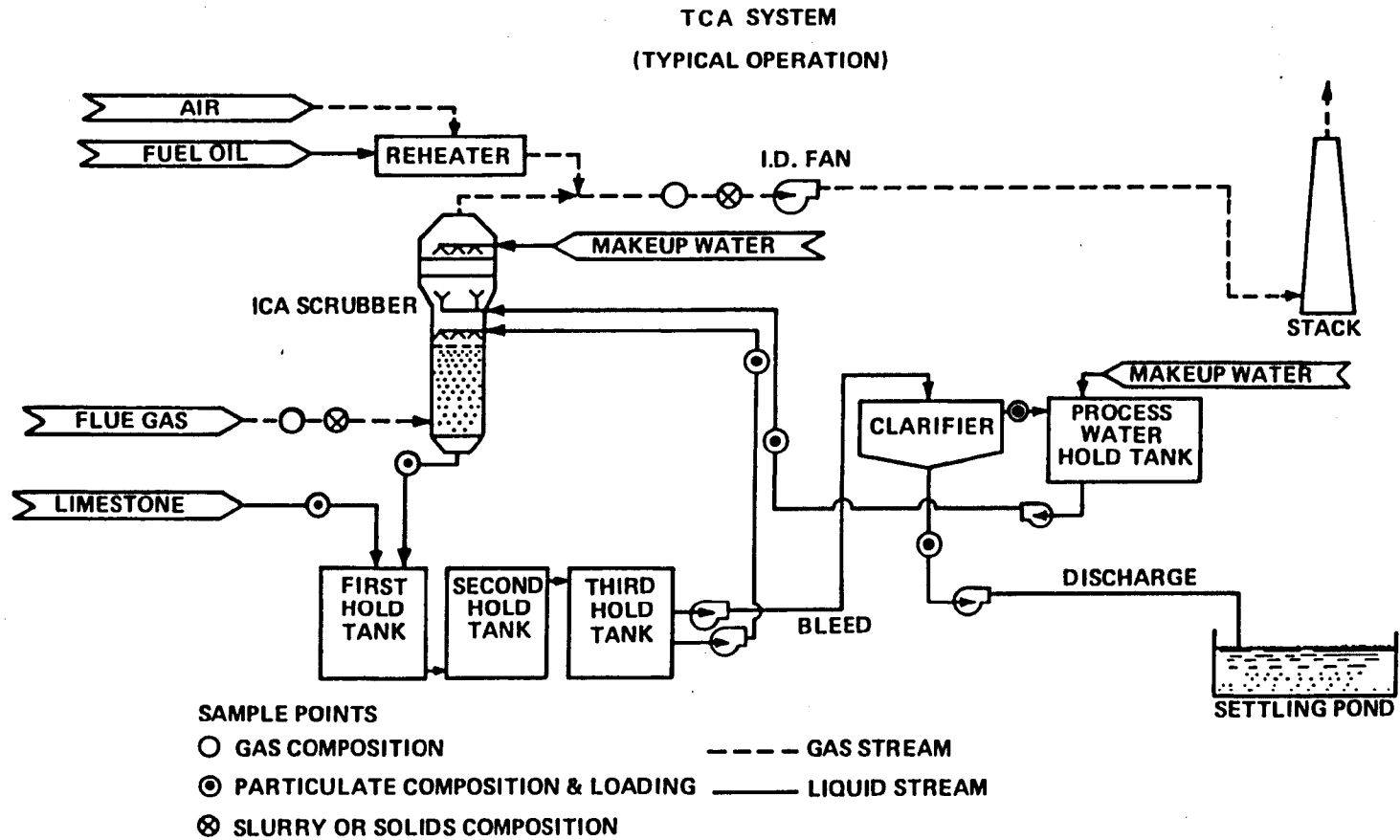


Figure 1. Flow diagram of typical scrubber.

small and needle-like in appearance, possessing poor dewatering characteristics that requires additional treatment (clarifiers and filters) to dewater the sludge enough to produce acceptable landfill material.

A solution to the sludge disposal problem would be to increase the crystal size of the gypsum product and to modify the habit to produce a crystal with acceptable dewatering properties.

One system that shows remarkable promise in producing a sludge with good dewatering characteristics is the Chiyoda Thoroughbred-121 FGD Process. Figure 2 shows a simplified flow diagram of the Chiyoda Thoroughbred-121 (CT-121) process. Inlet gas is cooled and saturated by water in a venturi before entering the jet bubbling reactor (JBR) where most of the SO_2 is removed. Air is added to the JBR to completely oxidize the absorbed SO_2 and to maintain a gypsum solids suspension. Powdered limestone is added to control pH. The exiting gas from the JBR passes through a mist eliminator before leaving the system through the stack. The gypsum is disposed of in a gypsum stack, where the solids settle out and the liquid flows through the stack and forms a surrounding moat.

The central feature of the CT-121 process is the jet bubbling reactor. SO_2 absorption, sulfite oxidation, lime-

SIMPLIFIED PROCESS FLOW DIAGRAM OF CHIYODA THOROUGHbred- 121
FLUE GAS SCRUBBING SYSTEM.

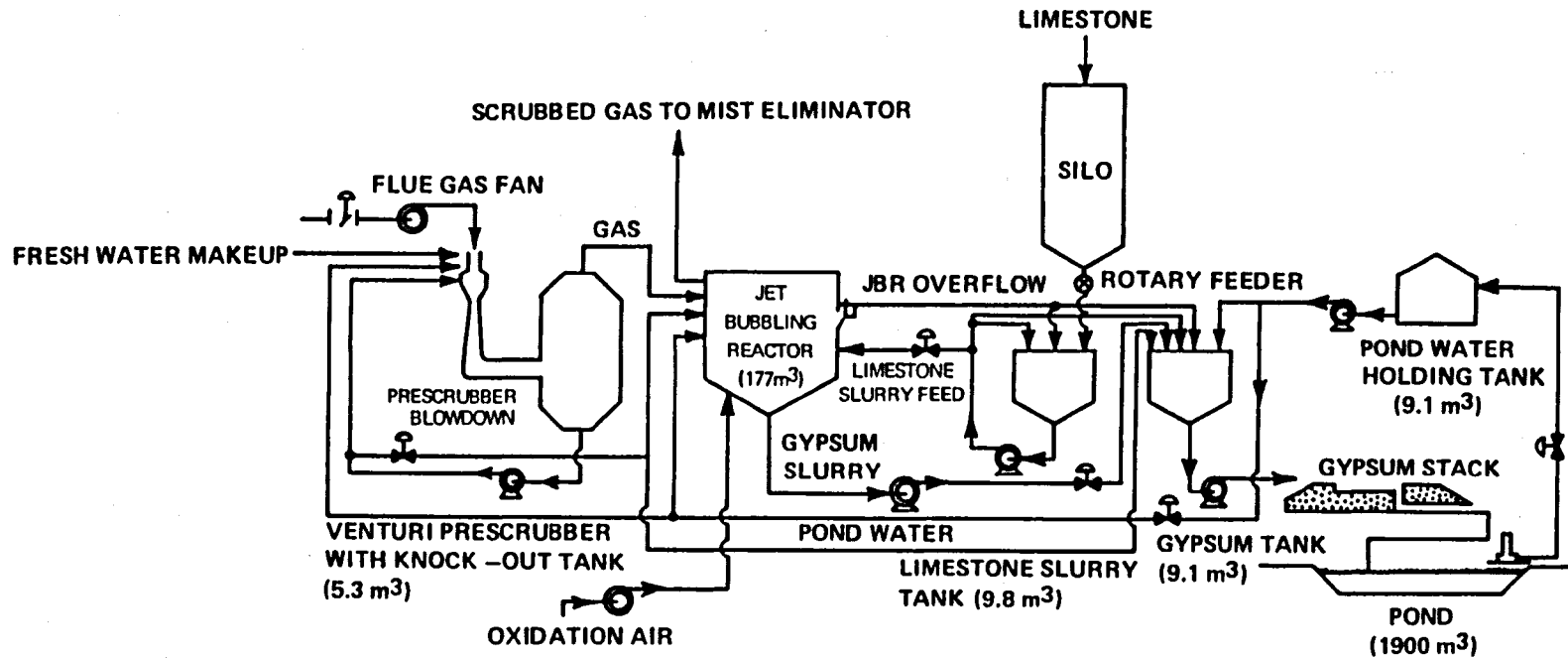


Figure 2. Flow diagram of Chiyoda Thoroughbred-121 flue gas scrubbing system.

stone dissolution, and gypsum crystallization reactions all occur within the JBR. Conventional FGD systems have separate vessels for absorption and reaction, an unfortunate concept that often results in high supersaturation and fine crystals. The JBR concept might lower the capital cost of a FGD system due to the reduction in number of vessels. A detailed report on the CT-121 FGD process is in the literature (Behrens and Hargrave, 1980).

Objectives of the Present Study

Research done at the University of Arizona by Mr. Dave Etherton, a recent graduate student of Dr. A. D. Randolph, determined the crystallization kinetics of gypsum in simulated stack gas scrubbing liquors. The kinetics were used in a computer simulation of a proposed crystallization design that increases the retention time of the solids without changing the retention time of the liquid phase. Computer results showed an increase in particle size using the proposed design. A better explanation of the proposed system will be discussed later. Furthermore, citric acid (as the citrate ion) shows promise as a gypsum crystal growth modifier to produce a rounded crystal habit. This habit modification and the variable solids/liquid residence time configuration, which might be used in conjunction to produce a superior gypsum product, was the central focus of the present study.

Thus the purpose of this study was to verify the computer predictions based on Etherton's kinetics using a bench-scale crystallizer of 9-liter capacity. H_2SO_4 and $\text{Ca}(\text{OH})_2$ solutions provide the supersaturation for gypsum crystallization. The crystallizer design used in this study to increase the retention time of the solids is called a double-drawoff (DDO) crystallizer. A schematic showing the DDO configuration is shown in Figure 3. The DDO crystallizer uses an internal settling device for size classification to settle out large particles and remove small particles at an accelerated rate. This retains the solids in the crystallizer for longer retention times, thus allowing the gypsum crystals to grow to larger sizes. The advantage of the DDO system is the increase in solids retention time without increasing vessel size or decreasing feed rates. Therefore an industrial crystallizer can be modified to use the double-drawoff system with size classification to increase the particle size of gypsum without any major changes in capital or operating costs, other than installation of an internal baffle for size classification.

Various system parameters were changed on the bench-scale crystallizer and their effect on nucleation rate, growth rate, slurry density, and mean particle size were studied. The same system changes were fed into the Mark V

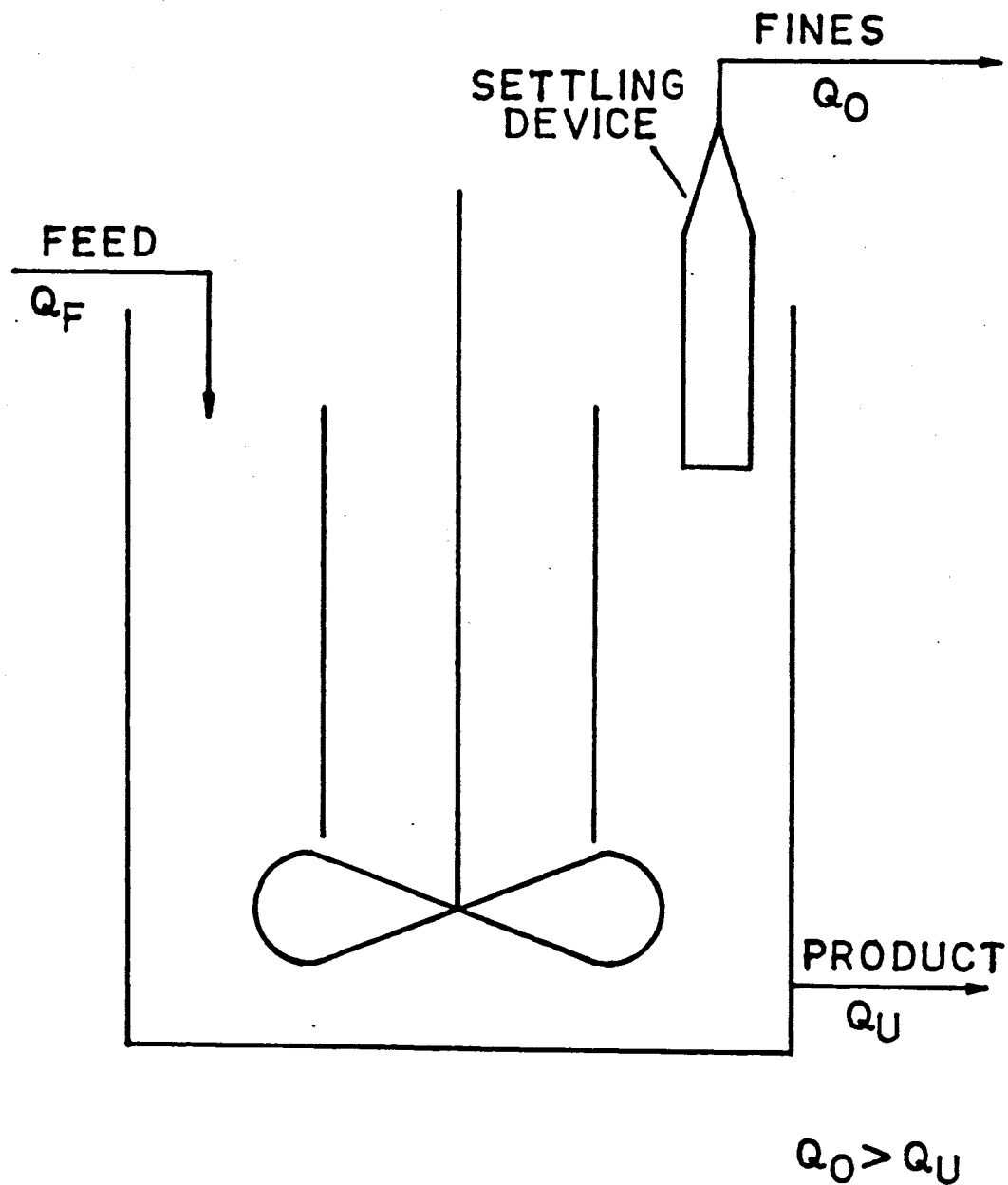


Figure 3. Schematic of double-drawoff crystallizer with accelerated fines removal.

CSD computer simulation program¹ along with gypsum crystallization kinetics. Computer and experimental results were compared.

The effect of citric acid on gypsum crystallization was also studied at various concentrations and different pH levels.

1. The Mark V CSD simulator was developed by William Silbert and Dr. Alan D. Randolph to simulate the interaction of process configuration and kinetics on the resultant CSD. The model is based on solution of simultaneous population and mass balances for the system.

APPARATUS

A schematic of the bench-scale crystallizer used in this study is illustrated in Figure 4. The crystallizer is a 9-liter plastic vessel that contains a stainless steel draft tube and heating coil. The coil and draft tube are supported by four stainless steel baffles. This allows circulation of the crystallizer slurry down the center of the draft tube and up the sides of the crystallizer. The heating coil uses a temperature bath to keep the crystallizer at 130° F. Supersaturation is achieved through chemical means by adding stoichiometric amounts of H_2SO_4 and $\text{Ca}(\text{OH})_2$ from their respective feed tanks. The crystallizer pH is continuously monitored and controlled by automatically adjusting the H_2SO_4 flow rate. The $\text{Ca}(\text{OH})_2$ tank is agitated to provide uniform suspension in the $\text{Ca}(\text{OH})_2$ slurry.

The feed tank contains about 110 liters of simulated mother liquor saturated with gypsum. Excess gypsum crystals are kept in the tank in order to desupersaturate all crystallizer exit streams returning to the feed tank. This allows the feed tank liquor to be recycled, therefore eliminating the task of making 110 liters of feed solution before each experiment. Steam is used to keep the feed tank around

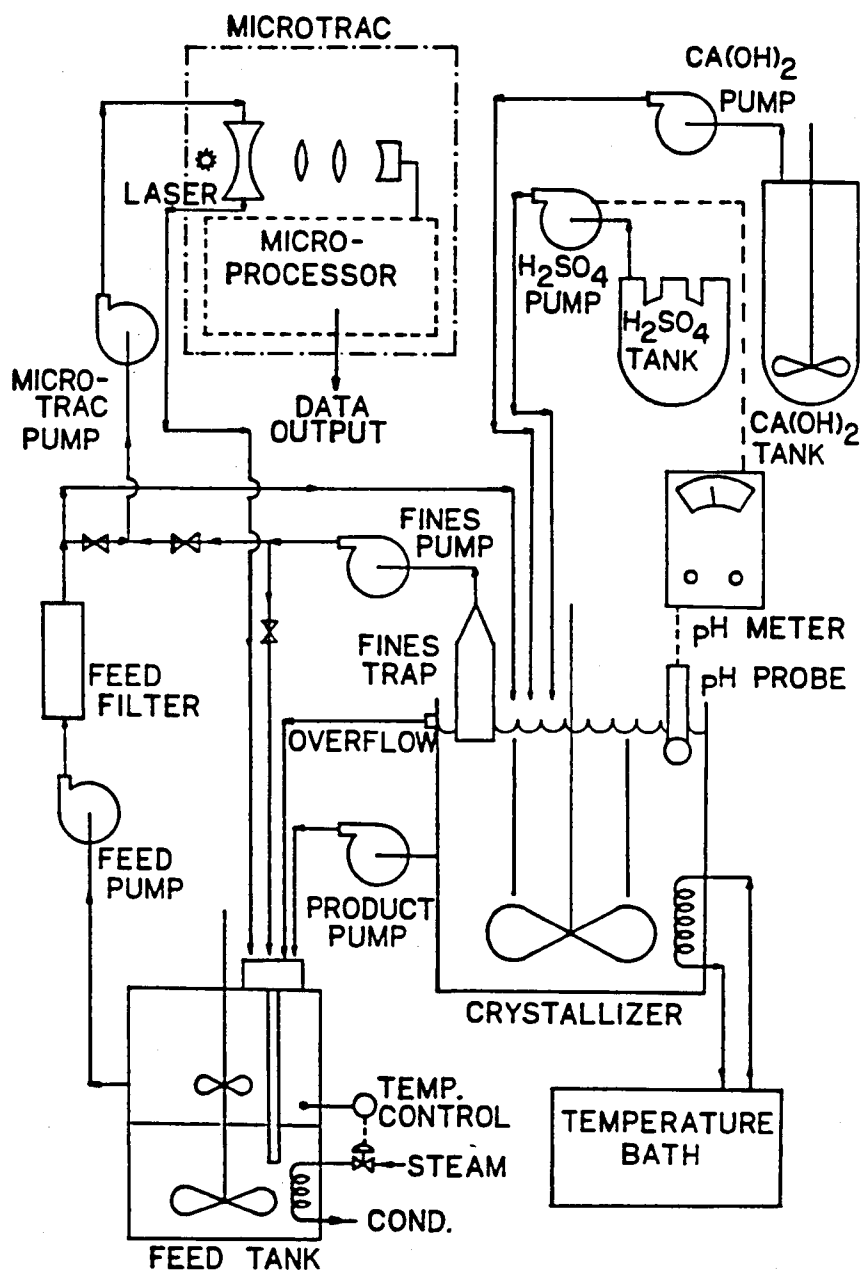


Figure 4. Schematic of apparatus.

130° F. Mild agitation is provided to reduce temperature and concentration gradients.

The fines trap, fines and product pumps create the DDO system. The fines trap is an inverted glass funnel designed to remove particles whose terminal velocity is less than the upward fluid velocity. Larger particles settle back into the crystallizer. This means that particles smaller than the size set by the fines trap and fines pump are removed at an accelerated rate relative to the large particles.

The product pump operates on a dual timer delay system. The pump runs for brief periods at a high flow rate and then remains off for long periods of time. This operation allows particle removal at high pumping velocities, thus reducing the possibility of classified product removal.

An overflow tube controls the level in the crystallizer using gravity flow to send any excess crystallizer liquor to the feed tank.

The feed tank liquor is used as makeup solution to control the liquid retention time in the crystallizer. The feed liquor is pumped through a filter to provide an unseeded feed solution for the crystallizer. The system is an open system because of the H_2SO_4 and $Ca(OH)_2$ reagents used, although nearly total recycle of mother liquor is achieved.

Measuring Devices

Determination of crystallization properties such as nucleation rate, growth rate, slurry density, and particle mean size from experimental samples was done using various measuring devices. The three most important particle sizing techniques, the Particle Data Inc. (PDI) Particle Counter; the Leeds & Northrup Microtrac Particle Size Monitor; and the Allen-Bradley Sonic Sifter, will be briefly described below.

Particle Data Inc. Celloscope[®] Particle Counter

The PDI particle counter is a zone sensing device that measures particle size. An illustration of the orifice tube and vicinity is shown on Figure 5. An electrolyte solution completes a circuit between two electrodes. One electrode (the inner electrode) is located inside the orifice tube. The outer electrode is placed in the sample solution. A vacuum pulls a known volume of sample through the orifice, causing particles to pass through the orifice, usually one at a time. The amount of current that passes through the orifice is related to the size (volume) of the particle passing through the orifice. The PDI measures changes in the current and calculates particle sizes. A distribution of particle sizes from the sample is sent to a

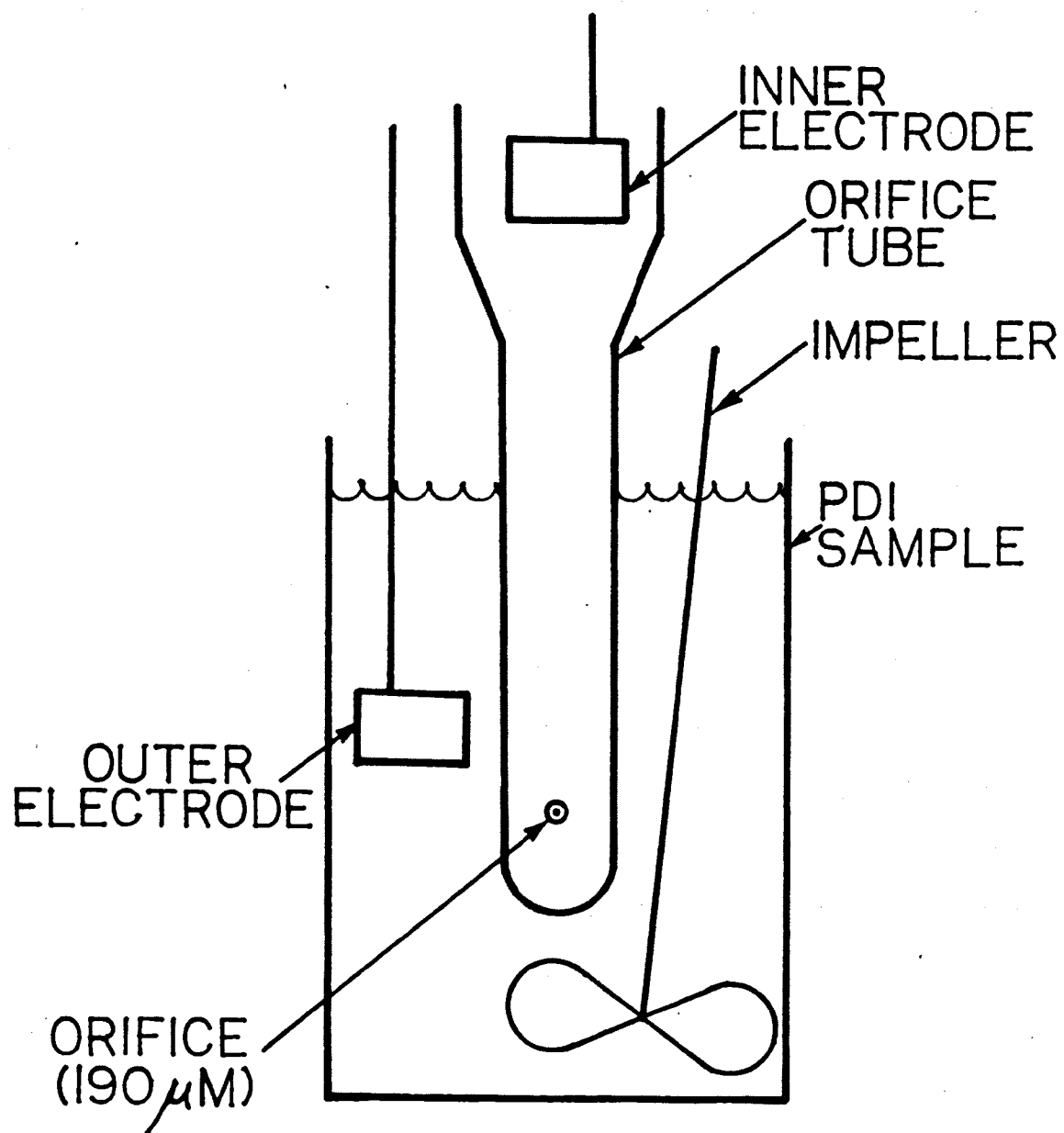


Figure 5. Orifice tube and vicinity.

PDP-8 minicomputer. The data is analyzed to calculate crystallization terms, e.g., nucleation rate (B^0), growth rate (G), and slurry density (M_T). Figure 6 shows a typical printout from the PDI particle counter and PDP-8 minicomputer.

Leeds & Northrup Microtrac Particle Size Monitor

The Microtrac is an on-line particle size monitor that uses light scattering to measure particle size distributions. A crystallizer sample diluted with clear mother liquor is pumped through a chamber in the Microtrac. A laser light beam is sent through the sample chamber and particles in the chamber scatter the light. Photo detectors placed at various positions outside the chamber measure the intensity of scattered light at various angles and send the information to a microprocessor that calculates the size distribution. A computer is used to convert the Microtrac data to a population density distribution and crystallization terms are obtained by fitting this population distribution to the theoretical MSMPR crystallizer form. The Microtrac can be used to measure samples continuously on a bench-scale or on an industrial level. Figure 7 shows a printout of Microtrac results.

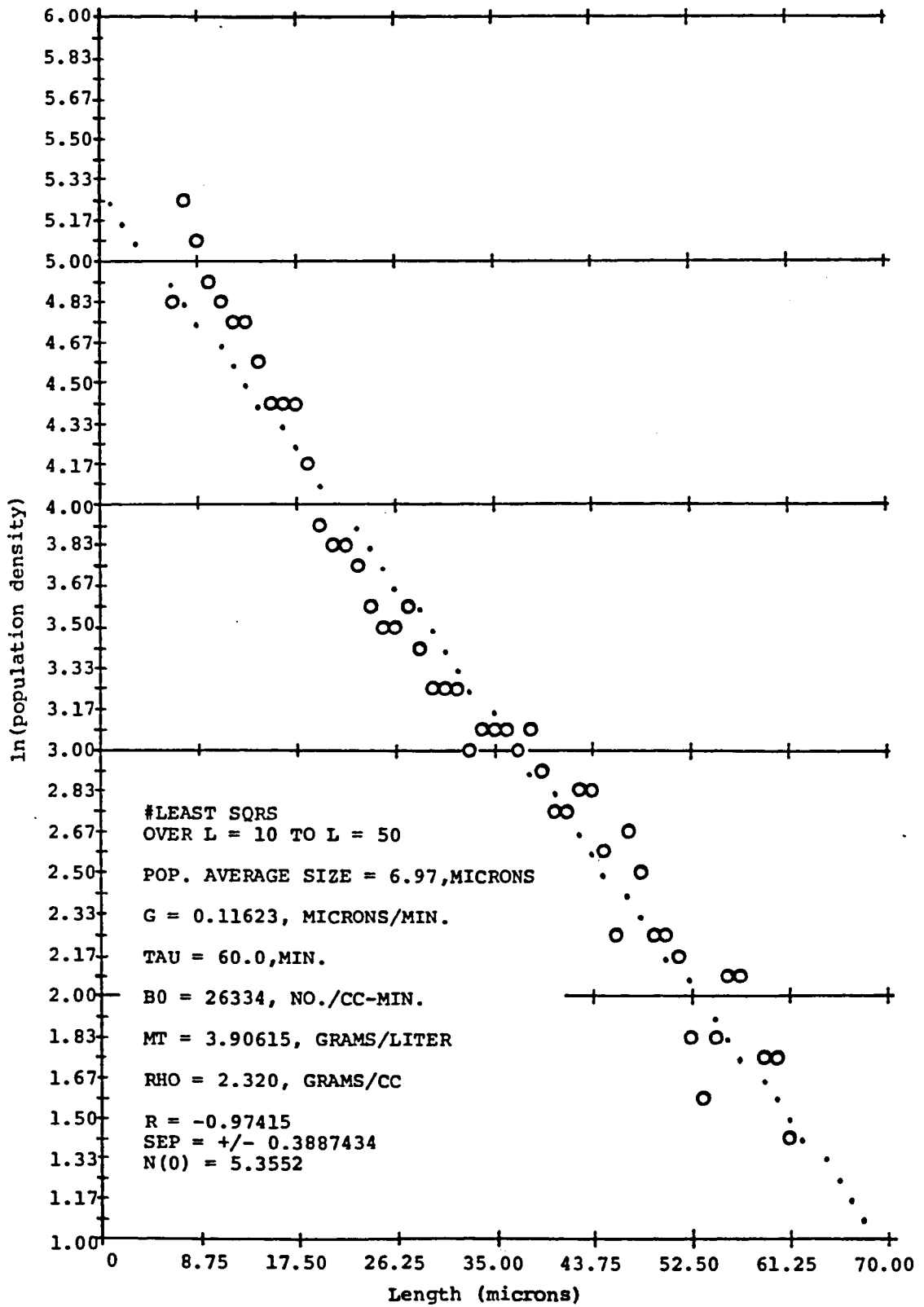


Figure 6. PDI printout.

Figure 7. Microtrac printout.

a. Microtrac data.

b. Microtrac plot.

*** GPL = 1.674E+00

*** RAW MICROTRAC PSM DATA FROM LAST RUN

DU	3	5	7	9	11	13
--	--	--	--	--	--	--
3.660E-01	1.700E+00	4.600E+00	5.200E+00	1.700E+01	9.400E+00	8.700E+00
2	4	6	8	10	12	14
--	--	--	--	--	--	--
2.800E+00	3.600E+00	5.600E+00	1.370E+01	1.960E+01	7.500E+00	0.000E-01

*** RESULTS AT 2:19:40 ON 6/12/81

TAU AT 1.000E+02 MINUTES
VOLUME AT 9.000E+03 CC
LOWER BOUND AT CHANNEL 4
UPPER BOUND AT CHANNEL 10

REGRESSION EQUATION

$N = 0.28786E+06 * \text{EXP}(-0.18994 * L \text{ AVE})$

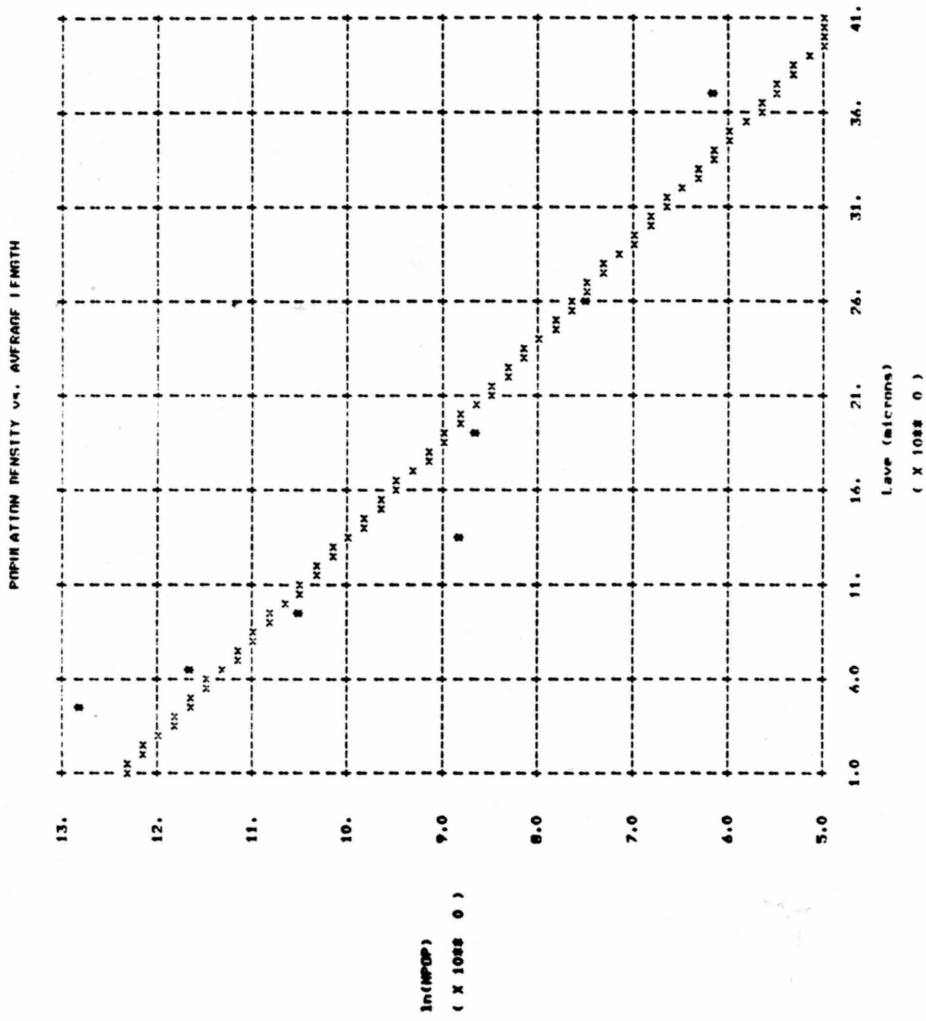
WHERE: N IS IN $\mu\text{L}/\text{CC}-\text{MICRON}$ L AVE IS IN MICRONS

G = 0.52648E-01 MICRONS/MIN
B = 15155. $\mu\text{L}/\text{CC}-\text{MIN}$

R-SQUARED = 0.89671

COEFFICIENT	VALUE	T
B0	0.28786E+06	22.102
B1	-0.18994	-6.5883

a. Microtrac data.



b. Microtrac plot.

Allen-Bradley Sonic Sifter

The Sonic Sifter uses sieve trays of increasing mesh size (decreasing average hole size) to classify particles by size. Sound waves are used to vibrate the crystals. Crystals fall through the sieve tray holes until a hole size too small for crystal passage is reached. Weighing the crystals from each sieve tray gives a weight distribution of the sample. The weight distribution is converted to a population distribution to calculate crystallization terms. Table 1 shows the results of a sample sieved by the Sonic Sifter.

Calibration of Equipment

Pumps

All the pumps were calibrated using the following procedure. A graduated cylinder and stop watch were employed. The pump was allowed to run while warming up. The time was measured to pump a given amount of liquid into the graduated cylinder. The volume was measured and a volumetric flow rate was calculated. Adjustments were made and the procedure was repeated until the correct flow rate was obtained.

Stirrers

The RPM of the crystallizer impeller was measured with a tachometer, then the correct value was set using a

Table 1. Typical Allen-Bradley sieve results. -- Sieve results from Run 27 after operating 36 hours. Mass of sieve sample = 10.00 g.

Sieve #	Weight (g)	%	Cumulative %	L_{avg}^* (μM)
10	0.05	0.50	100.0	-
11	0.29	2.91	99.50	386
12	0.36	3.61	96.59	324
13	0.25	2.51	92.98	273
14	0.46	4.61	90.47	229
15	1.60	16.05	85.86	193
16	1.89	18.96	69.81	162
17	1.98	19.86	50.85	136
18	0.85	8.53	30.99	115
19	0.85	8.53	22.47	96
20	0.64	6.42	13.94	81
21	0.70	7.02	7.52	68
R	<u>0.05</u>	0.05	0.05	-
	Σ 9.97			

* The top tray and residue (R) tray were not used in the calculation of the population distribution. Values of 420 μM and 31 μM were used for the top and residue trays, respectively, when the average particle mean size of the sieve sample was determined.

stroboscope while adjusting the stirrer speed. The feed tank stirrer ran at low speeds while the Ca(OH)_2 impeller ran at high speeds. Their RPMs were not measured.

Temperatures

The temperature in the crystallizer was measured with a thermometer. The temperatures of the feed tank and temperature bath were then adjusted to keep the crystallizer at 130°F .

pH

The pH meter was calibrated using buffer solutions of pH 4 and pH 7. Calibration was done occasionally. High and low set points on the controller were set during an experiment by adjusting the pH in the crystallizer and then adjusting the set points to maintain the desired pH.

PDI Particle Counter

A sample of ragweed pollen with a known mean size of $19.5 \mu\text{M}$ was used to calibrate the PDI. A solution of particle-free mother liquor was used to insure similar electrolyte conductance of calibration sample and crystallizer sample. Actual mechanics of calibration closely followed the calibration instructions in the PDI manual.

Microtrac

A known volume of clear mother liquor was circulated through the Microtrac to obtain a background count. A known mass of gypsum crystals was added to the circulating mother liquor to obtain a dV reading on the Microtrac. More gypsum crystals of known mass were added and another dV reading recorded. A plot of slurry density (concentration of gypsum crystals in solution) versus Microtrac dV readings was made from the data collected. The slope and intercept were determined and used in the on-line CSD measurement computer program to calculate the slurry density of the sample from its Microtrac dV reading.

Allen-Bradley Sonic Sifter

The Sonic Sifter did not require any calibration. The trays were cleaned periodically to prevent crystal blockage that could cause erroneous sieve results.

Solution Make-Up

The feed tank, $\text{Ca}(\text{OH})_2$, and H_2SO_4 solutions were made to simulate a stack-gas scrubbing liquor. The feed tank mother liquor had the following concentrations of ions: chloride, 2.51 g/L; magnesium, 0.20 g/L; and sodium, 0.05 g/L and was made up with the following salts: calcium chloride dihydrate, 10.09 g/L; magnesium sulfate heptahydrate,

20.03 g/L; and sodium chloride, 0.13 g/L. Gypsum was added to the feed tank in excess to saturate the mother liquor with calcium sulfate dihydrate. The salts were added to 110 liters of water in the feed tank and the solution was stirred and heated overnight. The feed tank solution was used for several runs. The feed tank was then cleaned and a new simulated stack-gas scrubbing liquor was made.

The $\text{Ca}(\text{OH})_2$ reagent solution was made with the following chemicals: calcium hydroxide, 88.82 g/L; calcium chloride dihydrate, 20.18 g/L; and sodium chloride, 0.26 g/L. To prevent nucleation in the $\text{Ca}(\text{OH})_2$ reagent tank, no sulfate ions were added to the $\text{Ca}(\text{OH})_2$ solution.

The H_2SO_4 reagent solution was made up with the following chemicals: sulfuric acid, 121.69 g/L; and magnesium sulfate heptahydrate, 4.06 g/L. To prevent nucleation in the H_2SO_4 reagent tank, no calcium ions were added to the H_2SO_4 solution.

Equal volumes of the two reagent solutions added to the crystallizer produced the feed tank ion concentrations with Ca^{++} and $\text{SO}_4^{=}$ ions creating the supersaturation for gypsum nucleation and growth.

650 ppm (weight basis) of the additive was used in the final runs; therefore 0.65 g/L and 1.3 g/L citric acid concentrations were in the feed tank and H_2SO_4 solutions,

respectively. These two concentrations produced a 650 ppm additive concentration in the mother liquor.

Experimental Set-Up

The day before an experiment all the equipment was briefly inspected to see if everything was operating correctly. Any system changes that needed to be done were performed. Calculations and calibrations were done to set the system variables at their correct value. The dual timer on-and-off time intervals were set for the product pump. The crystallizer (9-liter vessel, draft tube, baffles, and heating coil) and impeller were weighed after the scale from the previous experiment was removed. The crystallizer and impeller were put back into position and the necessary connections attached to it. Feed filters were replaced. The feed tank steam was turned on to heat the feed tank. The feed tank impeller was then turned on. The temperature bath was turned on and allowed to heat overnight. Ca(OH)_2 and H_2SO_4 solutions were made and added to their respective tanks. Minor cleanup of equipment area and preparations for sampling and data recording were then performed.

Start-Up

When the temperatures of the feed tank and temperature bath had stabilized around 130°F , the system was ready

to begin an experiment. The following procedure was done to start up an experiment.

1. Turn on the feed pump at a high flow rate (500 mL/min) to fill the crystallizer with mother liquor.
2. Turn on the Ca(OH)_2 tank impeller to mix the Ca(OH)_2 reagent slurry.
3. Turn on the pH meter and leave it on "Standby" to warm up.
4. Set the Ca(OH)_2 and H_2SO_4 systems to circulate distilled water to clean out the lines while warming up the pumps.
5. Put the fines trap (inverted glass funnel) in the clamp above the crystallizer.
6. Set up a circulating loop of the Ca(OH)_2 slurry to prime the Ca(OH)_2 pump.
7. When the crystallizer is full of mother liquor (excess liquor will be coming out of the overflow tube), lower the feed pump flow rate to the correct value.
8. Open the valve on the temperature bath to send hot water through the heating coil in the crystallizer.
9. Put the pH probe in the clamp above the crystallizer. The probe should be submerged as low as possible in the crystallizer. Check the fines trap to see that

its end is about 1 inch below the liquid level in the crystallizer.

10. Turn on the crystallizer impeller and adjust to the correct RPM.
11. Add seed crystals to the crystallizer. Usually crystals are obtained from a previous experiment. Obtain some gypsum crystals to use as seed if none are available from a previous experiment.
12. Switch pH meter from "Standby" to "pH."
13. Measure temperature of crystallizer and adjust pH meter to make corrections for that temperature.
14. Put discharge end of $\text{Ca}(\text{OH})_2$ pump into crystallizer in an area of high mixing (usually at bottom of crystallizer near the crystallizer wall).
15. Put discharge end of H_2SO_4 pump into center of draft tube. Make sure H_2SO_4 line does not wrap around impeller.
16. Adjust pH to correct value by adjusting H_2SO_4 flow rate manually. When desired pH is reached, set high and low set points to control pH at desired value ± 0.3 . Switch H_2SO_4 pump to automatic control (switch is in back of pump).
17. Turn on the fines pump and run at a flow rate high enough to prime the fines trap and pump. Then adjust flow rate to correct value.

18. Turn on the product pump. The dual timer was previously set but adjustments are made during the experiment to keep the level in the crystallizer fairly constant.
19. Watch the system for a few hours to see if everything is running smoothly. Make adjustments where necessary. Check for minor problems that can be corrected without completely shutting the system down.

Sampling

The PDI, Microtrac, and Sonic Sifter have different sample preparation procedures that are described below.

PDI

The PDI was only used to analyze samples from the MSMPR crystallizer configuration. Double-drawoff crystallizer experiments produced crystals too large for the PDI. The Microtrac and Sonic Sifter were used to analyze double-drawoff crystallizer samples.

Preparation of a sample to be analyzed by the PDI particle counter employs the use of a pipette, a magnetic stirrer, beakers, and a solution of clear mother liquor.

PDI samples are prepared as follows:

1. Obtain a product sample from the crystallizer.
2. Put the sample on a magnetic stirrer to reduce settling of solids.

3. Put a measured amount (100 mL) of filtered mother liquor in the PDI sample beaker.
4. Using a pipette, remove a known amount of sample and put it in the PDI sample beaker.
5. Place the PDI sample in a sonic bath for one minute to break up agglomeration.
6. Place the PDI sample on the PDI particle counter for analysis.

The filtered mother liquor in the PDI sample dilutes the sample so the orifice in the PDI will not plug. A dilution factor is used to correct for the mother liquor dilution.

Microtrac

The Microtrac was used for particle analysis on the small crystals (fines) from the fines trap. Because the Microtrac is a continuous on-line particle monitor, it only needs to be set up once during an experiment. The set-up procedure is below:

1. Turn on the Microtrac pump and set it at the desired flowrate (about 600 mL/min).
2. Adjust the feed pump flow rate to equal the sum of the Microtrac pump and crystallizer feed flow rates.
3. Open pinch clamp to send clear liquor to the Microtrac.

4. On top of the Microtrac is a corked tube. Remove the cork and shut off the Microtrac exit stream to fill up the Microtrac sample chamber.
5. Adjust the sample chamber liquid level by the trial and error procedure of uncorking the top of the chamber, draining a certain amount of liquid from the chamber, inserting the cork and observing the chamber level.
6. Turn on the Microtrac by turning the key to the "on" position.
7. Take background dV readings until they stabilize, then switch Microtrac to "run" mode.
8. Switch clamps to send fines diluted with filtered feed liquor to the Microtrac. Flow rates are adjusted to keep the crystallizer level constant.
9. Turn on the microprocessor, reset it, and turn on the computer terminal. Load the computer program and take sample readings.

Sonic Sifter

Product crystal samples were analyzed using the Sonic Sifter as these crystals were too large for either the PDI or Microtrac counters. Sonic Sifter samples were prepared using a glass funnel millipore filter, a vacuum flask, and acetone. A vacuum applied to the glass filter separated the

mother liquor from the product crystals. The mother liquor collected in the vacuum flask was poured into a graduated cylinder and the volume was measured. The gypsum crystals were dried using acetone and then weighed. Ten grams of the sample was put in the sifter. A weight distribution was obtained and converted to a population distribution to determine crystallization terms, e.g., nucleation rate, growth rate, and slurry density.

Shut-Down

After an experiment is completed, the following steps were performed to shut down the system:

1. Clamp the line to the Microtrac to shut off flow from the crystallizer to the Microtrac.
2. Reload computer program before turning off computer terminal, Microtrac, and microprocessor.
3. Drain Microtrac sample chamber by opening drain port and removing stopper at top of chamber.
4. Turn off the Microtrac pump.
5. Turn off all pumps associated with crystallizer.
6. Set up Ca(OH)_2 and H_2SO_4 systems for water circulation to clean out the lines.
7. Switch the pH meter to "Standby," place the pH probe in a beaker of water, and turn off the pH meter.
8. Turn off steam to feed tank and turn off feed tank impeller.

9. Turn off the temperature bath and close the valve to shut off water flow through the heating coils.
10. Siphon out crystallizer slurry while impeller is on. Be careful not to get tubing caught on the impeller. Save slurry for next experiment to be used as seed crystals.
11. Turn off crystallizer impeller.
12. Turn off $\text{Ca}(\text{OH})_2$ and H_2SO_4 pumps. Leave water circulation systems intact.
13. Turn off $\text{Ca}(\text{OH})_2$ impeller.
14. Seal $\text{Ca}(\text{OH})_2$ and H_2SO_4 tanks with stoppers to prevent any evaporation between runs.
15. Inspect crystallizer for extent of scale deposit.
16. Disconnect crystallizer from system. Disconnect impeller from motor drive.
17. Let crystallizer dry, then weigh crystallizer and impeller to determine amount of scale deposition.
18. Check system for damages or improvements.
19. Analyze data taken during experiment.

Analysis of Data

The results from the PDI, Microtrac, and Sonic Sifter were different in format. Therefore, some organization was needed to put the results in the same perspective. The following discussion will explain what was done with the results from the three particle measuring devices.

PDI Data

The PDI particle counter was only used to analyze Mixed Suspension Product Removal (MSMPR) crystallizer experiments. MSMPR crystallizers have only one exit stream which is the product stream, as there is no accelerated fines removal. Double-drawoff (DDO) crystallizer experiments produced crystals too large to be analyzed with the PDI. The Microtrac and Sonic Sifter were used to analyze DDO crystallizer samples. PDI results were compared with Microtrac and Sonic Sifter results to observe the effects of switching from MSMPR to DDO operation in the gypsum crystallizer.

A data printout from the PDP-8 minicomputer (PDI particle counter) is shown in Figure 8. Population average size ($L_{1,0}$), growth rate (G), nucleation rate (B^0), and slurry density (M_T) are the crystallization values of interest. The least squares fit of the data (correlation coefficient) was observed to see if the results were at a proper steady state.

Microtrac

A printout of Microtrac results is shown on Figure 9. Nucleation rate, growth rate, and slurry density are the important crystallization terms taken from the Microtrac output. The correlation coefficient is observed to see how well the regression equation fits the data. Because the

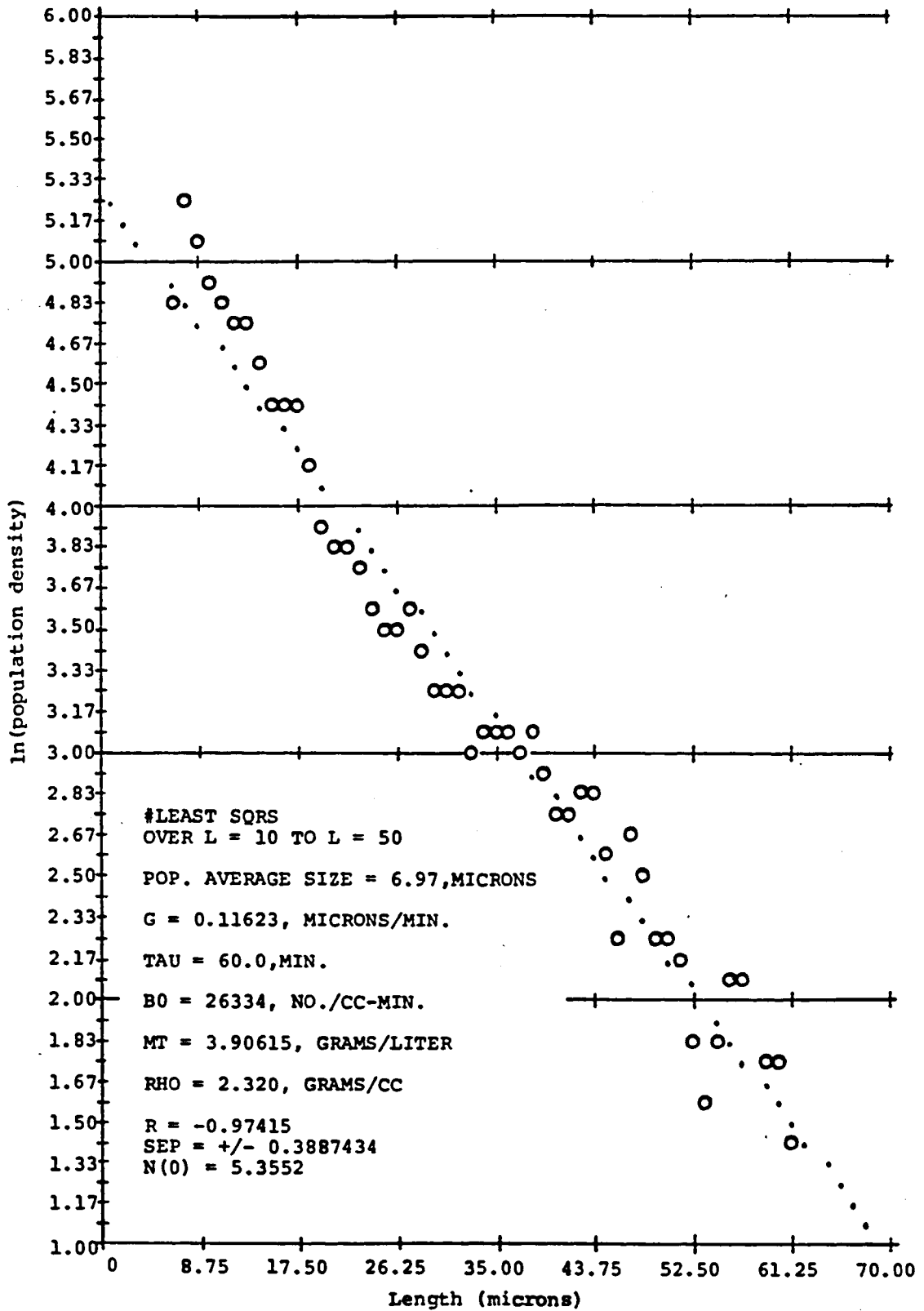


Figure 8. Printout used in data analysis.

Figure 9. Microtrac printout used in data analysis.

a. Microtrac data used in data analysis.

b. Microtrac plot used in data analysis.

*** GPL = 1.674E+00

*** RAW MICROTRAC PSM DATA FROM LAST RUN

DU	3	5	7	9	11	13
--	--	--	--	--	--	--
3.660E-01	1.700E+00	4.600E+00	5.200E+00	1.700E+01	9.400E+00	8.700E+00
2	4	6	8	10	12	14
--	--	--	--	--	--	--
2.800E+00	3.600E+00	5.600E+00	1.370E+01	1.960E+01	7.500E+00	0.000E-01

*** RESULTS AT 2:19:40 ON 6/12/81

TAU AT 1.000E+02 MINUTES
VOLUME AT 9.000E+03 CC
LOWER BOUND AT CHANNEL 4
UPPER BOUND AT CHANNEL 10

REGRESSION EQN:

$N = 0.28786E+06 * EXP(-0.18994 * L AVE)$

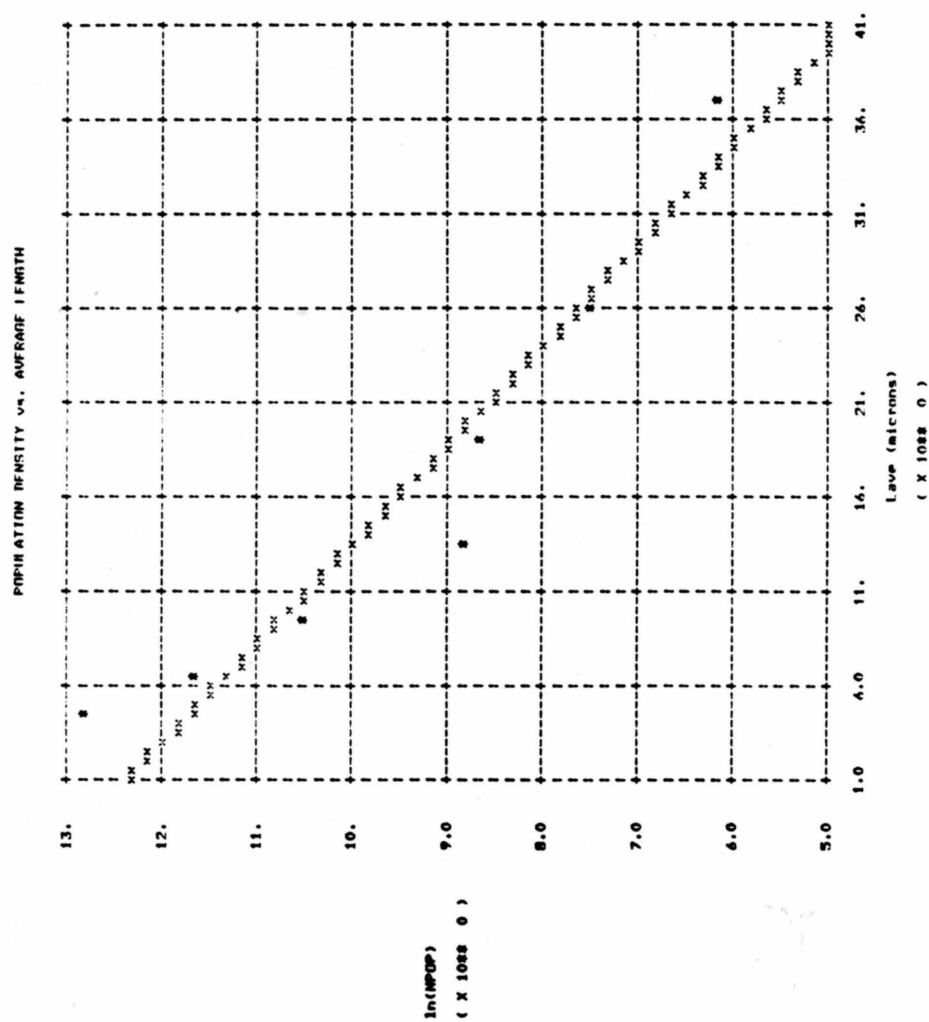
WHERE: N IS IN #/CC-MICRON L AVE IS IN MICRONS

G = 0.52648E-01 MICRONS/MIN
B = 15155. #/CC-MIN

R-SQUARED = 0.89671

COEFFICIENT	VALUE	T
B0	0.28786E+06	22.102
B1	-0.18994	-6.5883

a. Microtrac data used in data analysis.



Microtrac monitors only the overflow from the crystallizer, the population distribution calculated represent the crystallizer fines.

Sonic Sifter

Because the crystals from the sieve trays are weighed, the resulting weight distribution must be converted to a population distribution to couple the Sonic Sifter results with Microtrac results. The conversion equation is:

$$n_i = (\Delta W_i \cdot M_T) / (\Delta L_i \cdot \rho \cdot k_v \cdot L_{avg,i}^3 \cdot M_s) \quad (1)$$

where

n_i = population on tray i (#/mL· μ M)

ΔW_i = weight of crystals on tray i (g)

ΔL_i = aperture size difference between tray i and tray above tray i (μ M)

ρ = crystal density ($g/\mu M^3$)

k_v = volume shape factor

$L_{avg,i}$ = average particle size on tray i (μ M)

M_T = crystallizer slurry density (g)

M_s = mass of Sonic Sifter sample (g)

A least squares fit of $\ln n$ versus L_{avg} from converted Sonic Sifter data is made to obtain a population distribution equation representing the crystallizer product stream. Table 2 shows typical Sonic Sifter results.

Table 2. Sieve data conversion.* -- $k_v = \pi/6$, $\rho = 2.32 \times 10^{-12} \text{ g}/\mu\text{M}^3$, $M_s = 10.0 \text{ g}$, $v_{M_T(\text{exp})} = 30.58 \text{ g/L}$.

Sieve No.	ΔW (g)	ΔL (μM)	L_{avg} (μM)	$\ln n$
R	0.05	-	-	-
21	0.70	11	68	6.23
20	0.64	14	81	5.38
19	0.85	18	96	4.90
18	0.85	19	115	4.30
17	1.98	24	136	4.41
16	1.89	28	162	3.69
15	1.60	33	193	2.83
14	0.46	40	229	0.88
13	0.25	47	273	-0.42
12	0.36	57	324	-0.76
11	0.29	66	386	-1.65
10	0.05	-	-	-

*Results: $\ln n = 7.52 - 0.0257 \cdot L_{\text{avg}}$

$$r^2 = 0.9649$$

$$n^0 = 1850.6 \text{ \#/mL} \cdot \mu\text{M}$$

$$G = 0.0649 \text{ } \mu\text{M}/\text{min}$$

$$B^0 = 120.1 \text{ \#/mL} \cdot \text{min}$$

$$M_T(\text{cal.}) = 31.04 \text{ g/L}$$

Plotting both Microtrac and Sonic Sifter results produces the graph shown in Figure 10. Notice the difference in slopes as expected from DDO theory. An analysis of these data will be presented later.

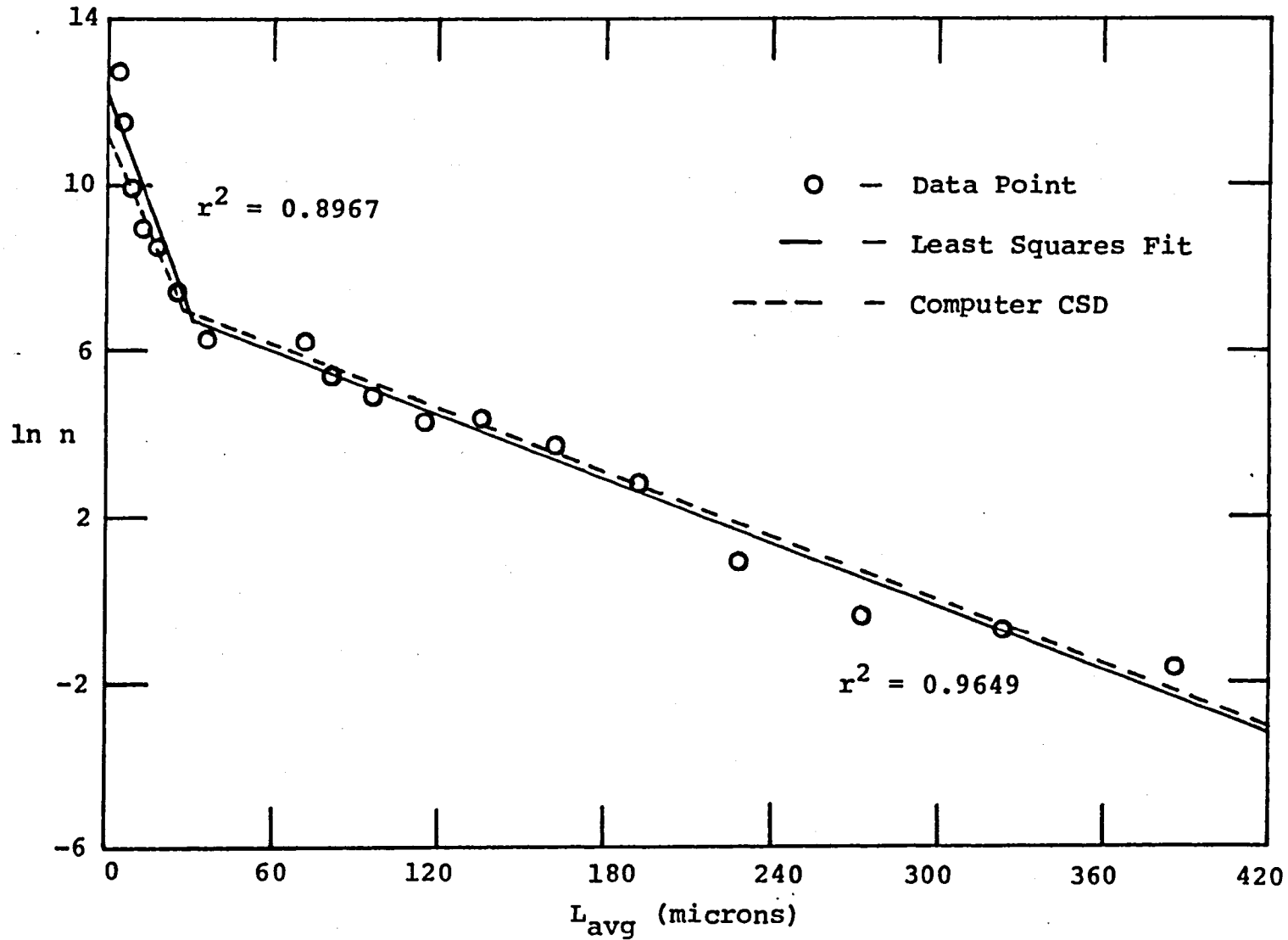


Figure 10. Plot of $\ln n$ versus L_{avg} using Microtrac and sieve data.

THEORY

A brief discussion of the mechanisms and kinetic formation of crystal nucleation and growth rates will precede a theoretical explanation of how the double-drawoff (DDO) system increases crystal size.

Nucleation

Formation of new crystals of a solute from a supersaturated solution is called nucleation. Three types of nucleation are recognized:

1. Homogeneous nucleation: the formation of new crystals from the liquid phase as a result of supersaturation alone. No pre-existing crystals are present or influence the formation of new grain.
2. Heterogeneous nucleation: the formation of new crystals in the presence of foreign substrates. Such substrates typically provide low-energy paths which increase the number of embryo clusters which eventually grow large enough to become stable nuclei.
3. Secondary nucleation: the formation of new crystals in the presence of seed crystals of the same material which therefore influences the formation of new grain.

The rate of homogeneous nucleation (B^0) is given by an Arrhenius rate expression:

$$B^0 = C \exp(\Delta G^*/kT) \quad (2)$$

where

B^0 = nucleation rate, #/mL·min

C = rate constant, #/mL·min

ΔG^* = free energy of formation of a nucleus, kcal/
nuclei

k = Boltzmann's constant, kcal/nuclei

T = absolute temperature, °K

The rate of heterogeneous nucleation is expressed as a similar equation with a term less than unity multiplying ΔG^* , which accounts for the lower energy barrier due to the impurities that act as nucleation sites. Homogeneous and heterogeneous nucleation both exhibit a metastable limit of supersaturation below which essentially no nucleation occurs (at least over any reasonable time interval). This level of supersaturation is higher than the supersaturation level at which industrial crystallizers typically operate. Therefore, some other mechanism (contact secondary nucleation) is thought to be responsible for creating nuclei in most inorganic industrial crystallizers.

Clontz and McCabe (1971) showed that nuclei can be formed at supersaturation levels below the metastable limit

by lightly tapping a crystal in solution with a solid object or another crystal. There was no visible damage to the crystal, even after creation of many nuclei. Therefore, it was proposed that nuclei are formed by dislodging a semi-ordered growth layer surrounding the crystal. Crystal-crystal, crystal-impeller, and crystal-wall contacts all result in secondary nucleation in an industrial crystallizer. Such secondary nucleation is called contact nucleation and has been shown to be proportional to the supersaturation and the intensity and frequency of the collisions (Chereminsinoff and Young, 1977; Larson and Timm, 1968; Randolph and Rajagopal, 1970).

The following power-law equation can often be used for correlation of secondary contact-type nucleation rate data:

$$B^o = k_n (\text{RPM}) G^i M_T^j \quad (3)$$

where

B^o = nucleation rate, #/mL·min

G = growth rate, $\mu\text{M}/\text{min}$

M_T = slurry density, g/L

k_n = constant

Growth rate in this equation is used as a measure of supersaturation driving force; growth rate is more easily measured. Slurry density is a measure of the amount of

crystals present (related to collision frequency). Collision intensity is related to the RPM of the impeller. This correlation has been successful in correlating much secondary nucleation rate data (Murray and Larson, 1965; Randolph and Larson, 1971; Timm and Cooper, 1971).

Growth

Crystal growth from solution is a two-step process. The first step is solute diffusion to the crystal surface. The second step is solute orientation into the crystal lattice (called the particle integration step). Growth can be diffusion-rate controlled or integration-rate controlled, depending on which step dominates the growth process. Non-agitated systems are usually diffusion-controlled whereas highly agitated systems are integration-controlled. A mechanism proposed for solute integration is the screw-dislocation theory presented by Burton, Cabrera and Frank (1951). This mechanism assumes solute molecules add to the crystal surface in a self-perpetuating spiral that provides a continuous supply of low-energy sites.

Supersaturation is the driving force for crystal growth. Theoretical predictions show growth as a function of concentration ratio, $S = C/C_{\text{sat}}$, as either:

$$G = k_G S \quad (4)$$

or

$$G = k_G S^2 \quad (5)$$

The concentration ratio S is sometimes referred to as the thermodynamic supersaturation. To correlate his experimental growth rate data, a power law of the form:

$$G = k_G s^a \quad (6)$$

was used by Etherton in his research study, where s is the stoichiometric supersaturation, $C - C_{sat}$. The stoichiometric supersaturation is convenient to use in mass balance calculations while the supersaturation ratio S is directly related to free energy changes which determine primary nucleation.

The gypsum crystallization study done by Etherton showed that secondary nucleation kinetics, e.g., Equation 3, correlated the data well. The following equations were determined from his research (Etherton, 1980):

$$B^0 = \exp(16.72) G^{1.48} M_T^{1.27} \quad (7)$$

$$G_s = \exp(13.11) s^{2.226}$$

Seed crystals were used in the present bench-scale crystallizer study to promote secondary nucleation. However, no attempt was made to verify Equations 7 and 8, but only to test Etherton's calculations that accelerated fines

removal in a bench-scale crystallizer would increase gypsum crystal size. Simulation of the bench-scale DDO results using Etherton's nucleation and growth model gave a good fit to the data which validates the reasonableness of his kinetics.

Accelerated Fines Removal

A theoretical explanation of the double-drawoff system will be discussed. A more detailed description is presented by Randolph and Larson (1971).

Population Balance

The macroscopic population balance for crystals in a mixed magma is given by Randolph and Larson (1971) as:

$$\frac{\partial n}{\partial t} + \frac{\partial(Gn)}{\partial L} + \frac{\partial(\ln V)}{\partial t} = -\sum_i \frac{n_i \bar{Q}_i}{V} + B(L) - D(L) \quad (9)$$

Assuming conditions of steady state, no crystal breakage, perfect mixing, no crystals in the feed, and G independent of L (ideal MSMR crystallizer plus McCabe's ΔL law), Equation 9 becomes:

$$G \frac{dn}{dL} = - \frac{n}{\tau} \quad (10)$$

which predicts a crystal population density distribution in the form:

$$n(L) = B^0/G \exp(-L/G\tau) \quad (11)$$

where

$n(L)$ = population density (number/micron mL)

G = linear growth rate (micron/min)

B^0 = nucleation rate (number/mL min)

L = linear particle size (micron)

τ = retention time (min)

A semilog plot of $n(L)$ versus L of Equation 11 produces a line with a slope and intercept of $-1/G\tau$ and B^0/G , respectively.

The DDO crystallizer is similar to a MSMPR crystallizer except that two exit streams leave the DDO crystallizer. Equation 9 reduces to the following form for a DDO crystallizer:

$$VG \frac{dn}{dL} = -Q_B C_w(L)n \quad (12)$$

The $C_w(L)$ term is a size-dependent removal function that makes Equation 12 a variable coefficient equation. Development of the removal function is presented by Randolph and Larson (1971). Q_B is a reference flow, usually net liquor flow. Particles less than some size L_F are removed at the total liquor flow rate, while over-size particles are removed at the discharge rate. If the discharge rate is chosen for the reference flow Q_B , then the $C_w(L)$ term can be written as follows:

$$C_w > 1, L < L_F \quad (13)$$

$$C_w = 1, L > L_F \quad (14)$$

which simulates size-dependent removal in a DDO crystallizer. Letting C_w equal some value greater than one (say R) for L values less than L_F , the population balance predicts the following distributions:

$$n = B^0/G \exp\left[-\frac{RL}{G\tau}\right], \quad L < L_F \quad (15)$$

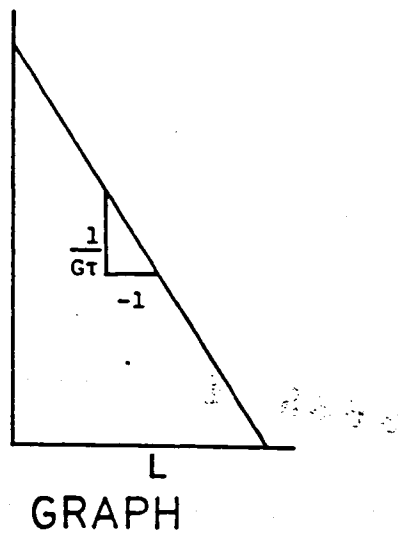
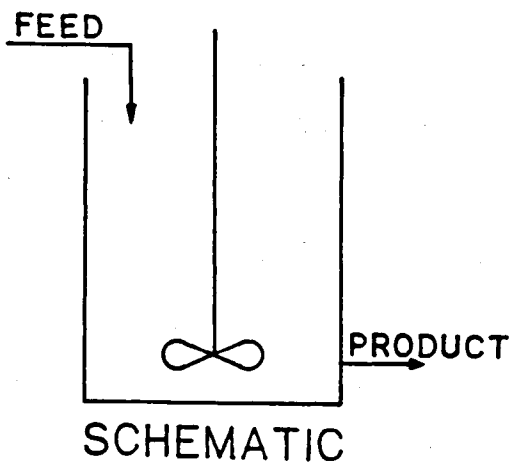
$$n = B^0/G \exp\left[-(R-1)\frac{L_F}{G\tau}\right] \exp\left(-\frac{L}{G\tau}\right), \quad L > L_F \quad (16)$$

A plot comparing population density distributions with and without DDO accelerated fines removal is illustrated in Figure 11. Note the increase in large crystals with the DDO configuration. Accelerated fines removal produces the difference in slopes ($R > 1$ in Equation 14). Mass balance constraints make the growth rate increase, creating the less steep slope for particles greater than L_F . Thus from a theoretical standpoint, accelerated fines removal in a DDO crystallizer will increase the crystal size of product.

System Design

The bench-scale DDO crystallizer used in this study employed an inverted glass funnel to create a settling zone for particle classification. Calculations of particle

MSMPR CRYSTALLIZER



DDO CRYSTALLIZER

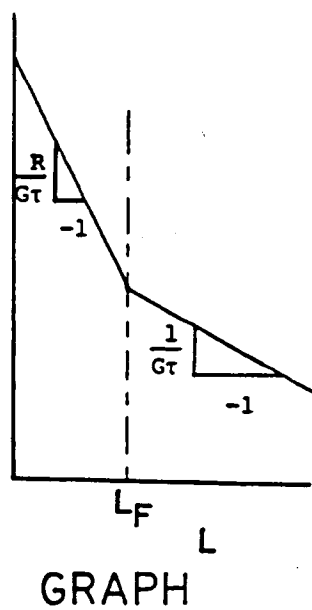
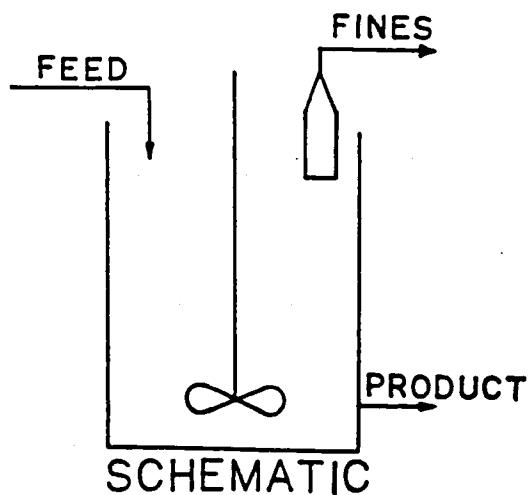


Figure 11. Crystallizer configuration comparison.

terminal velocity using Stokes Law settling were done to determine the particle cut-off size.

Etherton's nucleation rate correlation was fed into the Mark I CSD simulator to determine how accelerated fines removal would affect gypsum crystal size distribution. The Mark I CSD simulator is an earlier version of the Mark V CSD simulation used in this study. Table 3 and Figure 12 show the three cases simulated together with the predicted mass-weighted mean sizes. The proposed design shows a significant increase in crystal size. In the present study bench-scale crystallizer experiments were performed to closely match Etherton's computer simulation parameters, thus facilitating comparison of these predictions with experimental results.

Table 3. Mark I results.

Configuration	Mass Mean Size (μM)
MSMPR	71
Current Design	67
Proposed Design	83-130

The proposed design in Figure 12 has a clarifier that returns small crystals (less than 15 μM) to the crystallizer.

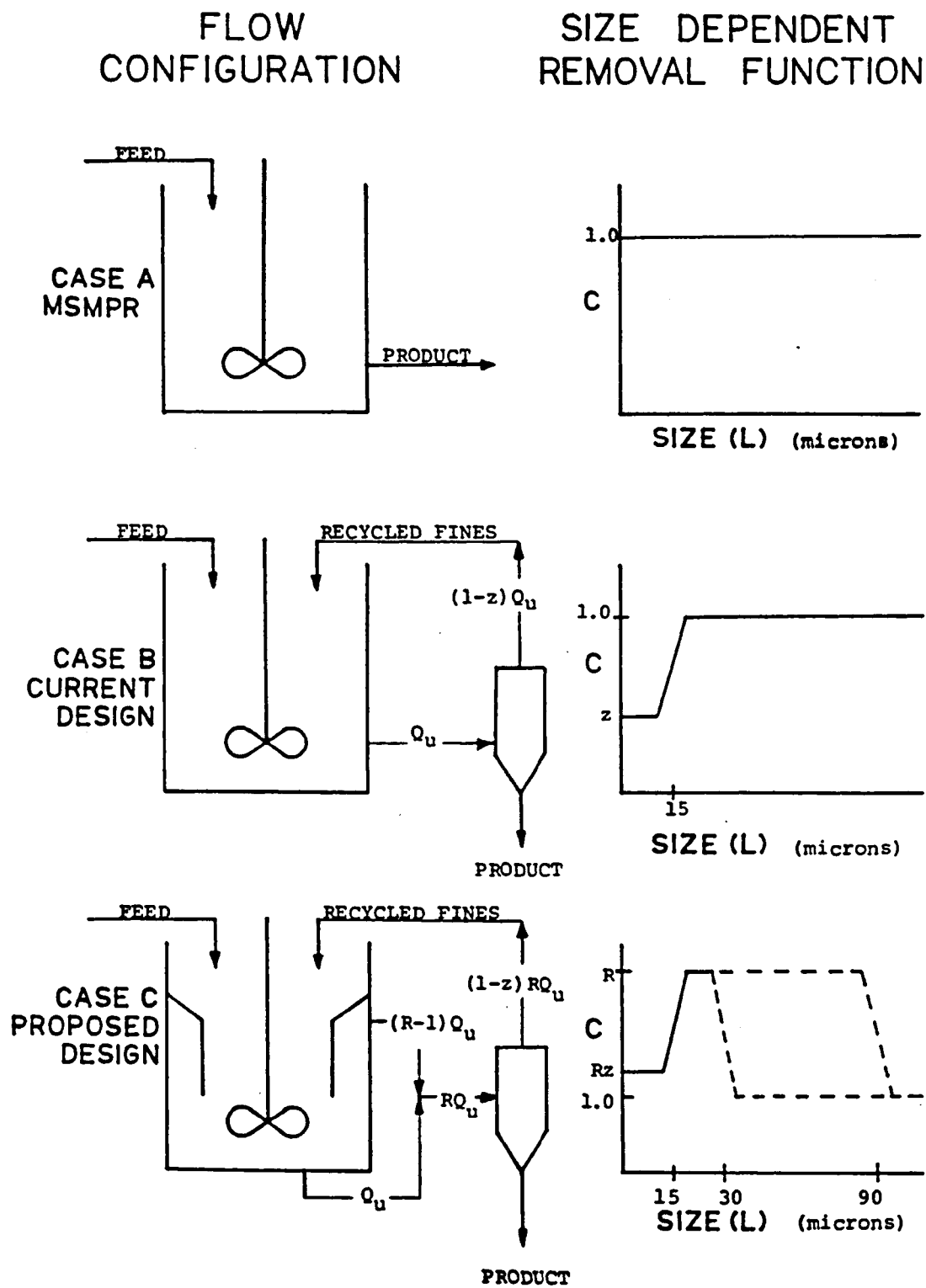


Figure 12. Configurations simulated by Mark I (after Etherton, 1980).

Bench-scale experiments did not employ a clarifier. Small crystals were filtered out before returning the liquor to the crystallizer. Therefore, Etherton's computer simulations cannot be compared exactly to the experimental results of this study. However, experimental runs closely matching Etherton's CSD simulations were run, except that no clarifier return was present. These runs adequately captured the flavor of DDO operation and were used to demonstrate the validity of the CSD simulation model.

Computer Simulation

The Mark V CSD computer simulation program, developed by William Silbert at the University of Arizona, is designed to simulate the interaction of process configuration and kinetics on the resultant CSD. The model is based on solution of simultaneous population and mass balances for the system.

Three equations are solved simultaneously in the Mark V program. They are listed below:

Solute Balance:

$$Q_F(C_F - C) = \frac{GV\rho k_a m_2}{2} \quad (17)$$

Gypsum Kinetics:

$$B^0 = \exp(16.72) \cdot G^{1.48} \cdot M_T^{1.27} \quad (18)$$

Supersaturation-Growth Rate Correlation:

$$G = \exp(13.11) \cdot (C - C_s)^{2.226} \quad (19)$$

Analytical and numerical solutions to the above equations are in Appendix A.

Substituting the following values into the solute balance:

$$V = 9,000 \text{ mL}$$

$$e = 2.32 \text{ g/mL}$$

$$k_a = 3.0$$

will give the following solute balance equation:

$$Q_F \cdot (C_F - C) = 31320 \cdot G \cdot m_2 \quad (20)$$

Substitution of other constants and definition of terms will be given in Appendix A and the Nomenclature section, respectively.

PRESENTATION OF EXPERIMENTAL RESULTS

Experiments using the bench-scale crystallizer were performed under various conditions. Certain parameters (DDO ratio, rate of make, pH, impeller speed, and retention time) were changed to study their effect on the crystal habit and size distribution. Initial experiments used the MSMR configuration to establish a base for comparison with DDO runs. The effects of citric acid modifier were also studied in early experiments. Later runs with the DDO system always used citric acid modifier. It was discovered that a run time of at least 48 hours was needed to achieve steady state results. Therefore, only data from the final runs were used for evaluation of process behavior.

Experimental results are listed in Table 4 for observation and comparison. Plots of corresponding runs follow in the text, together with plots comparing experimental, computer, and calculated results. In general, the experimental and computer-simulated values were in reasonable agreement.

The Microtrac was inoperable during some runs and therefore a few graphs do not have Microtrac results. The fines distribution in these cases was extrapolated from

Table 4. Experimental results.

a. Bench-scale crystallizer results.

Run No.	DDO Ratio	τ_L (min)	RPM	pH	Rate of Make (g/L min)	$G \times 10^2$ ($\mu\text{M}/\text{min}$) Exp	$B^0 \times 10^{-3}$ ($\#/mL \cdot \text{min}$) Exp	$n^0 \times 10^{-5}$ ($\#/mL \cdot \mu\text{M}$) Exp	M_T (g/L) Exp	L_{avg} (μM) Exp	L_F (μM) Exp
13 ^a	0	60	425	6	0.125	11.6	26.3	5.27	3.65	28	0
26	9:1	60	407	4	0.125	5.96	10.6	1.81	39.5	179	21
27	5:1	100	406	4	0.125	6.03	11.9	2.12	30.6	159	31
28	9:1	60	407	4	0.125	5.27	8.16	1.56	45.0	171	13
29 ^b	9:1	100	405	4	0.125	3.27	15.4	4.67	41.4	150	17
31	5:1	60	485	4	0.125	9.15	13.2	1.48	16.3	130	28
32	5:1	60	406	4	0.188	9.40	12.4	1.51	46.6	175	27
33	5:1	60	406	5	0.125	8.00	10.8	1.35	30.4	110	22
34 ^b	5:1	60	400	4	0.125	13.4	5.23	0.390	39.1	170	36

a = MSMPR run

b = No Microtrac data

Table 4. Experimental results.

b. Mark V CSD simulator results.

Run No.	DDO Ratio	τ_L (min)	RPM	pH	Rate of Make (g/L min)	$G \times 10^2$ ($\mu\text{M}/\text{min}$) Comp	$B^0 \times 10^{-3}$ ($\#/mL \cdot \text{min}$) Comp	$n^0 \times 10^{-5}$ ($\#/mL \cdot \mu\text{M}$) Comp	M_T (g/L) Comp	L_{avg} (μM) Comp	L_F (μM) Comp
13 ^a	0	60	425	6	0.125	24.3	3.29	0.136	5.86	58	0
26	9:1	60	407	4	0.125	8.45	12.8	0.51	58.5	200	27
27	5:1	100	406	4	0.125	6.45	4.75	0.73	36.5	154	27
28	9:1	60	407	4	0.125	8.45	12.8	1.51	58.5	200	27
29 ^b	9:1	100	405	4	0.125	5.20	6.59	1.27	61.0	206	27
31	5:1	60	485	4	0.125	10.5	9.15	0.873	34.9	149	27
32	5:1	60	406	4	0.188	10.3	15.8	1.53	54.7	146	27
33	5:1	60	406	5	0.125	10.5	9.15	0.873	34.9	149	27
34 ^b	5:1	60	400	4	0.125	10.5	9.15	0.873	34.9	149	27

a = MSMPR run

b = No Microtrac data

sieve data. The extrapolation procedure along with other data analysis methods are discussed in Appendix B.

Crystallizer Runs

The range of operating conditions is listed in Table 5, and the specific conditions for each run are listed in Table 6. The crystallizer temperature was maintained close to 130° F. Any small deviations in temperature should not significantly affect the results. The length of a run depended on what happened first; i.e., achievement of a steady state CSD, equipment failure, or operator fatigue.

Table 5. Range of variables (DDO runs only).

Variable	Range	Units
Rate of make	0.125 - 0.188	g/L min
Retention time	60 - 100	min
DDO ratio	5:1 - 9:1	
pH	4 - 5	
Temperature	130 - 134	°F
Impeller speed	402 - 485	rev/min
Citric acid conc.	625 - 650	ppm

The increase in the additive concentration between runs 13 and 26 was necessary due to the pH change from 6 to 4. Citric acid's modifying ability depends on its concentration and the crystallizer pH. When the pH is lowered,

Table 6. Summary of run conditions.

Run No.	Date	Run Time (hours)	Rate of Make (g/L min)	Retention Time (min)	DDO Ratio	pH	Temp (°F)	RPM	Citric Acid Conc. (ppm)
13 ^a	1/23/81	3	0.125	60	0	6	133	430	50
26	6/ 8/81	21	0.125	60	9:1	4	132	407	650
27	6/11/81	36	0.125	100	5:1	4	132	406	650
28	6/16/81	46	0.125	60	9:1	4	134	407	650
29	6/29/81	53	0.125	100	9:1	4	134	405	650
31	7/14/81	49	0.125	60	5:1	4	130	485	650
32	7/20/81	44	0.188	60	5:1	4	131	406	650
33	7/27/81	56	0.125	60	5:1	5	130	406	650
34 ^b	8/12/81	47	0.125	60	5:1	4	133	402	650

a = MSMR run

b = Base conditions for comparing DDO runs

more citric acid modifier is needed to change the crystal habit. A possible explanation of this behavior will be discussed later.

A variable that was not changed but which affects the CSD is the particle cut-off size. A fixed classification size of about 27 microns was used in all the computer runs. Data analysis of experimental runs produced a varying classification size, even though conditions were set to maintain a fairly constant cut-off size (see L_F results in Table 6). The effects of classification size on the crystallizer and product mean sizes are discussed by Etherton (1980).

MSMPR crystallizer data were analyzed using the PDP-8 minicomputer that prints out the results determined from the data received from the PDI particle counter. Double-drawoff CSD's were determined from Microtrac and Allen-Bradley Sonic Sifter data. Therefore, plots of the two crystallizer configurations will be different. However, the results can still be compared to observe the effect size classification has on the CSD.

Results

Table 4 lists the crystallizer conditions and results by experiment (Run No.). The results of computer-simulated runs under similar crystallizer conditions are also listed for comparison.

Graphs

The following figures are plots of the experimental and computer crystal size distributions. The correlation coefficients indicate how well the linear regression equations fit the Microtrac and Allen-Bradley Sonic Sifter data. The dashed line in each plot is the CSD determined from computer results to compare with the experimental CSD.

The data points exhibit a hump in several plots. This represents an unsteady state CSD caused by either uncontrolled changes in the crystallizer during a run or too short a run time. In general, the experimental and computer plots agree fairly well. It should be recalled that there are no adjustable parameters in the model to bring about this data fit; a priori system kinetics and process parameters were used in the CSD simulations.

Run 26

Run 26 was done at the following crystallizer conditions: DDO ratio, 9:1; retention time, 60 min; impeller speed, 407 rev/min; pH, 4; and rate of make, 0.125 g/L min.

In run 26 the DDO ratio was increased from the base condition of 5:1 to a value of 9:1. This change increases the solids retention time from 6 hours to 10 hours, which should thus increase the mean size, slurry density, nucleation rate, and nuclei density. The growth rate should

decrease with an increase in the DDO ratio. A plot of the computer and experimental CSD's are shown in Figure 13. The experimental and computer results of runs 26 and 34 (base run) are shown in Table 7.

The results of the DDO ratio increase agree qualitatively with the computer predictions. The experimental data points create an unsteady state hump in the CSD (see Figure 13). Linear regression is used to produce the best fit line which is assumed to be a steady state CSD. The computer results showed a CSD with flatter slopes and more crystals at a given size. In conclusion, an increase in the DDO ratio does improve the product quality by increasing the mean size and slurry density. Fouling was also reduced at the higher DDO ratio.

Run 27

Run 27 was done at the following crystallizer conditions: DDO ratio, 5:1; retention time, 100 min; impeller speed, 406 rev/min; pH, 4; and rate of make, 0.125 g/L min.

In run 27 the retention time was increased to 100 min from the base condition to 60 min. This change increases the solids retention time from 6 hours to 10 hours, similar to the DDO ratio increase of run 26. Runs 26 and 27 will be compared to see if an increase in retention time produces the same results an increase in the DDO ratio would produce.

Table 7. Results of runs 26 and 34.

Run No.	$G \times 10^2$ ($\mu\text{M}/\text{min}$)		$B^o \times 10^{-3}$ ($\#/\text{mL} \cdot \text{min}$)		$n^o \times 10^{-5}$ ($\#/\text{mL} \cdot \mu\text{M}$)		M_T (g/L)		L_{avg} (μM)	
	Comp	Exp	Comp	Exp	Comp	Exp	Comp	Exp	Comp	Sieve
34	10.5	13.4	9.15	5.23	0.873	0.390	34.9	39.1	149	170
26 ^a	8.45	5.96	12.8	10.6	1.51	1.81	58.5	39.5	200	179

a = DDO ratio increase

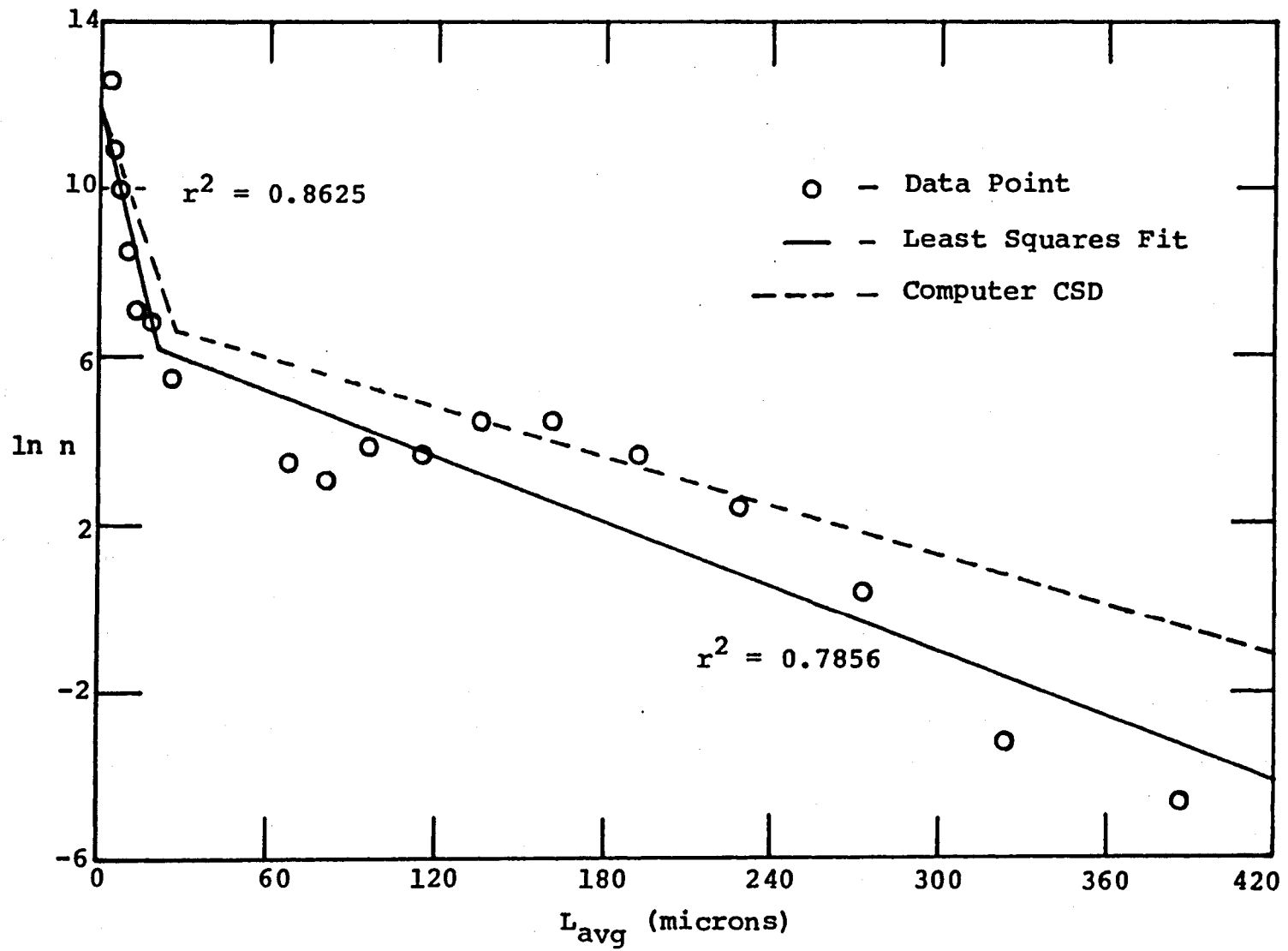


Figure 13. Plot of Microtrac and sieve data from run 26.

The solids retention time is the same in both systems, but the procedure of achieving the 10-hour holding time is different. Experimental and computer results of runs 26, 27, and 34 are shown in Table 8 for comparison.

The computer simulation predictions show that both changes increase L_{avg} and M_T while lowering G , but a DDO ratio increase raises the mean size and slurry density more than the retention time increase. Comparing run 27 to run 34, computer B^0 and n^0 values dropped in both cases. In conclusion, a DDO ratio increase changes (increases) the slurry density and crystal size more effectively than an increase in the mother liquor retention time.

A plot of run 27 is shown in Figure 14. Run 27 shows excellent agreement between experimental and computer results, indicating that the kinetics used in the computer program well describe gypsum secondary nucleation.

Run 28

Run 28 is a duplicate of run 26 to evaluate normal run-to-run variance in the system. Results from these two runs are listed in Table 9. The results of these two runs agree quite well except for the measured slurry density. Equipment operating problems are probably the reason for this difference. Figure 15 is a plot of the CSD from run 28. Note the unsteady state hump in the data similar to run 26.

Table 8. Results of runs 26, 27, and 34.

Run No.	$G \times 10^2$ ($\mu\text{M}/\text{min}$)		$B^0 \times 10^{-3}$ ($\#/\text{mL} \cdot \text{min}$)		$n^0 \times 10^{-5}$ ($\#/\text{mL} \cdot \mu\text{M}$)		M_T (g/L)		L_{avg} (μM)	
	Comp	Exp	Comp	Exp	Comp	Exp	Comp	Exp	Comp	Sieve
34	10.5	13.4	9.15	5.23	0.873	0.390	34.9	39.1	149	170
26 ^a	8.45	5.96	12.8	10.6	1.51	1.81	58.5	39.5	200	179
27 ^b	6.47	6.03	4.75	11.9	0.733	2.12	36.5	30.6	154	159

a = DDO ratio increase

b = retention time increase

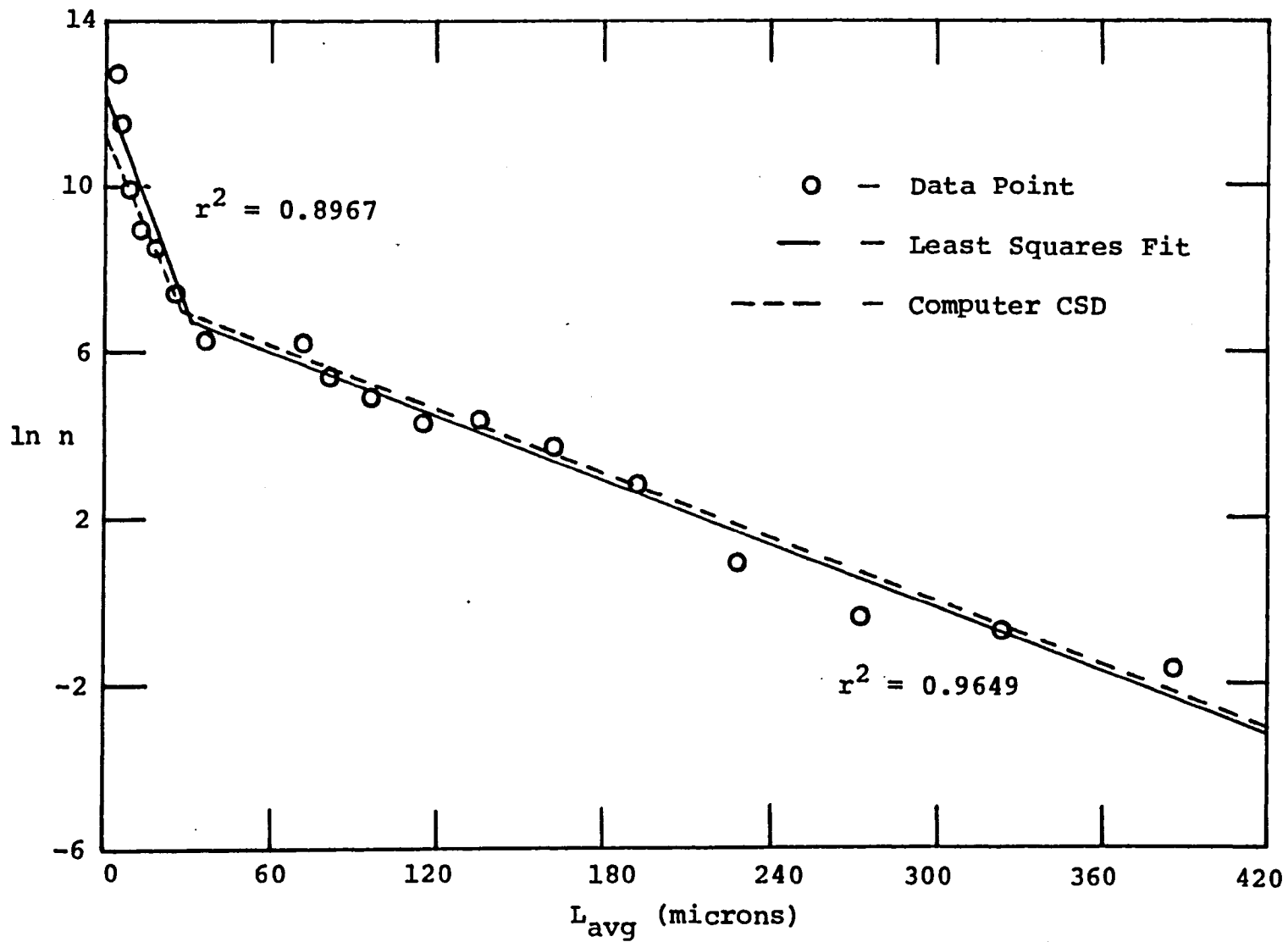


Figure 14. Plot of Microtrac and sieve data from run 27.

Table 9. Results of runs 26 and 28.

Run No.	$G \times 10^2$ ($\mu\text{M}/\text{min}$)		$B^0 \times 10^{-3}$ ($\#/\text{mL} \cdot \text{min}$)		$n^0 \times 10^{-5}$ ($\#/\text{mL} \cdot \mu\text{M}$)		M_T (g/L)		L_{avg} (μM)	
	Comp	Exp	Comp	Exp	Comp	Exp	Comp	Exp	Comp	Sieve
26	8.45	5.96	12.8	10.6	1.51	1.81	58.5	39.5	200	179
28	8.45	5.27	12.8	8.16	1.51	1.56	58.5	45.0	200	171

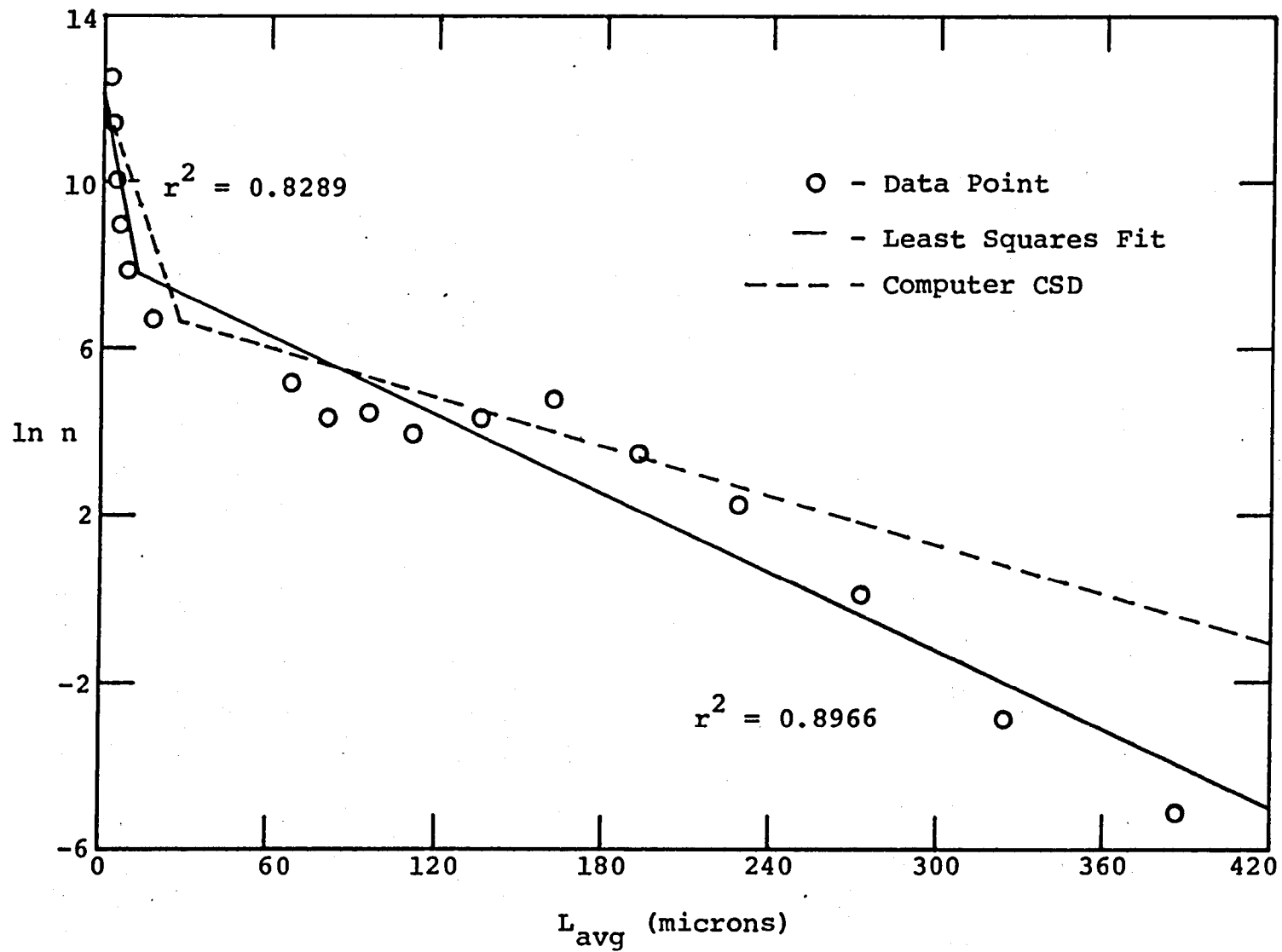


Figure 15. Plot of Microtrac and sieve data from run 28.

Runs 26 and 28 show that reproducible results can be achieved in the bench-scale crystallizer.

Run 29

The following conditions were used for run 29: DDO ratio, 9:1; retention time, 100 min; impeller speed, 406 rev/min; pH, 4; and rate of make, 0.125 g/L min.

The conditions of run 29 create a solids retention time of 1000 min (16-2/3 hours). This should produce a large mean size and slurry density together with a low growth rate. The results of run 29 are shown in Table 10.

Run 29 computer predictions show the highest L_{avg} and M_T values and the lowest growth rate of all the predicted runs. Comparing run 29 with the base conditions, the computer B^0 values dropped while the n^0 values increased.

Examination of the experimental results shows a smaller increase in slurry density than indicated by computer predictions. Particle mean size went down instead of increasing. The experimental growth rate is the lowest of all the runs. No Microtrac data were taken during run 29 or the base run. The fines distribution in these cases was extrapolated from the Allen-Bradley Sonic Sifter data. Therefore, the experimental n^0 and B^0 values might have been different if the Microtrac had been used to calculate the fines CSD.

Table 10. Results of runs 29 and 34.

Run No.	$G \times 10^2$ ($\mu\text{M}/\text{min}$)		$B^0 \times 10^{-3}$ ($\#/\text{mL} \cdot \text{min}$)		$n^0 \times 10^{-5}$ ($\#/\text{mL} \cdot \mu\text{M}$)		MT (g/L)		L_{avg} (μM)	
	Comp	Exp	Comp	Exp	Comp	Exp	Comp	Exp	Comp	Sieve
34 ^b	10.5	13.4	9.15	5.23	0.873	0.390	34.9	39.1	149	170
29 ^b	5.20	3.27	6.59	15.4	1.27	4.67	61.0	41.4	206	150

b = No Microtrac data

Unfortunately, the Microtrac was inoperable during runs 29 and 34.

A graph showing the computer and experimental CSD's of run 29 is given in Figure 16. In general, the two CSD's agree even with the extrapolated data. The one main difference is the slope of the CSD for large crystal sizes. This difference was caused by conditions in the crystallizer environment.

Runs 31 Through 33

Runs 31, 32, and 33 employ a variable change in impeller speed, rate of make, and pH, respectively. The other variables are similar to base conditions. The change performed in each run is listed below.

Run 31	RPM raised from 406 to 485
Run 32	Rate of make changed from 0.125 g/L min to 0.188 g/L min
Run 33	pH raised from 4 to 5

The remaining variables in each run were set at base conditions. The computer simulation program does not predict changes in impeller speed or pH; therefore, the computer results of runs 31 and 33 are identical. The experimental results of the two runs are compared with the experimental base condition results.

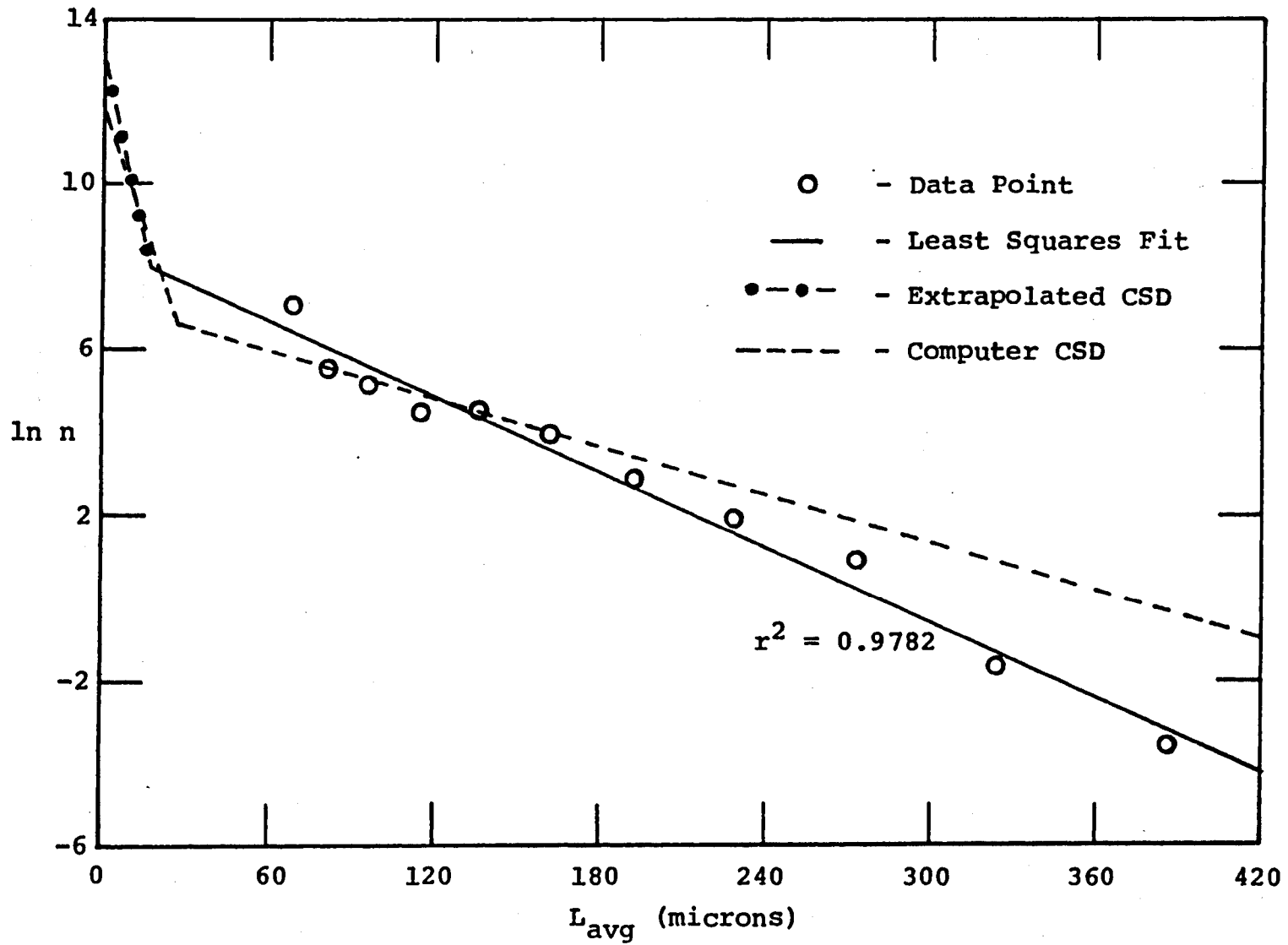


Figure 16. Plot of sieve data from run 29 with extrapolated fines CSD.

The results of run 32 will be discussed first because the computer program can simulate a rate of make change. Results of runs 32 and 34 are shown in Table 11.

The experimental results follow the computer-predicted value changes except for L_{avg} . Experimental results from run 32 show an increase in mean size while the computer results predict a decrease. Conditions in the crystallizer environment, e.g., fouling, are probably a reason for this discrepancy.

Run 32 crystal size distribution is plotted in Figure 17. The experimental and computer CSD's show good agreement. The apparent discontinuity in the data points near L_F is possibly due to Microtrac error.

The results of runs 31 and 33 along with the base condition results are in Table 12. Increasing the impeller speed is detrimental to slurry density build-up and mean size. More nuclei are produced and more exist in the crystallizer (B^0 and n^0 values increase). Less scale forms in the crystallizer, but this reduction in fouling does not make up for the decrease in product quality (determined by the mean size and slurry density).

Increasing the pH produces similar results as increasing the impeller speed. The factor creating these results is related to the modifier. The amount of citric

Table 11. Results of runs 32 and 34.

Run No.	$G \times 10^2$ ($\mu\text{M}/\text{min}$)		$B^{\circ} \times 10^{-3}$ ($\#/\text{mL} \cdot \text{min}$)		$n^{\circ} \times 10^{-5}$ ($\#/\text{mL} \cdot \mu\text{M}$)		M_T (g/L)		L_{avg} (μM)	
	Comp	Exp	Comp	Exp	Comp	Exp	Comp	Exp	Comp	Sieve
34	10.5	13.4	9.15	5.23	0.873	0.390	34.9	39.1	149	170
32 ^a	10.3	9.40	15.8	12.4	1.53	1.51	54.7	46.6	146	175

a = Rate of make increase

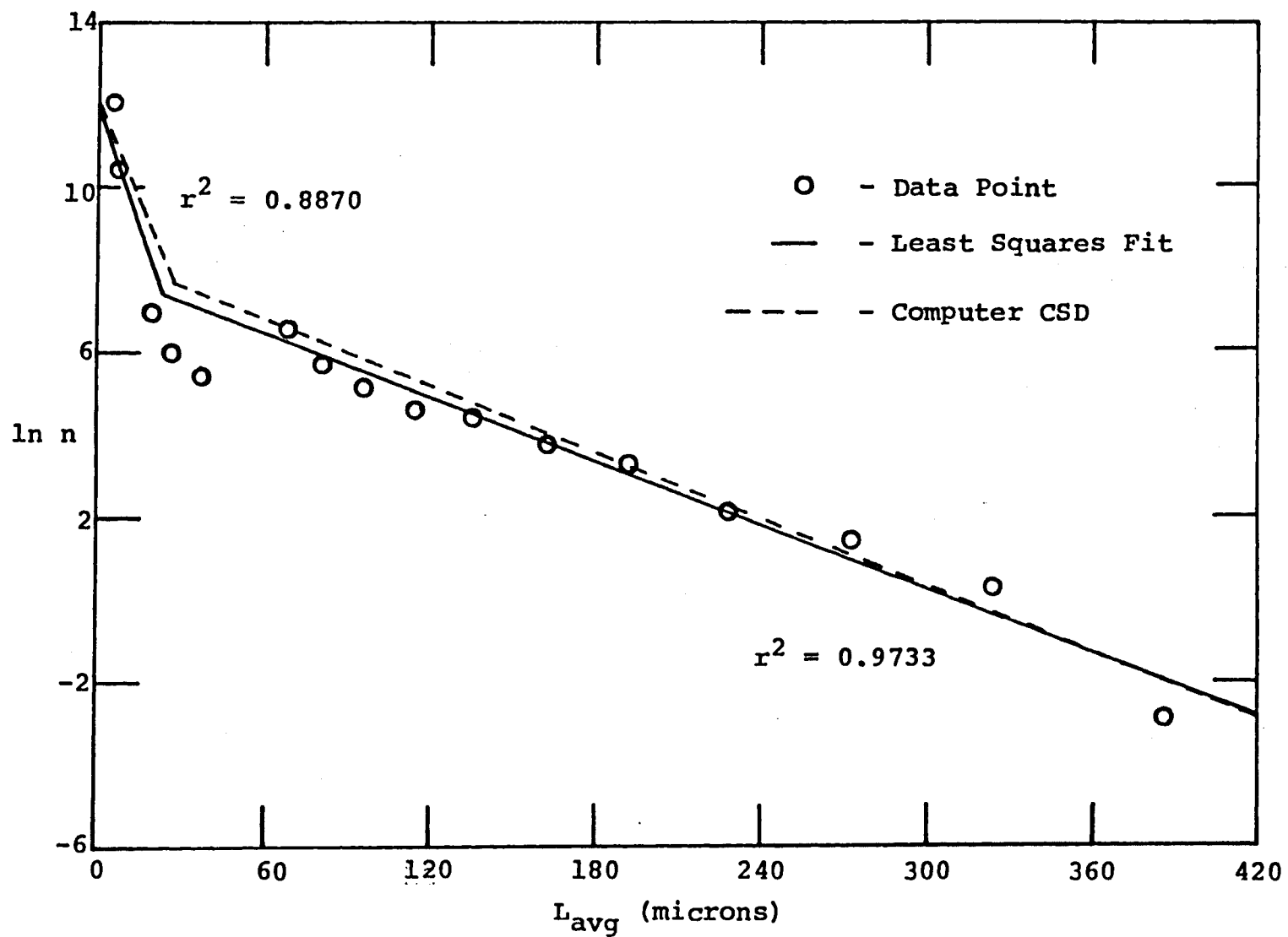


Figure 17. Plot of Microtrac and sieve data from run 32.

Table 12. Results of runs 31, 33, and 34.

Run No.	$G \times 10^2$ ($\mu\text{M}/\text{min}$)		$B^{\circ} \times 10^{-3}$ ($\#/\text{mL} \cdot \text{min}$)		$n^{\circ} \times 10^{-5}$ ($\#/\text{mL} \cdot \mu\text{M}$)		M_T (g/L)		L_{avg} (μM)	
	Comp	Exp	Comp	Exp	Comp	Exp	Comp	Exp	Comp	Sieve
34	10.5	13.4	9.15	5.23	0.873	0.390	34.9	39.1	149	170
31 ^a	10.5	9.15	9.15	13.2	0.873	1.48	34.9	16.3	149	130
33 ^b	10.5	8.00	9.15	10.8	0.873	1.35	34.9	30.4	149	110

a = Impeller speed increase

b = pH increase

acid in the crystallizer coupled with the crystallizer pH will affect the results even though the other variables remain constant. An explanation of this phenomenon will be discussed later.

Figures 18 through 20 plot experimental and computer results from runs 31, 33, and 34. Figure 18 shows good agreement of computer and experimental crystal size distributions, indicating again that the bench-scale crystallizer results can be predicted using computer simulation with Etherton's kinetics.

Figures 19 and 20 show unsteady state CSD data points. Figure 19 (run 33) has a steeper-than-predicted slope. This is caused by a lower growth rate which produces a lower mean size. The experimental and computer slopes intersect in Figure 20 (run 33). The difference in computer and experimental results is related to crystallizer conditions that sometimes give unsteady state results and/or poor data fit to the model.

The MSMPR results (see Table 4) are discussed here to stress the fact that all the double-drawoff runs significantly increased both slurry density and mean size relative to the MSMPR case, as predicted from computer simulation and theoretical considerations.

Figures 21 through 25 are plots comparing the experimental results with calculated and computer results.

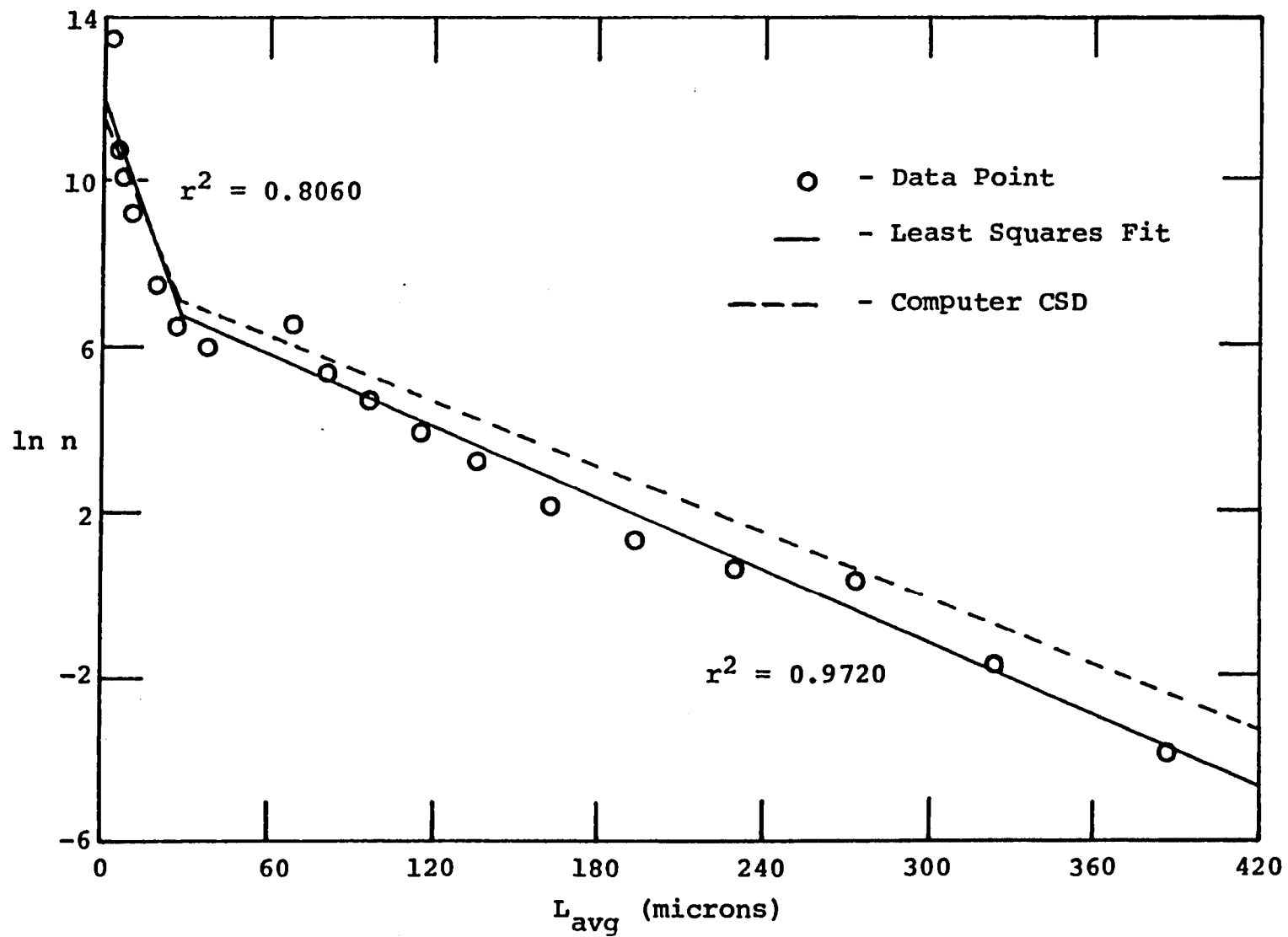


Figure 18. Plot of Mictotrac and sieve data from run 31.

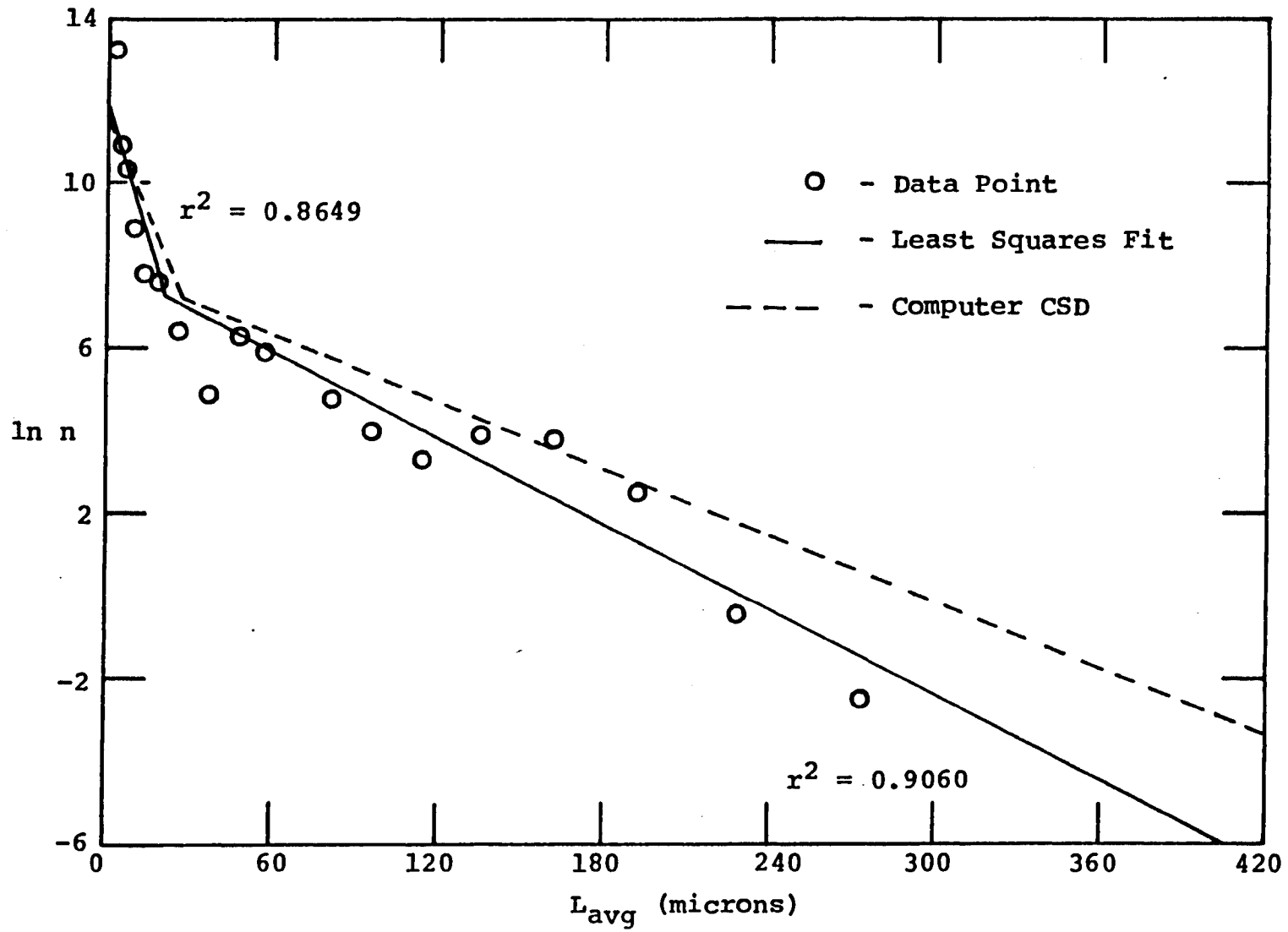


Figure 19. Plot of Microtrac and sieve data from run 33.

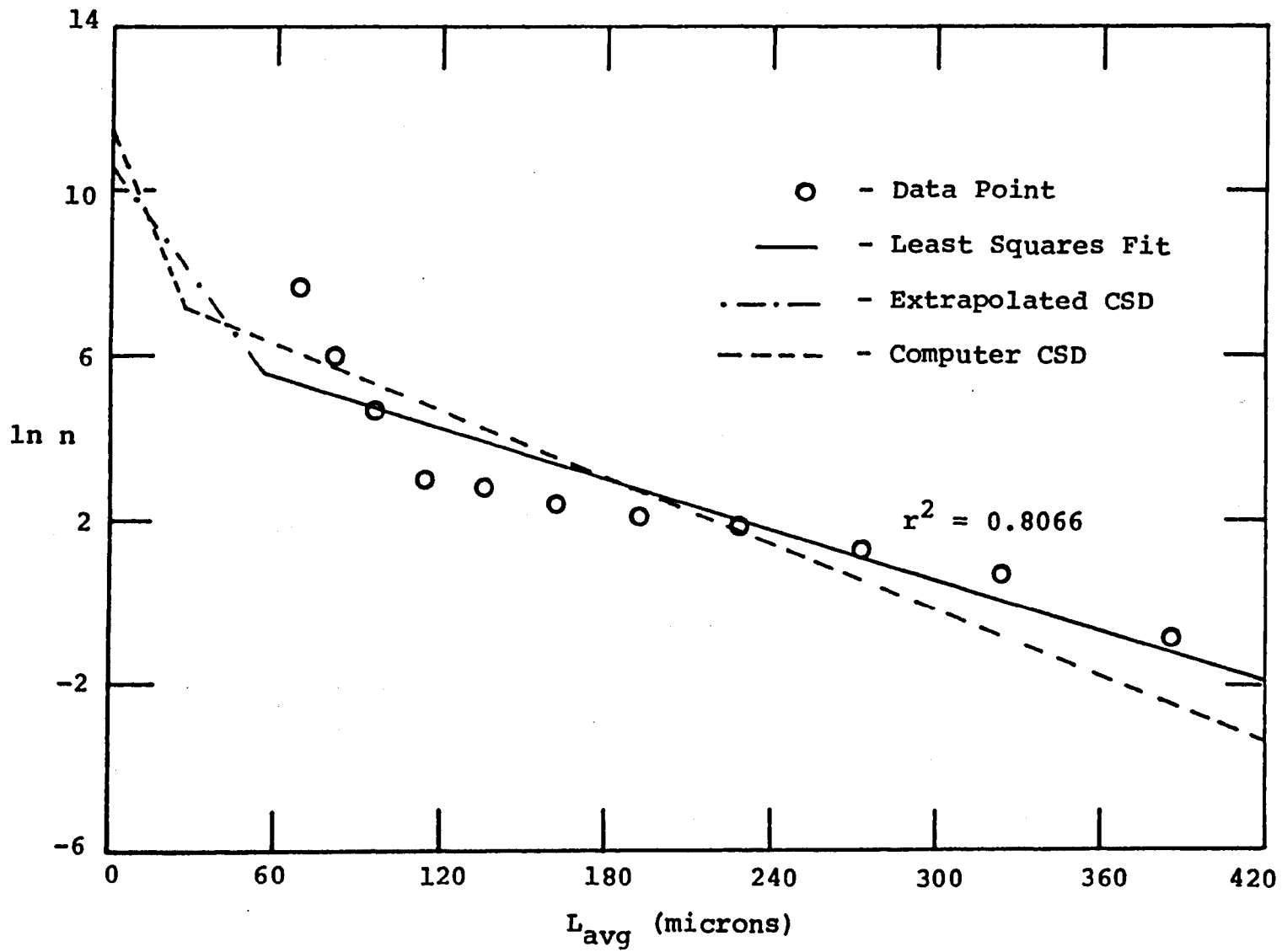


Figure 20. Plot of sieve data from run 34 with extrapolated fines CSD.

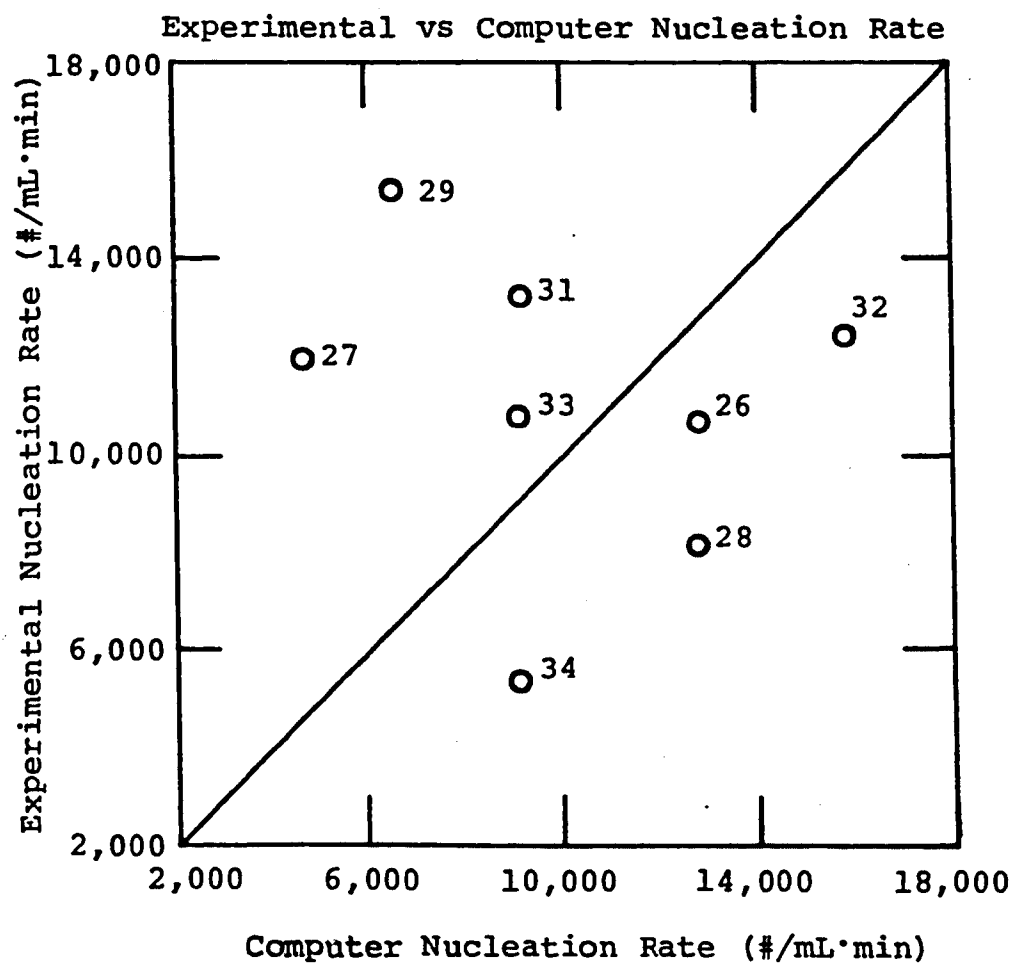


Figure 21. Experimental versus computer nucleation rate.

Experimental vs Calculated Nucleation Rate

$$\text{Equation: } B^{\circ} = \exp(16.72) G^{1.48} M_T^{1.27}$$

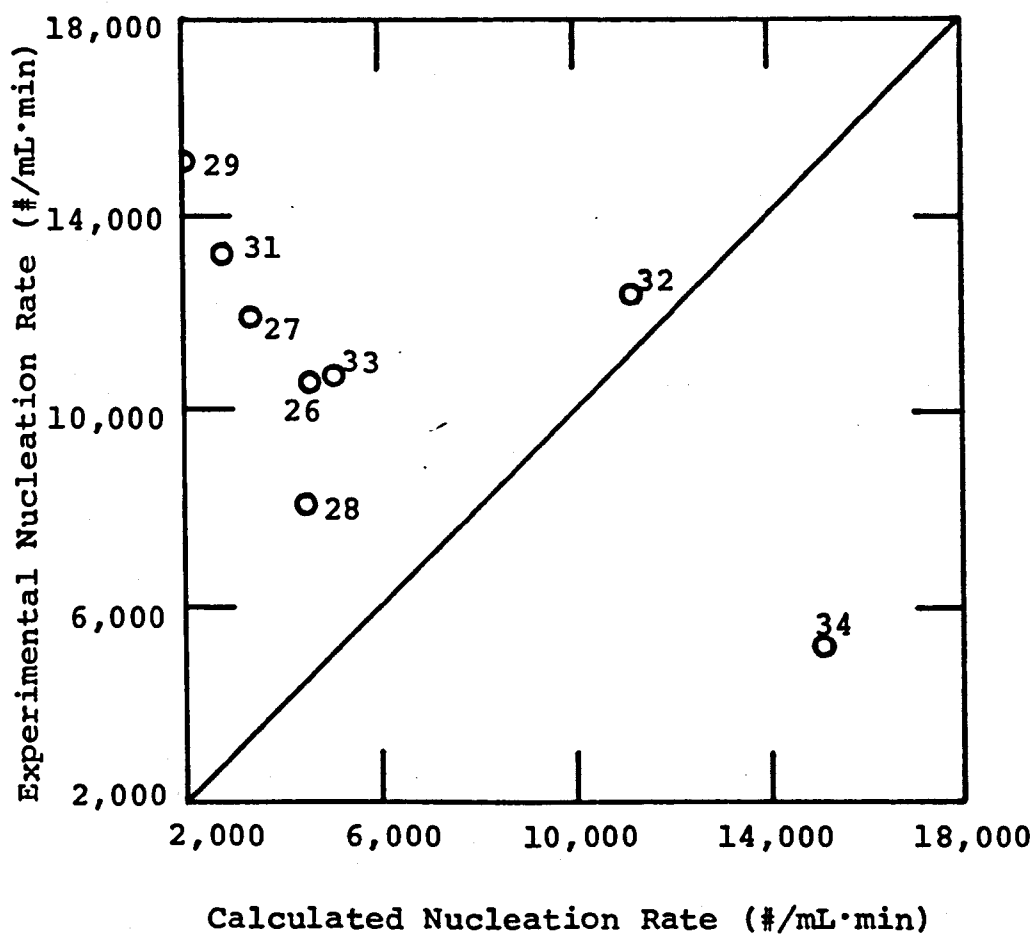


Figure 22. Experimental versus calculated nucleation rate.

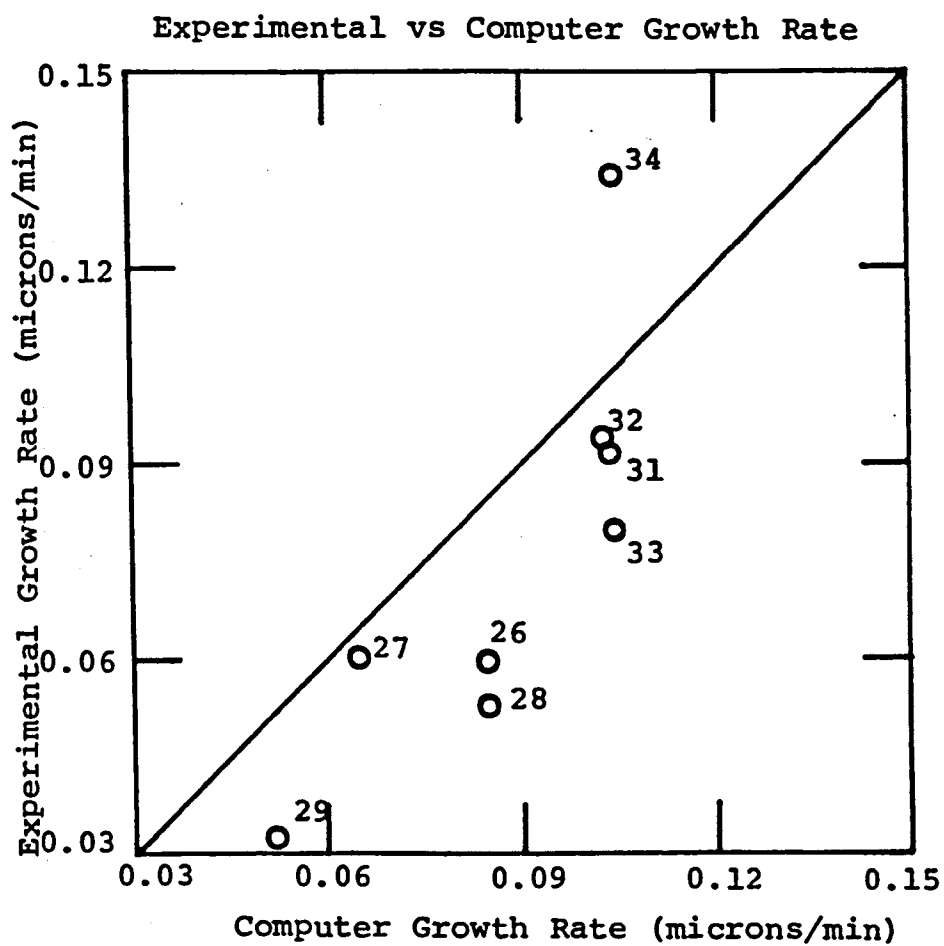


Figure 23. Experimental versus computer growth rate.

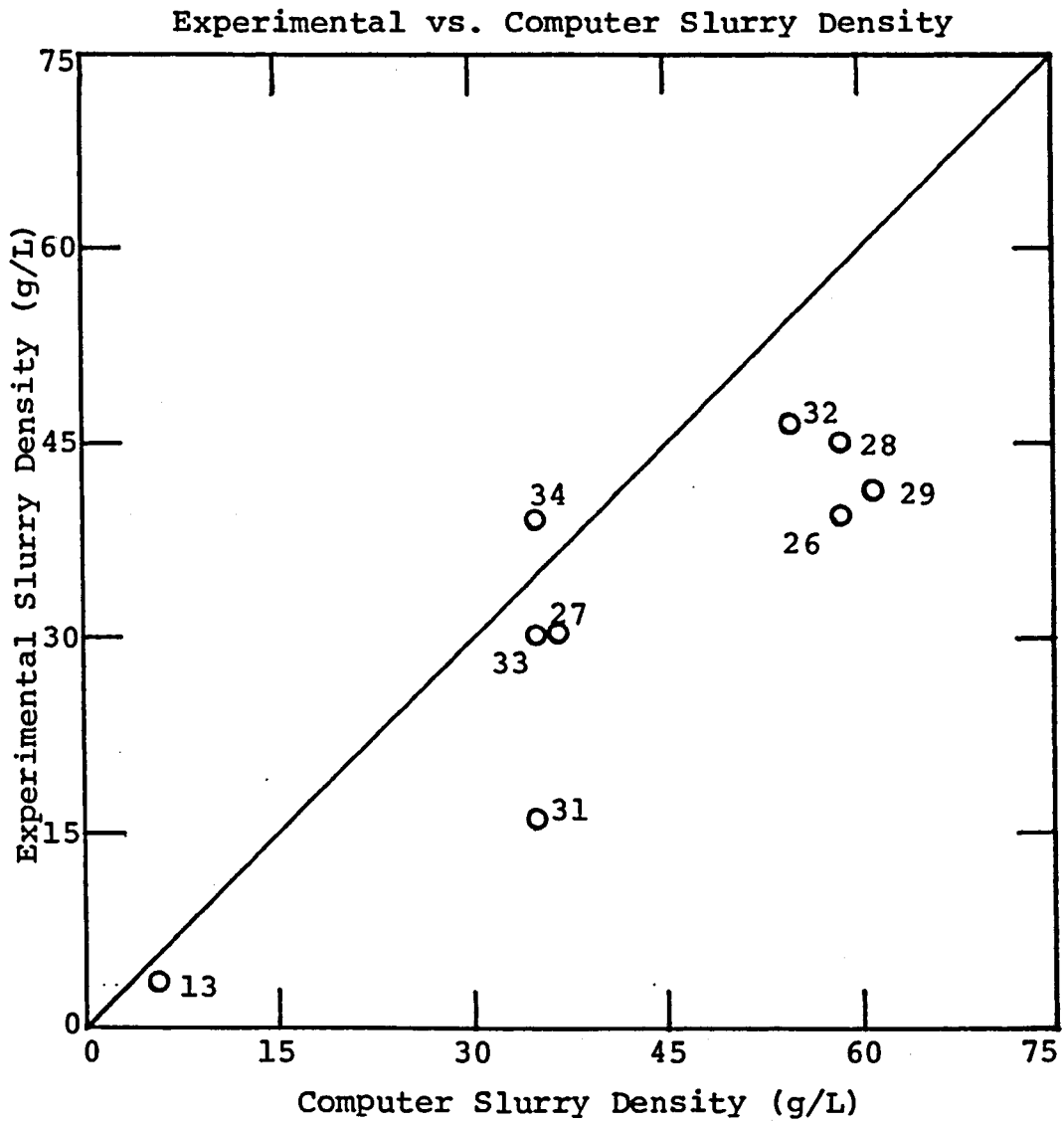


Figure 24. Experimental versus computer slurry density.

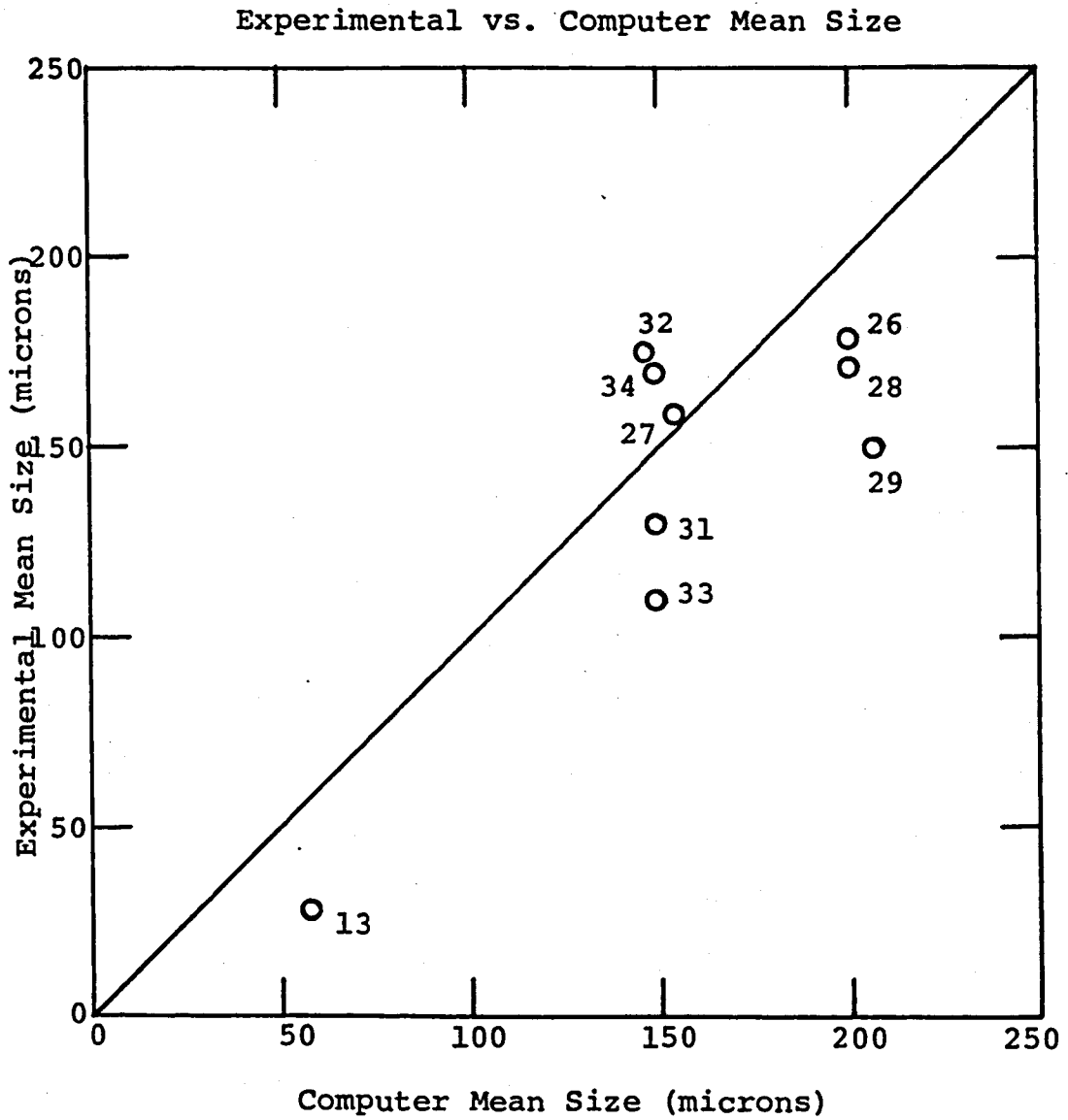


Figure 25. Experimental versus computer mean size.

The results compared are nucleation rate, growth rate, slurry density, and mean size. The calculated nucleation rates were obtained using the experimental growth rates and slurry densities in the kinetic equation. The experimental results are lower than the computer results in Figures 23, 24, and 25 with a few exceptions. Nucleation rate comparisons based on computer predictions versus evaluation of Etherton's kinetics show different results, as illustrated by Figures 21 and 22. In Figure 21 the data scatter shows no pattern. The experimental nucleation rates are higher than the calculated nucleation rates in Figure 22. Conditions in the crystallizer that are not accounted for in the computer program (e.g., fouling, RPM, pH) are the reasons why experimental and computer results disagree. The experimental slurry densities (see Figure 24) are almost always lower than predicted by computer simulation, undoubtedly due to wall fouling which would lower the experimental value. However, the mean particle size was fairly well predicted by computer simulation, as shown in Figure 25.

In conclusion, Etherton's kinetics used in the computer program are a valid representation of secondary nucleation for the gypsum system and more importantly, the CSD follows the theoretical DDO crystallizer predictions. Different crystallizer conditions produced consistent changes approximating the computer results. Therefore, computer

simulation using the Mark V CSD algorithm should be a useful tool for process scale-up. Experimental results shown in Table 4 indicate that the DDO configuration is truly effective in increasing the slurry density and mean crystal size. Increasing the double-drawoff ratio produces large increases in these variables. Deviations between experimental and computer results can largely be explained due to conditions in the bench-scale crystallizer not simulated in the computer program (i.e., wall fouling, or pH and RPM changes).

DISCUSSION OF RESULTS

The following will discuss the experimental and computer results shown in the "Presentation of Experimental Results" section. Reasons why computer and experimental results disagree will be discussed first, followed by explanations of how variable changes affect crystallizer performance. The results of operating parameter changes are compared with the base run results. Finally, the unrelieved supersaturation, crystal habit modifier, and crystal appearance will be discussed.

Disagreement between Computer and Experimental Results

Table 4 shows the difference in experimental and computer-simulated results. The respective crystal size distribution forms, however, show better agreement (see Figures 13 through 20) than specific crystallizer variables, e.g., B^0 , G , and M_T agreement (see Figures 21 through 25).

The main reason experimental and computer results differ is because of conditions that affect the environment of one system but not the other. The following discussion will explore these conditions and how they affect the results.

Scale

Scale build-up is a condition that is present in the bench-scale crystallizer but is not simulated in the computer program. Scale accumulation on the crystallizer walls decreases the amount of supersaturation available for nucleation and growth. This causes a decrease in growth rate, slurry density, and mean size. The decrease in slurry density creates less crystal surface area available for crystal growth. Lower growth rates with essentially the same nucleation rate produces larger nuclei densities and thus results in finer crystals with smaller average size. Computer simulation does not consider scale formation; therefore, computer results are not affected by scale formation. Scale formation tends to lower growth rate (G), slurry density (M_T), and mass mean size (L_{avg}) and increases nucleation rate (B^0) and the nuclei density (n^0). These changes can be seen in the results (Table 4 and Figures 21 through 25).

Kinetics

Etherton (1980) did a gypsum kinetic study using a 1-liter glass vessel called a Mini-nucleator. Etherton's research found that the following equations:

$$B^0 = \exp(16.72) G^{1.48} M_T^{1.27} \quad (21)$$

$$G = \exp(13.11) s^{2.226} \quad (22)$$

correlated with his data. The above equations were used in a computer simulation program (Mark V) developed at the University of Arizona to predict the results of the bench-scale crystallizer. The bench-scale crystallizer used in this study is a 9-liter plastic bucket. Crystallizer kinetics depend on the crystallizer and its environment; therefore the kinetics developed from mini-nucleator experiments may not be representative for the bench-scale crystallizer. Figures 21 and 22 show the disagreement in experimental, computer, and calculated nucleation rates. However, the computer and experimental crystal size distributions (Figures 14 and 18) agree well. This indicates that Etherton's kinetics used in the computer program predict the bench-scale crystallizer results with reasonable accuracy. The disagreement in experimental and computer results is mainly caused by other factors in the crystallizer (i.e., scale).

Dynamics

The computer program considers only steady state solutions to the CSD problem. Experimental runs often have fluctuations in the fixed parameters that affect the results. It was assumed that any fluctuations present were small and did not significantly affect the crystallizer's results. But if a situation develops where a temporary mechanical failure occurs and is repaired without stopping

the run, then the incident would certainly create dynamic changes in the crystallizer that would take many hours to damp out. A few plots of the experimental data produced a hump that represents an unsteady state CSD (see Figures 13 and 15). Long run times were needed to achieve steady state conditions in these cases, but equipment failure usually prevented extremely long runs (longer than 60 hours).

In conclusion, differences in experimental and computer results are caused by conditions that occur in one system and not the other. Scale formation is a principal reason why computer and experimental values disagree. The agreement in experimental and computer CSD's prove that the kinetics used predict the bench-scale crystallizer results with reasonable accuracy. Less fouling in the crystallizer or scale simulation in the computer program probably would make the computer predictions and experimental results agree better.

Parameter Changes

The bench-scale DDO crystallizer was run under different conditions to study how a parameter change will affect the results. Computer runs under similarly varied conditions were also carried out, using Etherton's kinetics. The variables changed and their range of operation are listed in Table 5. The run conditions are shown in Table 6.

The following are the conditions in Run 34: DDO ratio, 5:1; retention time, 60 min; impeller speed, 406 rev/min; pH: 4; and rate of make, 0.125 g/lit min were used as base conditions to compare with the other runs.

The results of the variable changes are listed in another section of this report (Presentation of Experimental Results). This section will discuss how variable changes affect the results. The results of a run and the base run will be shown, followed by a discussion of the experimental results.

This section will examine only parameter changes dealing with the DDO crystallizer; therefore MSMPR results will not be discussed. However, note that the change from the MSMPR configuration to the DDO configuration produced the largest single change in the results (see Table 6). These results plus the CSD plots verify that the DDO configuration does increase the crystal size and does produce a CSD that matches theoretical predictions.

Comparison of Runs

Run 26

The DDO ratio was increased from 5:1 to 9:1 in run 26. The results are shown in Table 13.

Computer results predict that a DDO ratio increase will decrease the growth rate (G) and increase the nucleation

Table 13. Results of runs 26 and 34.

Run No.	$G \times 10^2$ ($\mu\text{M}/\text{min}$)		$B^0 \times 10^{-3}$ ($\#/\text{mL} \cdot \text{min}$)		$n^0 \times 10^{-5}$ ($\#/\text{mL} \cdot \mu\text{M}$)		M_T (g/L)		L_{avg} (μM)	
	Comp	Exp	Comp	Exp	Comp	Exp	Comp	Exp	Comp	Sieve
34	10.5	13.4	9.15	5.23	0.873	0.390	34.9	39.1	149	170
26	8.45	5.96	12.8	10.6	1.51	1.81	58.5	39.5	200	179

rate (B^0), nuclei density (n^0), slurry density (M_T), and mass mean size (L_{avg}). Increasing the DDO ratio removes the fines (crystals of size less than L_F , the classification size) at a faster rate and increases the retention time of the product crystals. This produces an increase in slurry density and mean size because the retained crystals grow to larger sizes. The increase in slurry density decreases the growth rate. This allows the supersaturation to promote nucleation, therefore increasing the nucleation rate and nuclei density. Even though the growth rate is lower and nuclei density higher, the mean size increases because of the longer solids retention time. Therefore, computer simulation predicts that an increase in the DDO ratio will increase the slurry density and mean size. The nuclei density and nucleation rate also increase while the growth rate decreases. The change in G , B^0 , and n^0 are undesirable, but the increase in M_T and L_{avg} outweighs these changes and a larger-sized product is produced with less fouling tendency (less supersaturation).

The experimental results followed the same pattern predicted by computer simulation (i.e., G decreased while the other variables increased). However, the magnitudes of the respective value changes were different. This difference is caused by scale formation in the crystallizer. Scale robs

the crystallizer of supersaturation that promotes nucleation and growth. Therefore, scale in the crystallizer caused the DDO ratio increase to produce larger changes in the experimental results.

Run 27

The overall liquid phase retention time was increased from 60 min to 100 min in run 27. The results are shown in Table 14.

Computer simulation predicts that an increase in the retention time decreases G , B^0 , and n^0 . It also increases M_T and L_{avg} . The conditions of runs 26 and 27 were set up to create identical solids retention times (600 minutes). The computer results show that a DDO ratio increase produces a larger mean size (more fines removed relative to product) and slurry density compared to a retention time increase. The DDO ratio increase removes fines at a faster rate, thus promoting crystal growth of the product crystals. Increasing the retention time will actually decrease the overall (underflow plus overflow) fines removal rate because all the flow rates are reduced to increase the liquid phase retention time. Therefore, a larger crystal size range is retained in the crystallizer and subjected to crystal growth which thus produces a smaller average size relative to a similar DDO ratio increase. The increase in the surface area available

Table 14. Results of runs 27 and 34.

Run No.	$G \times 10^2$ ($\mu\text{M}/\text{min}$)		$B^\circ \times 10^{-3}$ ($\#/\text{mL} \cdot \text{min}$)		$n^\circ \times 10^{-5}$ ($\#/\text{mL} \cdot \mu\text{M}$)		M_T (g/L)		L_{avg} (μM)	
	Comp	Exp	Comp	Exp	Comp	Exp	Comp	Exp	Comp	Sieve
34	10.5	13.4	9.15	5.23	0.873	0.873	34.9	39.1	149	170
27	6.47	6.03	4.75	11.9	0.733	0.733	36.5	30.6	154	159

for crystal growth decreases supersaturation and hence both B^0 and G . The effect on B^0 is compounded both by changes in supersaturation (decreases B^0) and solids concentration (increases B^0). Thus the net increase in mean particle size due to the retention time increase is small compared to the M_T and L_{avg} increases caused by the DDO ratio increase (see Table 8).

The experimental results do not follow computer predictions. Scale formation again is the probable reason for these incongruencies. The longer retention time promotes scale formation. The result is a further reduction in available supersaturation, which in turn lowers the experimental M_T , G , and L_{avg} values. Experimental n^0 and B^0 values are higher because nucleation is enhanced by scale formation. It appears that scale formation is definitely a cause of the discrepancy in computer and experimental results. These two runs (26 and 27) also indicate that a preferable mode of increasing solids retention time is by increasing the DDO ratio rather than cutting back total liquid flow.

Run 28

The conditions and results of runs 28 are similar to run 26; therefore discussion of run 28 will be omitted. The slight difference in the two runs was due to slightly different crystallizer conditions. Also scale formation again

created some incongruencies in the experimental results of runs 26 and 28.

Run 29

Two variables, the DDO ratio and the retention time, were increased in this run. Run 29 conditions will be compared with runs 26 and 27 to see if the DDO ratio increase improves the crystal size more efficiently than a retention time increase. Results of runs 26, 27, and 29 and 34 are shown in Table 15.

Runs 26 and 27 have been discussed earlier. Their results will be used for comparison with the results of run 29. Computer predictions show that the DDO ratio increase coupled with the retention time increase produced the highest mean size, the highest slurry density, and the lowest growth rate of all the runs. Comparisons of run 29 with runs 26 and 27 indicate that the DDO ratio increase affects the crystal size more than the retention time increase. The retention time change raised the mean size about 5 microns. The DDO ratio change increased the mean size about 50 microns. The slurry density increase due to the DDO ratio change is about 15 times greater than the slurry density increase caused by the retention time change. The DDO ratio increase produced large crystals. The retention time increase also increases crystal size, but on a smaller scale. The retention time

Table 15. Results of runs 26, 27, 29, and 34.

Run No.	$G \times 10^2$ ($\mu\text{M}/\text{min}$)		$B^{\circ} \times 10^{-3}$ ($\#/\text{mL} \cdot \text{min}$)		$n^{\circ} \times 10^{-5}$ ($\#/\text{mL} \cdot \mu\text{M}$)		M_T (g/L)		L_{avg} (μM)	
	Comp	Exp	Comp	Exp	Comp	Exp	Comp	Exp	Comp	Sieve
34 ^a	10.5	13.4	9.15	5.23	0.873	0.390	34.9	39.1	149	170
26 ^b	8.45	5.96	12.8	10.6	1.51	1.81	58.5	39.5	200	179
27 ^c	6.47	6.03	4.75	11.9	0.733	2.12	36.5	30.6	154	159
20 ^d	5.20	3.27	6.59	15.4	1.27	4.67	61.0	41.4	206	150

a = base conditions

b = 9:1 DDO ratio, 60 min retention time

c = 5:1 DDO ratio, 100 min retention time

d = 9:1 DDO ratio, 100 min retention time

increase lowers B° and n° . This decrease will compensate for the increase in nucleation rate and nuclei density created by the DDO ratio change. Therefore, according to computer predictions, a DDO ratio increase coupled with a retention time increase will produce large crystals, increase the slurry density, and keep nucleation down.

Experimental results did not produce the same changes as computer results. The discrepancy in experimental and computer values is again attributable to scale formation. These experimental conditions produced the lowest mean size of the four runs shown. The growth rate is extremely low, and n° and B° values are high.

In conclusion, large DDO ratios with the correct retention time will produce a gypsum product with adequate landfill characteristics. The only problem that should be solved is wall scale formation which is detrimental to the gypsum product quality and crystallizer operation. However, in a large-scale commercial operation the amount of wall fouling relative to liquor flows will be vastly lower and the CSD simulation could be used with confidence to design and guide operation of the process.

Runs 31 Through 33

Impeller speed, rate of make, and pH were changed in runs 31, 32, and 33, respectively. The other variables were

set at base conditions. The results of each run will be examined.

Run 31

The impeller speed was raised from 406 RPM to 485 RPM in run 31. Computer results do not predict any changes as RPM was not correlated in the nucleation kinetics, but it is assumed that the increased agitation will increase n^0 and B^0 and decrease M_T , L_{avg} , and G . The results are compared with standard conditions (run 34) in Table 16.

Because computer results are identical, only the experimental results will be examined. The results agree with the assumption that increased agitation will create more nuclei, increasing n^0 and B^0 . Accelerated fines removal will remove a large amount of the nuclei formed, but fewer crystals grow to larger sizes. This reduces M_T , G , and L_{avg} . Scale formation is less because supersaturation is lower and/or the crystal-wall collision frequency is higher, which scours the surface. M_T is lowered because a larger fraction of the finer crystals that are created escape in the overflow.

In conclusion, increasing the impeller speed does create less scale, but the end result is a big reduction in slurry density and particle mean size. Too low an impeller speed, however, will cause settling of the slurry and uneven

Table 16. Results of runs 31 and 34.

Run No.	$G/10^2$ ($\mu\text{M}/\text{min}$)		$B^0 \times 10^{-3}$ ($\#/\text{ML} \cdot \text{min}$)		$n^0 \times 10^{-5}$ ($\#/\text{mL} \cdot \mu\text{M}$)		M_T (g/L)		L_{avg} (μM)	
	Comp	Exp	Comp	Exp	Comp	Exp	Comp	Exp	Comp	Sieve
34	10.5	13.4	9.15	5.23	0.873	0.390	34.9	39.1	149	170
31	10.5	9.15	9.15	13.2	0.873	1.48	34.9	16.3	149	130

mixing in the crystallizer. These conditions will promote fouling and nucleation, thus producing a poor gypsum product. Therefore control of agitation is important and an impeller speed operating range must be determined to insure production of a gypsum product with suitable dewatering and filtering properties.

Run 32

The rate of make was increased from 0.125 g/L min to 0.188 g/L min in run 32. This should increase the supersaturation level in the crystallizer because the reagents are added at a faster rate. The results are shown in Table 17.

Computer results predict slight decreases in G and L_{avg} with increases in B^0 , n^0 , and M_T . The higher level of supersaturation created more nuclei and increased the slurry density, but its effects on G and L_{avg} were minimal. Increasing the rate of make under certain conditions will produce more crystals but essentially retain the same mean size.

Experimental results show an increase in L_{avg} instead of a decrease. The other variables changed according to computer predictions. A possible reason for the improved L_{avg} value is that the combination of more crystal surface area plus the formation of scale in the crystallizer lowered the supersaturation to a level that promoted more growth than

Table 17. Results of runs 32 and 34.

Run No.	$G/10^2$ ($\mu\text{M}/\text{min}$)		$B^{\circ} \times 10^{-3}$ ($\#/\text{mL} \cdot \text{min}$)		$n^{\circ} \times 10^{-5}$ ($\#/\text{mL} \cdot \mu\text{M}$)		M_T (g/L)		L_{avg} (μM)	
	Comp	Exp	Comp	Exp	Comp	Exp	Comp	Exp	Comp	Sieve
34	10.5	13.4	9.15	5.23	0.873	0.390	34.9	39.1	149	170
32	10.3	9.40	15.8	12.4	1.53	1.51	54.7	46.6	146	175

nucleation. Scale in this case is more helpful than harmful to the product quality. But scale is still undesirable because of the maintenance problems it creates.

In conclusion, increasing the rate of make produced opposing effects on computer and experimental L_{avg} values while the other values followed predicted changes. Scale formation is a possible cause for this discrepancy.

Run 33

The pH was raised from 4 to 5 in run 33. This will affect the concentration of citrate ion, believed to be the crystal habit modifier of gypsum. Again computer results will not change and only the experimental results will be examined. The results of runs 33 and 34 are shown in Table 18.

Increasing the pH produced the smallest mean size of all the DDO runs. Nuclei density and nucleation rate increased considerably while slurry density and growth rate decreased. The higher pH shifts the citric acid equilibrium and allows more citrate ion into solution. Citrate ion increases nucleation rate, perhaps by lowering the energy level needed to form nuclei. The more citrate ion present, the more nuclei formed. Therefore, higher pH promotes nucleation. The result is a decrease in G , M_T and L_{avg} . Also, scaling might be increased if the energy barrier for scale formation is also lowered due to the citrate ion.

Table 18. Results of runs 33 and 34.

Run No.	$G/10^2$ ($\mu\text{M}/\text{min}$)		$B^{\circ} \times 10^{-3}$ ($\#/\text{mL} \cdot \text{min}$)		$n^{\circ} \times 10^{-5}$ ($\#/\text{mL} \cdot \mu\text{m}$)		M_T (g/L)		L_{avg} (μM)	
	Comp	Exp	Comp	Exp	Comp	Exp	Comp	Exp	Comp	Sieve
34	10.5	13.4	9.15	5.23	0.873	0.390	34.9	39.1	149	170
33	10.5	8.0	9.15	10.8	0.873	1.35	34.9	30.4	149	110

However, if the citrate ion concentration is too low, the gypsum product will have a needle-like crystal habit which possesses poor filtering and landfill properties. The citrate ion concentration can be lowered by either reducing the amount of citric acid added to the mother liquor or by lowering the solution pH. Too low a pH will create a poor crystal habit whereas too high a pH will lower the slurry density and mean size due to excessive nucleation. Therefore, a pH range must be determined that produces satisfactory results. This range will depend on the amount of citric acid added to the mother liquor. Industrial crystallizers run at a low pH to enhance limestone dissolution and conversion to sulfate. Therefore, other factors must be considered to determine the correct pH operating range.

In conclusion, experimental results show that a pH rise will lower the mean size by increasing nucleation. A satisfactory pH operating range will depend not only on crystallization properties, but other factors occurring in an industrial crystallizer.

Conclusions

The computer-simulated results and experimental results agree in general with the theoretical DDO crystallizer configuration predictions. The double-drawoff configuration definitely increases the crystal size by removing small

crystals (fines) at an accelerated rate relative to under-flow product. All the DDO runs produced a mean size greater than the MSMR results (see Table 4). The runs conducted at different crystallizer conditions give an idea of how such parameter changes affect the gypsum product. Increasing the DDO ratio produces a significant increase in mean size. Increasing the impeller speed and crystallizer pH appears to be detrimental and to decrease the mean size. Control of these variables will be important in an industrial crystallizer to insure production of a material with suitable dewatering, filtering and other end use properties. Some of the variables (pH, impeller speed, etc.) require a range of operation to produce a satisfactory gypsum product. Maintaining these operating ranges would be important in an industrial crystallizer.

Unrelieved Supersaturation

Computer-simulated runs used a supersaturation-growth correlation:

$$G = \exp(13.11) s^{2.226} \quad (23)$$

to calculate the unrelieved supersaturation (s) exiting the crystallizer. Table 19 lists the unrelieved supersaturation for each of the runs along with the computer results. Unrelieved supersaturation values are placed next to the growth rate values for comparison.

Table 19. Results of computer runs.

Run No.	DDO Ratio	τ (min)	RPM	pH	Rate of Make (g/L·min)	$s \times 10^4$ (g/mL)	$G \times 10^2$ ($\mu\text{M}/\text{min}$)	$B^0 \times 10^{-3}$ (#/mL·min)	$n^0 \times 10^{-5}$ (#/mL· μM)	M_T (g/L)	L_{avg} (μM)	L_F (μM)
13 ^a	0	60	425	6	0.125	14.7	24.3	3.29	0.136	5.86	58	0
26	9:1	60	407	4	0.125	8.4	8.45	12.8	1.51	58.5	200	27
27	5:1	100	406	4	0.125	8.1	6.47	4.75	0.733	36.5	154	27
28	9:1	60	407	4	0.125	8.4	8.45	12.8	1.51	58.5	200	27
29 ^b	9:1	100	405	4	0.125	7.3	5.20	6.59	1.27	61.0	206	27
31	5:1	60	485	4	0.125	10.0	10.5	9.15	0.873	34.9	149	27
32	5:1	60	406	4	0.188	10.0	10.3	15.8	1.53	54.7	146	27
33	5:1	60	406	5	0.125	10.0	10.5	9.15	0.873	34.9	149	27
34 ^b	5:1	60	400	4	0.125	10.0	10.5	9.15	0.873	34.9	149	27

a = MSMR run

b = No Microtrac data

Assuming the computer results describe the bench-scale crystallizer results reasonably well (as described in the last section), the steady state unrelieved supersaturation will then be the supersaturation available for scale formation. Decreasing the residual solute concentration should decrease the amount of fouling. Etherton's supersaturation-growth correlation equation in the computer program predicts the amount of unrelieved supersaturation for different crystallizer conditions. These predictions make it possible to design a DDO crystallizer configuration that produces an adequate gypsum product with minimum fouling.

The MSMR crystallizer results shown in Table 19 have the highest growth rate (G) and unrelieved supersaturation (s) values of any of the runs made and indeed the MSMR crystallizer produced more scale than any of the DDO crystallizer runs. For example, the computer results show a large amount of unrelieved supersaturation for run 13 (MSMR run) compared to the DDO runs, and run 13 indeed exhibited a large amount of fouling. It is reasonable then to relate the amount of fouling in the crystallizer to the amount of unrelieved supersaturation predicted by computer simulation.

Table 19 shows that increases in the retention time or the DDO ratio decreased the solute concentration. Retention time affects the unrelieved supersaturation more than

the DDO ratio. Increasing both parameters produces the lowest solute concentration. Fortuitously, high DDO ratios and long retention times also produce large crystals and heavy slurry densities.

Impeller speed and pH changes do not affect the computer results, but an increase in impeller speed will promote nucleation and decrease growth. The growth rate reduction will decrease the solute concentration (supersaturation) and hence lower the tendency to foul. Unfortunately, the decrease in fouling that occurs with high RPM would also lower the mean size and slurry density. In conclusion, increasing the impeller speed would reduce fouling, but also reduce the product size and slurry density.

Increasing the pH at a given citric acid concentration will also promote nucleation, therefore decreasing growth and unrelieved supersaturation (s). However, a considerable amount of fouling occurred during the high pH run. An explanation of this fouling is that the modifier lowers the energy barrier for heterogeneous surface nucleation and is more effective at the higher pH's (more citrate ion form) which produces fouling even with a decrease in the unrelieved supersaturation. Further, the mean size at high pH was the lowest of all the DDO runs. Therefore, increasing pH and impeller speed produces a poor gypsum product (smaller size), and there is more fouling in the former case.

A rate of make increase produced the same s value as base conditions. Small variations in the rate of make do not affect the unrelieved supersaturation because the growth rate constant k_G is relatively large. The growth rates in runs 32 and 33 were: 10.3 $\mu\text{M}/\text{min}$ and 10.5 $\mu\text{M}/\text{min}$, respectively. The supersaturations calculated from these growth rates are essentially identical. Therefore, large fluctuations in the feed concentration should produce little or no change in fouling.

An attempt was made in runs 33 and 34 to measure the amount of scale occurring during a run. The crystallizer was weighed before and after a run to determine the weight of scale formed. Dividing the weight by the run time and the crystallizer feed flow rate gave an average concentration drop in the crystallizer due to scale formation. Values of 5.11×10^{-4} g/mL and 5.84×10^{-4} g/mL were calculated for runs 33 and 34, respectively. The computer predicted an unrelieved supersaturation value of 10×10^{-4} g/mL for both runs. Assuming the computer value is correct, approximately half of the unrelieved supersaturation forms scale. The other half leaves the crystallizer in solute form. These measurements confirm the importance of varying levels of scale formation in the interpretation of these bench-scale runs. However, in large-scale operation, wall fouling should be of less

relative importance in determining the residual supersaturation and the computer simulation should more accurately predict the effects of changes in operating conditions. Fouling in run 33 (high pH run) was higher. The pH increase allowed the modifier to lower the scale formation energy barrier, therefore increasing the amount of fouling in run 33.

Scale formation measurements were not done in the other runs, but the experimental runs with lower computer-predicted supersaturation values were observed to have less fouling. Computer simulation should be extremely useful in designing a double-drawoff crystallizer configuration that will produce an acceptable gypsum product with less crystallizer fouling.

Conclusions

Using the supersaturation-growth correlation in the computer simulation program can predict an unrelieved supersaturation that is related to the amount of fouling occurring in the crystallizer. Therefore computer simulation should be extremely useful in designing a DDO crystallizer that produces an acceptable gypsum product with less crystallizer fouling.

Crystal Habit Modifier

Citric acid was the additive used to modify the crystal habit of gypsum. Etherton used a citric acid concentration of 1000 ppm. A brief batch crystallization study was made to see if lower concentrations would also change the crystal habit to a more equant growth. Figure 26 shows the laboratory apparatus used to test the effects of lower concentrations of the additive on gypsum. Sodium sulfate and calcium chloride were the reagents used to generate supersaturation. A small amount of seed crystals were added to promote secondary nucleation. A sample of crystals was put in a sonic bath for one minute to break up any agglomeration and then optical microscope photographs of the crystals were taken. The results are shown in Figures 27 and 28. Note the increasing amount of clusters. Citric acid concentrations about 20 were effective in modifying the habit of gypsum crystals. The pH of the above experiments was above 6.

Bench-scale MSMPR experiments were done at a pH of 6 using no additive and then with an additive of 50 ppm. Figure 29 shows photographs of the crystals grown with and without citric acid. Note the "potato-like" equant growth of the crystals grown in the presence of citric acid compared to the needle-like growth of gypsum when no additive is present. At this pH most of the citric acid would be present as the citrate ion.

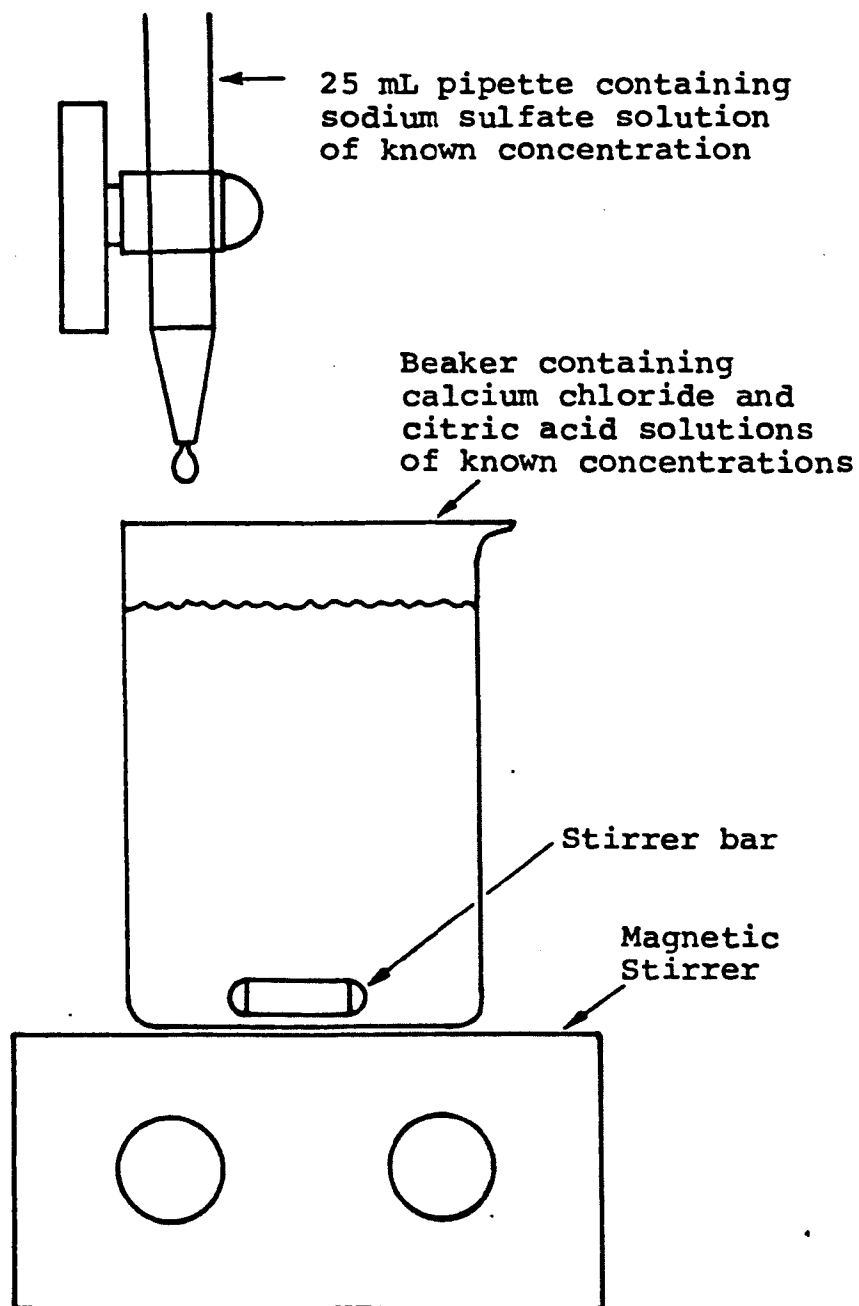


Figure 26. Apparatus used for citric acid experiments.

Citric Acid Concentration

0 ppm

5 ppm

10 ppm

20 ppm

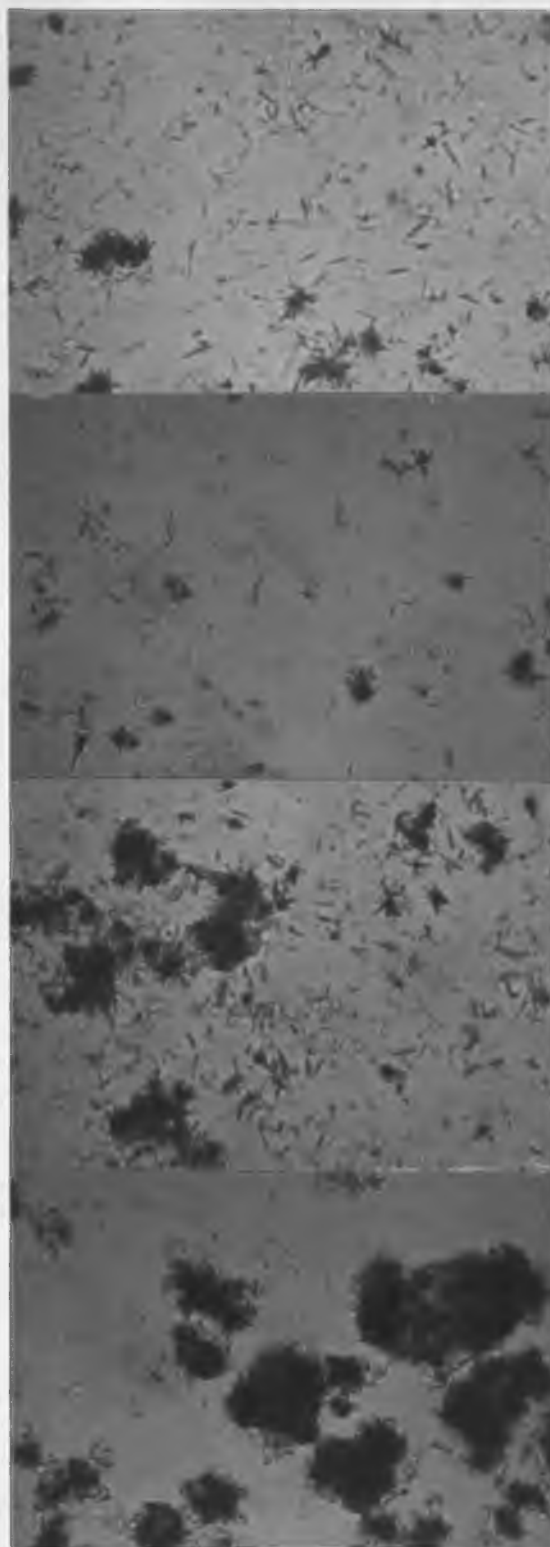


Figure 27. Crystals grown in low citric acid concentrations (0 ppm to 20 ppm).

Citric Acid Concentration

50 ppm

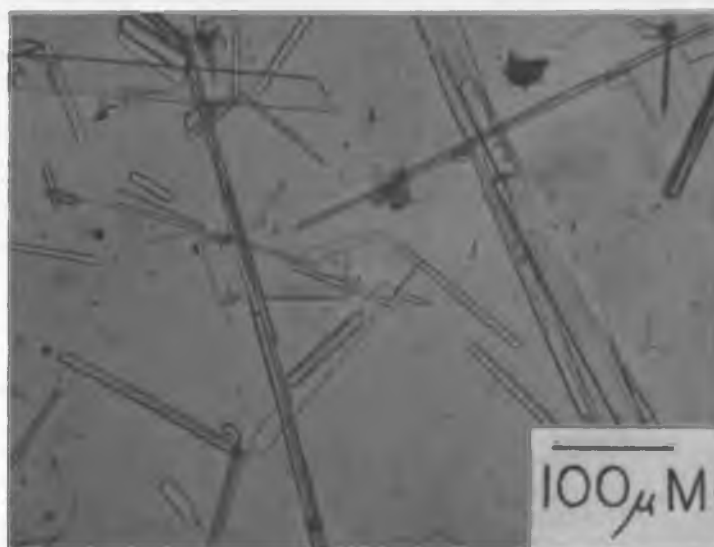
68 ppm

125 ppm

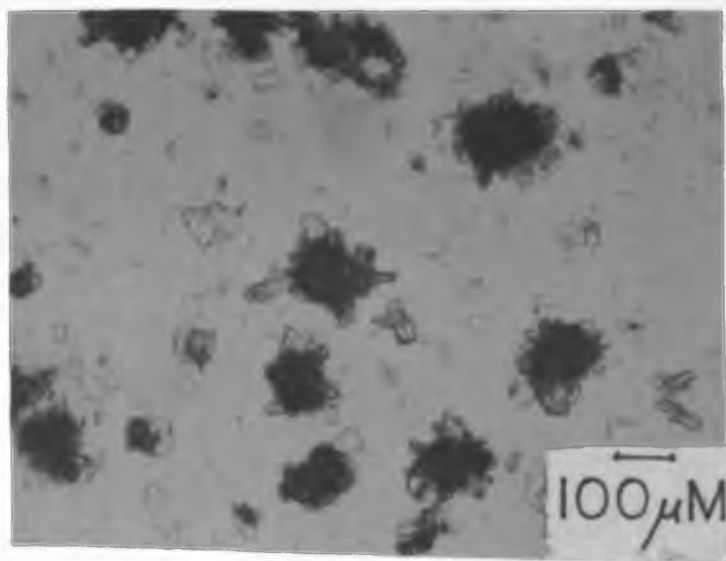
250 ppm



Figure 28. Crystals grown in high citric acid concentrations ((50 ppm to 250 ppm)).



No Additive



50 ppm Additive Concentration

Figure 29. Crystals grown with and without additive.

Bench-scale experiments at a pH of 4 produced needle-like crystals, even with the 50 ppm citric acid concentration. Citrate ion is thus believed to be the actual crystal habit modifier. The concentration of citrate ion in solution depends on the solution pH. Acid-base equilibrium constants were taken from the literature (Dean, 1979) and used to calculate Figure 30, which shows that citrate ion concentration decreases dramatically with decreasing pH. Increasing the citric acid concentration at a lower pH will provide enough citrate ion to promote crystal habit modification. Bench-scale runs were conducted at an additive concentration of 650 ppm and the crystals produced were again potato-like in structure. Therefore, the concentration of modifier needed depends greatly on the crystallizer pH. Low pH values enhance limestone dissolution and conversion to sulfate in industrial crystallizers; therefore the citric acid concentration must be high enough to change the crystal habit, even at these low pH values.

Conclusions

Citric acid is an excellent crystal habit modifier. It produces a gypsum product with improved settling and filtering properties. Citrate ion, believed to be the actual modifier, has a strong acid concentration dependence on pH. Low pH experiments required higher citric acid concentrations

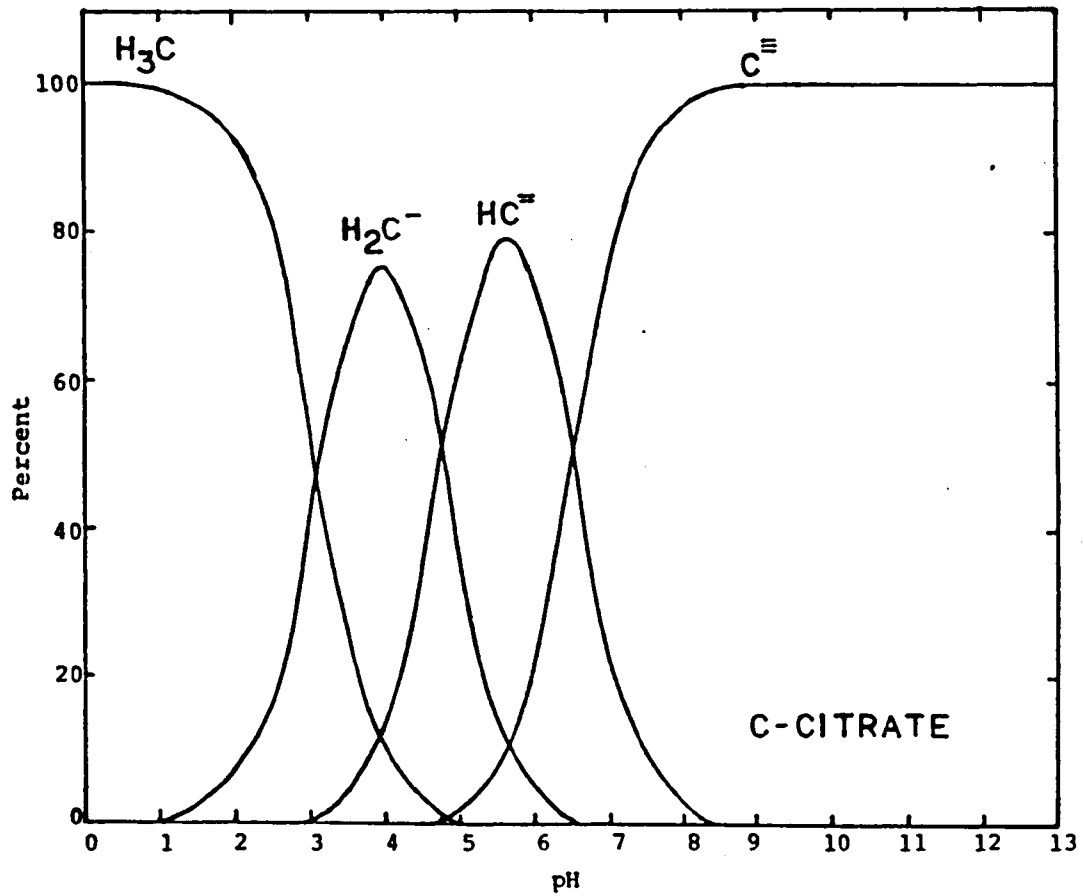


Figure 30. Citric acid breakdown versus pH.

to maintain the desired crystal habit. Further research should be done to determine the actual mechanism of crystal habit change with citrate ion.

Crystal Appearance

Scanning electron microscope (SEM) photographs of the gypsum crystals produced in the bench-scale crystallizer were taken to study the crystal habit. Figures 31 through 33 show SEM and optical microscope photographs of these gypsum crystals.

Figure 31 shows SEM photographs of two different but typical gypsum crystals. Both crystals have rough crystal surfaces, but Crystal A (top photo) has a large, smooth crystal surface (left side) with random crystal faces on the right side. Crystal B (bottom photo) has random crystal faces over its entire surface.

Dual magnification SEM photographs (Figure 32) were taken to get a close-up of the crystal surface. Close inspection of a crystal surface reveals needle-like crystal growth either joined together by aggregation or growing in all directions from a single site. Smooth and rough surfaces are present, with the rough surfaces dominating. The needle-like growth creates numerous recesses in the crystal surface.

Optical microscope photographs (Figure 33) were taken to view the crystals under visible light. Photo A (top

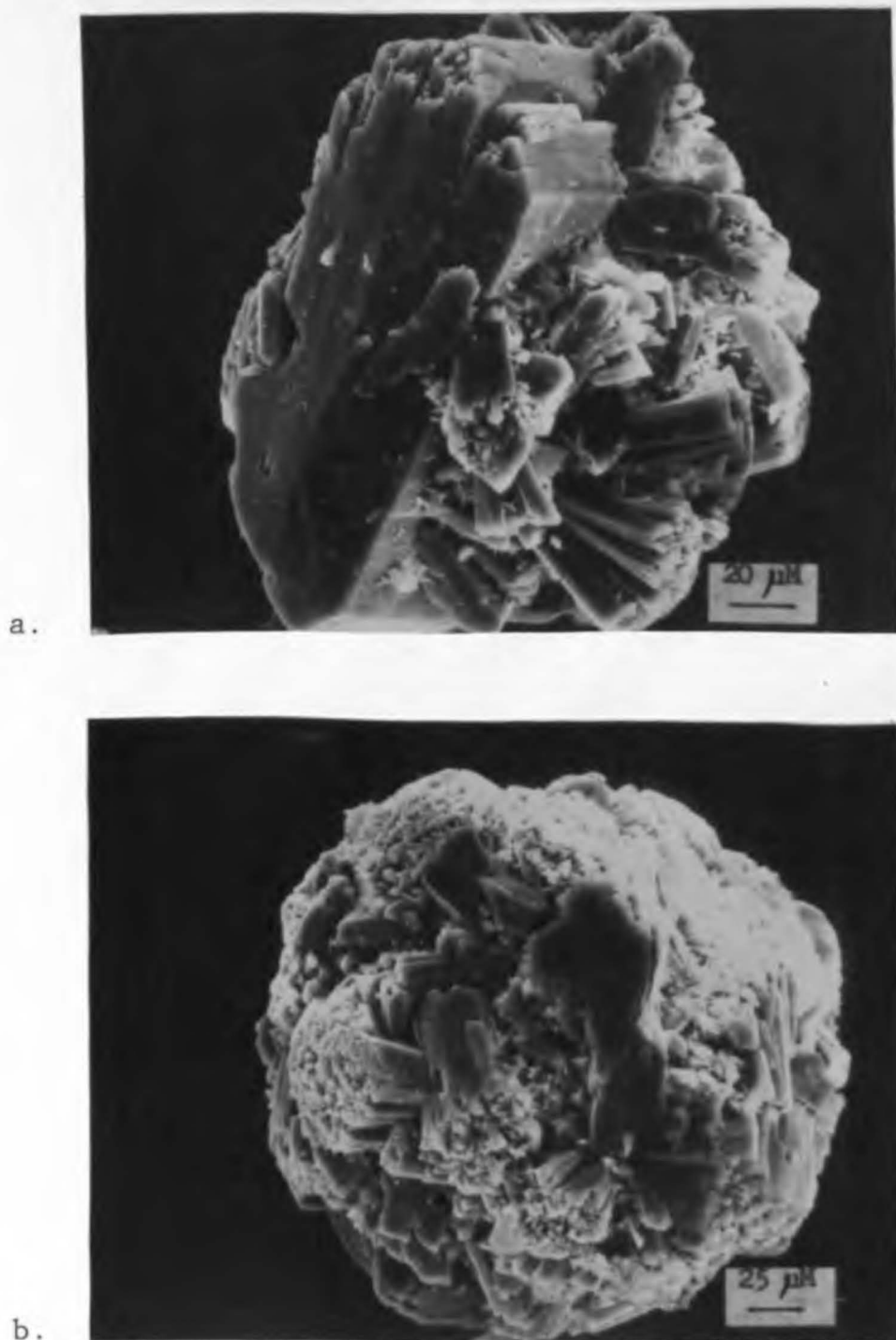


Figure 31. SEM photographs of gypsum crystals. --
(a) Crystal A; (b) Crystal B.

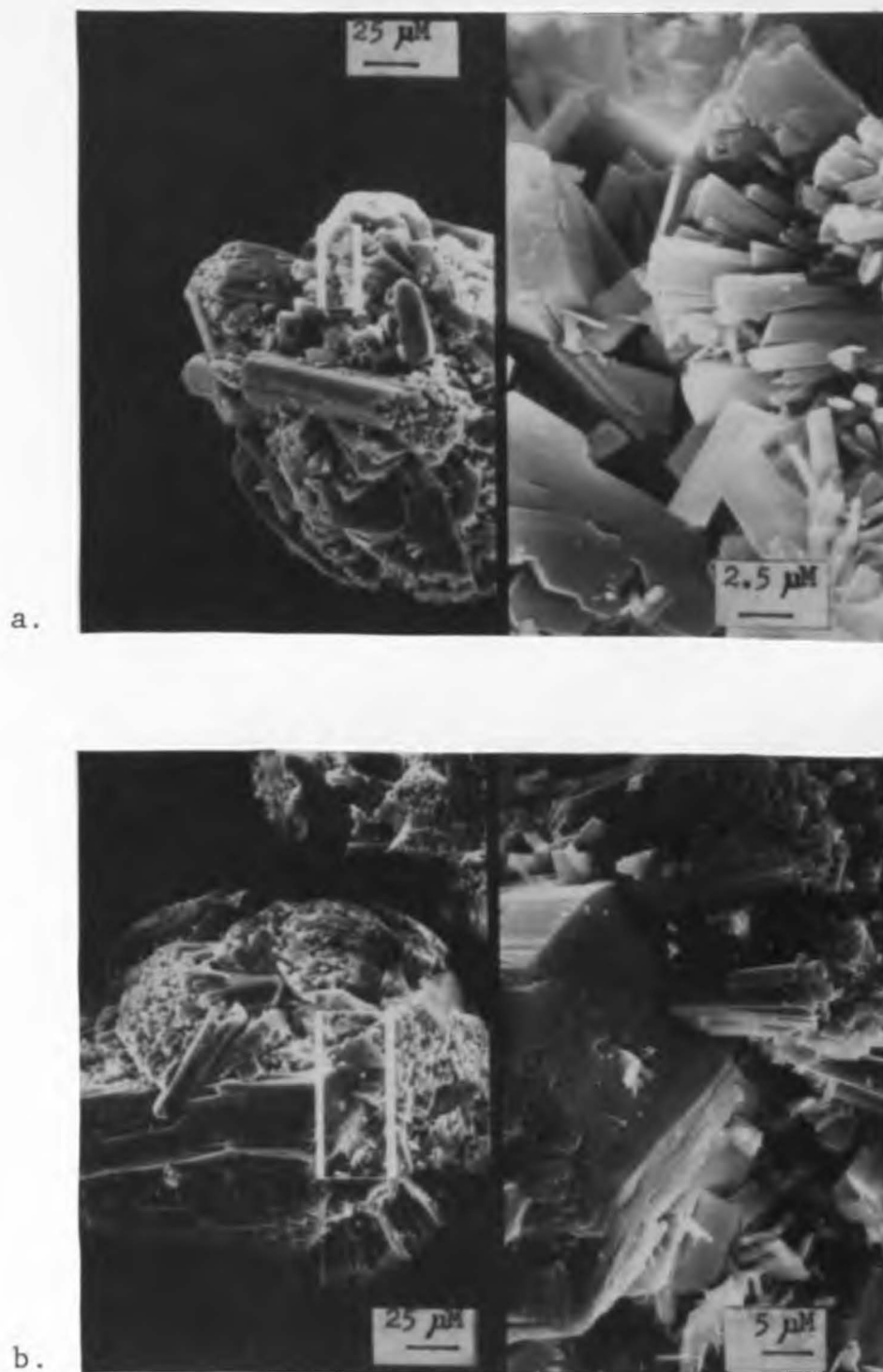


Figure 32. Dual magnification SEM photographs of gypsum crystals. -- ((a) SEM with 10x dual magnification; (b) SEM with 5x dual magnification.

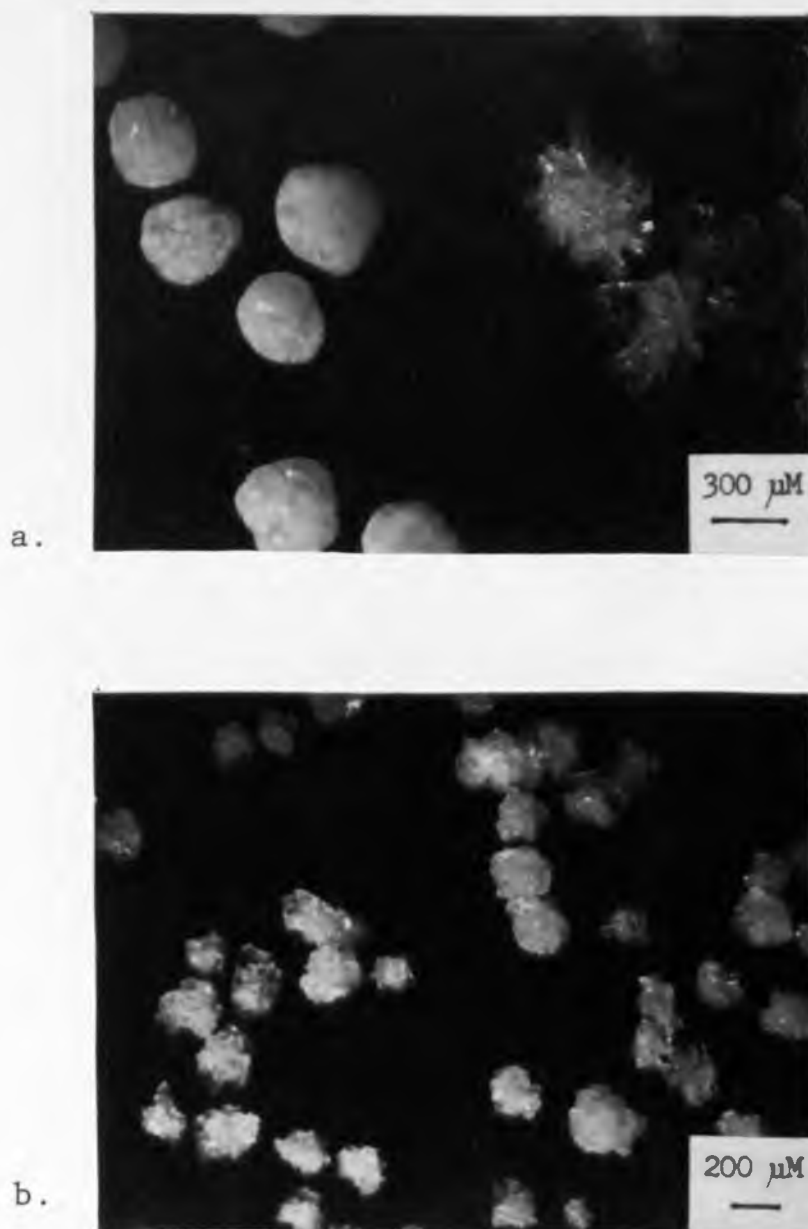


Figure 33. Optical microscope photographs of gypsum crystals. -- (a) Crystallizer sample (left) and mini-nucleator crystals (right); (b) Crystallizer product crystals.

photo) compares gypsum crystals produced in the bench-scale crystallizer (left) with Etherton's crystals grown in the mini-nucleator experiments (right). Both crystal samples were sieved to achieve similar crystal sizes for comparison. Note the more spherical-shaped crystals on the left (bench-scale crystallizer sample) compared to the blockier mini-nucleator crystals. The mini-nucleator crystals were used in many separate runs and thus represent an average of several different chemical environments. Crystal collisions in the bench-scale crystallizer produced the rounded crystal shapes. Mini-nucleator experiments were done with low supersaturation levels and low slurry densities compared to bench-scale crystallizer runs. Therefore, the crystal collisions were less frequent and the driving forces for nucleation and growth were smaller in the mini-nucleator, thus producing the blockier crystals. Furthermore, citric acid was not routinely used in the mini-nucleator experiments. Additional bench-scale crystallizer gypsum crystals are shown in Photo B (bottom photo) in Figure 33. Note the crystal faces in Photo B that are similar to the crystal faces on the mini-nucleator crystals, showing that similar crystal habits can be produced. The difference in the two crystallizer environments produced the difference in the overall crystal shapes (as seen in Photo A, Figure 33), especially the citric acid used in the bench-scale runs.

Two possible mechanisms for the new crystal habit are discussed as follows. One possible mechanism is aggregation with needle-like crystals still being produced in the crystallizer. The additive would then act as a glue to attract and bind the crystals together. Crystal growth and aggregation continue on all sides of the crystal, increasing its size. This could explain why the crystal surface is rough with random crystal faces.

Another mechanism is a sequence of events that produces big, bulky crystals. The additive creates a low-energy site on the crystal surface. Needle-like crystals grow in all directions from the site. The multidirectional growth creates recesses where supersaturated liquor is trapped. Crystallization and growth occur in these recesses to fill the area. The above sequence of events occurs at other sites, causing the crystal to grow in all directions.

Both mechanisms produce a rough crystal surface with random crystal faces and having a needle-like crystal habit. The additive either promotes aggregation or it provides a low-energy site for multidirectional spiny crystal growth. The SEM photographs do not distinguish between these two mechanisms.

Laboratory experiments done using various citric acid concentrations (see Figures 27 and 38) show clusters of what

appear to be needle-shaped crystals. These pictures suggest that aggregation is promoted in the presence of the additive. However, if aggregation is the crystal habit mechanism, then the bench-scale crystallizer would have a mixture of needle-shaped crystals and aggregated crystals in the product.

Photo B in Figure 33 shows no needle-like crystals. Therefore the crystal habit mechanism of multidirectional spiny crystal growth from a low-energy site is the more realistic mechanism of the two mechanisms proposed. Chemical analysis of the gypsum crystals by Radian Corp., Austin, Texas, detected no citrate ion in the crystals down to 500 ppm.

Therefore, citrate ion is not consumed in the crystal habit change and doesn't strongly chemabsorb.

Conclusions

SEM photographs of bench-scale crystallizer samples produced with citric acid show gypsum crystals with rough surfaces and a random arrangement of needle-like crystal faces. Multidirectional needle-like crystal growth from a site is believed to be the mechanism that produces the modified crystal habit. Citrate ion acts as an agent that creates a low-energy site to promote multidirectional growth of the gypsum crystals. Growth occurs on all sides of the crystal, thus increasing its size. The spherical shape of the crystals is due to collisions in the crystallizer that

shape the crystals. Citrate ion additive is very effective in producing these habit changes which result in better dewatering properties.

SUMMARY

Experiments were performed on a 9-liter bench-scale crystallizer employing the double-drawoff (DDO) crystallizer configuration that increases the solids retention time without changing the liquid retention time. Experimental and computer simulation (Mark V CSD simulator) results using various DDO crystallizer conditions were compared to study the effects of parameter changes on the growth rate, nucleation rate, slurry density, and particle mean size and also test the validity of Etherton's kinetics used in the computer program. Results show that the DDO configuration increases the mass mean size and slurry density and decreases fouling when compared to the MSMPR configuration with its equal solid/liquid retention times. Also the computer and experimental results agree reasonably well, proving that Etherton's kinetics are a valid model of gypsum secondary nucleation. The Mark V also calculated an unrelieved supersaturation using a supersaturation-growth correlation from Etherton's research that is a means of determining the amount of fouling a particular DDO crystallizer configuration design will have.

Batch and bench-scale experiments using citric acid were done to study the additive's effect on gypsum at various additive concentrations and pH levels. The modifier produced a gypsum product with satisfactory dewatering and filtering properties. Also citrate ion concentration was found to have a strong dependence on pH.

CONCLUSIONS

1. The crystal size distributions determined experimentally from the DDO crystallizer agree with the hypothetical crystal size distributions associated with particle size classification theory. The experimental crystal size distributions differ somewhat because of the various parameter changes performed, but the general shape of the crystal size distribution matches the theoretical predictions.
2. The double-drawoff crystallizer configuration markedly increases the mass mean size and slurry density. The MSMPR crystallizer slurry density and mean size were significantly smaller than the corresponding double-drawoff crystallizer product, thus confirming Etherton's predictions.
3. Calculated and experimental CSD's agree well when the variable amount of wall fouling was taken into account. The DDO computer model with Etherton's kinetics can be reliably used to simulate a gypsum crystallizer.
4. Variable changes simulated by the Mark V computer program did not produce results similar to those

observed experimentally. Deviation between simulation and experimental results were probably due to varying degrees of fouling on the crystallizer walls which changed the supersaturation level. As fouling on an industrial scale would have less effect on the operating supersaturation level, the use of CSD simulation for design of a large-scale unit is fully warranted.

5. The operating range for crystallizer conditions, e.g., pH and agitation, must be determined on a larger scale to specify the optimum conditions to make an acceptable gypsum product. However, the range of these variables was certainly bracketed in the present study.
6. The supersaturation-growth correlation used in the computer simulation model calculated unrelieved supersaturation values for the various crystallizer conditions. These values can be a means of estimating the tendency to foul in the crystallizer. Thus, computer simulation can be used to design a crystallizer that will produce a satisfactory gypsum product and also have minimum fouling.
7. Citric acid concentration and crystallizer pH both appear to affect the crystal habit. However, citrate

ion is believed to be the actual crystal habit modifier. A pH change will change the amount of citrate ion in solution and therefore the amount of additive needed will depend on the system pH. Photographs of gypsum crystals show that citric acid produces an equant crystal habit with improved dewatering properties.

8. SEM photographs of gypsum crystals from bench-scale crystallizer runs show a rough crystal surface with random arrangement of crystal faces produced by the additive promoting multidirectional needle-like growth from a low-energy site. Chemical analysis by Radian Corp., Austin, Texas, detected no citrate ion in the crystals down to 500 ppm; therefore, citrate ion is not consumed in the crystal habit change and doesn't strongly chemabsorb. The resulting crystal habit shows that citrate ion additive is very effective in producing a gypsum crystal with better dewatering properties.

NOMENCLATURE

NOMENCLATURE

- B^0 = nucleation rate, $\#/mL \cdot min$
 C = steady state crystallizer solute concentration, g/mL
 C = rate constant in Arrhenius rate expression,
 $\#/mL \cdot min$
 C_F = crystallizer feed concentration, g/mL
 C_S = gypsum concentration in saturated solution, g/mL
 G = linear growth rate, $\mu M/min$
 G' = estimated linear growth rate, $\mu M/min$
 k = Boltzmann's constant, $kcal/nuclei \cdot ^\circ K$
 k_a = surface area shape factor
 k_G = rate constant in supersaturation-growth correlation,
 $(\mu M/min) (mL/g)^{2.226}$
 k_N = rate constant in secondary nucleation model,
 $(\#/mL \cdot min) (min/\mu M)^{1/48} (mL/g)^{1.27}$
 k_v = volume shape factor
 L = linear particle size, μM
 L_i = i^{th} linear particle size in Mark V computer program
CSD, μM
 $L_{avg,i}$ = average particle size on Sonic Sifter tray i , μM
 L_F = classification size in double-drawoff crystallizer,
 μM
 M_S = mass of sample used in Allen-Bradley Sonic Sifter, g
 M_T = crystallizer slurry density, g/mL

$m_k = k^{\text{th}}$ population moment ($\# \cdot \mu\text{M}^k$)/mL

$m'_k = k^{\text{th}}$ population moment calculated using guessed nuclei density ($\# \cdot \mu\text{M}^k$)/mL

$m_2 =$ second population moment ($\# \cdot \mu\text{M}^2$)/mL

$m_3 =$ third population moment ($\# \cdot \mu\text{M}^3$)/mL

$n =$ population density, $\#/\text{mL } \mu\text{M}$

$n_i(L_{\text{avg},i}) =$ population density on sieve tray i , $\#/\text{mL } \mu\text{M}$

$n_i(L_i) =$ population density from CSD in Mark V computer program, $\#/\text{mL } \mu\text{M}$

$n^0 =$ nuclei density, $\#/\text{mL } \mu\text{M}$

$n_C^0 =$ calculated nuclei density from solute balance,
 $\#/\text{mL } \mu\text{M}$

$n_G^0 =$ guessed nuclei density in Mark V computer program,
 $\#/\text{mL } \mu\text{M}$

$Q_F =$ crystallizer feed flow rate, mL/min

$Q_O =$ crystallizer fines flow rate, mL/min

$Q_u =$ crystallizer product flow rate, mL/min

$R =$ ratio of solids retention time to liquid retention
time

$S =$ thermodynamic supersaturation

$s =$ stoichiometric supersaturation, g/mL

$T =$ absolute temperature, $^{\circ}\text{K}$

$V =$ crystallizer volume, mL

$\Delta L_i(\text{Mark V}) = i^{\text{th}}$ size interval for Mark V numerical integration, μm

ΔL_i (sieves) = aperture size difference between sieve tray i
and sieve tray above tray i , μM

ΔW_i = crystal mass on sieve tray i , g

ΔG^* = free energy of formation of a nucleus, kcal/nuclei

ρ = crystal density, g/mL

τ = solids retention time, min

τ_L = liquid phase retention time, min

APPENDIX A

MARK V COMPUTER SIMULATION EQUATIONS

MARK V COMPUTER SIMULATION EQUATIONS

Analytical and numerical solutions to three equations: the solute balance, gypsum kinetics, and supersaturation-growth correlation will be discussed. Development of these equations is discussed by Randolph and Larson (1971).

The three equations solved simultaneously in the Mark V computer program are as follows:

$$Q_F(s_F - s) = (1/2)GV\rho k_a m_2 \quad (\text{A.1})$$

$$B^0 = k_N G^i M_T^j \quad (\text{A.2})$$

$$G = k_G s^a \quad (\text{A.3})$$

Equations A.1, A.2, and A.3 are the solute balance, gypsum kinetics, and supersaturation-growth correlation equations, respectively. The above equations are analytically reduced to the equations shown below:

$$G = \left[\frac{(Q_F[s_F - s])^{1-j} V_H(G)}{\rho k_N k_a V \tau^3 H(G)} \left(\frac{V_H(G)}{\tau D_T(G)} \right)^j \right]^{\frac{1}{i+3}} \quad (\text{A.4})$$

$$s = \left[\frac{G}{k_G} \right]^{1/a} \quad (\text{A.5})$$

where

$$B^0 = n^0 / G \quad (\text{A.5})$$

$$D_T(G) = 2R^{-4} [1 - \exp(-P_F) (1 + P_F + \frac{1}{2}P_F^2 + \frac{1}{6}P_F^3)] + \exp(-P_F) (1 + x_F + \frac{1}{2}x_F^2 + \frac{1}{6}x_F^3) \quad (\text{A.7})$$

$$H(G) = R^{-3} [1 - \exp(-P_F) (1 + P_F + \frac{1}{2}P_F^2)] + \exp(-P_F) (1 + x_F + \frac{1}{2}x_F^2) \quad (\text{A.8})$$

$$P_F = \frac{RL_F}{G\tau} \quad (\text{A.9})$$

$$x_F = \frac{L_F}{G\tau} \quad (\text{A.10})$$

$$R = \frac{Q_o}{Q_u} + 1 \quad (\text{A.11})$$

with other terms defined in the Nomenclature section.

Using an estimated growth rate, trial-and-error methods are used to find a growth rate that satisfies Equations A.4 and A.5. Then the other crystallization terms (e.g., nucleation rate, slurry density, mass mean size, etc.) are calculated.

Numerical integration performed in the Mark V computer program uses a guessed nuclei density (about 40 #/mL μM) to calculate a CSD that is needed to generate the population moments (m_2 and m_3). Because the CSD is exponential, the population moments are directly proportional to the nuclei density. Therefore the following relationship holds:

$$m'_k / m_k = n_G^o / n_C^o \quad (\text{A.12})$$

where

$$m'_k = k^{\text{th}} \text{ population moment calculated using guessed } n^o$$

$$m_k = \text{the actual } k^{\text{th}} \text{ population moment}$$

n_G^o = guessed nuclei density

n_C^o = calculated (actual) nuclei density

Substituting Equation A.12 into Equations A.1 and A.2, rearranging, and using numerical integration (trapezoidal rule) results in the following equations:

$$n_C^o = \frac{2n_G^o Q_F (s_F - s)}{G \rho V k_a m_2} \quad (\text{A.13})$$

$$G = \left[\frac{n_C^o}{k_N M_T^J} \right]^{i-1} \quad (\text{A.14})$$

Equations A.13 and A.14 are the solute balance and gypsum kinetics, respectively. The numerical integration routine uses the following equations:

$$m_k' = \sum_{i=2}^N \bar{n}_i (\bar{L}_i)^k \Delta L_i \quad (\text{A.15})$$

$$M_T = \rho k_v m_3 \left(\frac{n_C^o}{n_G^o} \right) \quad (\text{A.16})$$

$$\bar{n}_i = \frac{n_i + n_{i-1}}{2} \quad (\text{A.17})$$

$$\bar{L}_i = \frac{L_i + L_{i-1}}{2} \quad (\text{A.18})$$

$$\Delta L_i = L_i - L_{i-1} \quad (\text{A.19})$$

with the following trial-and-error procedure:

1. Estimate a growth rate (G').
2. Calculate s using Equation A.5.
3. Using the guessed nuclei density (n_G^0), calculate m_2' and m_3' .
4. Calculate the true nuclei density using Equation A.13.
5. Using Equation A.16, calculate the true slurry density.
6. Use Equation A.14 to calculate a growth rate (G).
7. If $G' = G$, then the equations are solved. If $G' \neq G$, estimate a new G' and return to step 2.

The CSD used in the numerical integration (n_i and L_i values) were calculated using the method of characteristics to solve the steady state population balance.

Numerical integration produces round-off errors, but the errors are negligible. Therefore, the Mark V CSD simulator solves simultaneous population and mass balances to simulate the interaction of process configuration and kinetics on the resultant CSD. Also the Mark V calculates unrelieved supersaturation in the crystallizer that could be used to estimate crystallizer fouling.

The constants fed into the Mark V computer program are listed in Tables A.1 and A.2. Substituting the constants into Equations A.4 and A.5 produced the analytical

Table A.1. Permanent constants used in Mark V.

Symbol	Values	Units
a	2.226	()
i	1.48	()
j	1.27	()
k_a	3.0	()
k_G	$\exp(13.11)$	$(\mu\text{M}/\text{min})(\text{mL}/\text{g})^{2.226}$
k_N	$\exp(16.72)$	$(\#/ \text{mL} \cdot \text{min}) \cdot (\text{min}/\mu\text{M})^{1.48} \cdot (\text{mL}/\text{g})^{1.27}$
L_F	27.0	(μM)
V	9000.0	(mL)
ρ	2.32	(g/mL)

Table A.2. Parameter changes for each run.

Run No.	Q_F (mL/min)	S_F (g/mL)	τ (min)	R
26, 28	150	0.0075	600	10
27	90	0.0075	600	6
29	90	0.0075	1000	10
31, 33, 34	150	0.0075	360	6
32	150	0.01125	360	6

equations solved using the Mark V. Equation A.4 shown below:

$$s = \left[\frac{G}{\exp(13.11)} \right]^{1/2.226}$$

was the same for all the runs. Equation A.5 substitutions are listed below.

Runs 26 and 28:

$$G = 0.0288 \left[\frac{150(0.0075-s)}{H(G)} \right]^{-0.0603} D_T(G)^{-0.283}$$

$$P_F = 0.450/G, \quad x_F = 0.0450/G$$

Run 27:

$$G = 0.0288 \left[\frac{90(0.0075-s)}{H(G)} \right]^{-0.0603} D_T(G)^{-0.283}$$

$$P_F = 0.270/G, \quad x_F = 0.045/G$$

Run 29:

$$G = 0.0177 \left[\frac{90(0.0075-s)}{H(G)} \right]^{-0.0603} D_T(G)^{-0.283}$$

$$P_F = 0.270/G, \quad x_F = 0.0270/G$$

Runs 31, 33, and 34:

$$G = 0.0469 \left[\frac{150(0.0075-s)}{H(G)} \right]^{-0.0603} D_T(G)^{-0.283}$$

$$P_F = 0.450/G, \quad x_F = 0.075/G$$

$$G = 0.0469 \left[\frac{150(0.01125-s)}{H(G)} \right]^{-0.0603} D_T(G)^{-0.283}$$

$$p_F = 0.450/G, \quad x_F = 0.075/G$$

Trial-and-error methods were used to find a growth rate that satisfied the equations. p_F and x_F values were used in Equations A.7 and A.8 to calculate $H(G)$ and $D_T(G)$. s was calculated using Equation A.4. The Mark V computer program did not use the analytically reduced equations; but the Mark V's numerical methods did solve Equations A.1 through A.3 with accurate results.

APPENDIX B

DATA ANALYZING METHODS

DATA ANALYZING METHODS

Estimation of Fines Crystal
Size Distribution

Microtrac data was not available in runs 29 and 34; therefore the fines CSD was extrapolated from Allen-Bracley Sonic Sifter results. The following equations were used to calculate the nuclei density (n^0).

$$n^0 = n_p^0 \exp[(R-1)x_F] \quad (\text{B.1})$$

$$M_T = 6\rho k_v n^0 (G\tau)^4 D(G) \quad (\text{B.2})$$

where

$$D(G) = R^{-4} [1 - \exp(-P_F) (1 + P_F + \frac{1}{2}P_F^2 + \frac{1}{6}P_F^3)] + \exp[-P_F] [1 + x_F + \frac{1}{2}x_F^2 + \frac{1}{6}x_F^3] \quad (\text{B.3})$$

$$P_F = \frac{RL_F}{G\tau} \quad (\text{B.4})$$

$$x_F = \frac{L_F}{G\tau} \quad (\text{B.5})$$

with other terms defined in the Nomenclature section.

There are two unknowns (n^0 and L_F). Equations B.1 and B.2 are solved simultaneously by trial-and-error and a fines cut-off size (L_F) and a nuclei density (n^0) calculated. CSD plots of runs 29 and 34 (Figures 17 and 21) agree with DDO crystallizer theory.

Microtrac Data

Some Microtrac size-monitoring channels produced erroneous data. To minimize errors, several Microtrac readings were taken 24 hours after starting a run (fines CSD at steady state). The data was averaged with any erroneous measurements omitted. Linear regression was performed using a programmable calculator. The above procedure reduced the error in Microtrac results by minimizing errors in Microtrac data.

Growth Rate

Experimental growth rates were calculated from both Microtrac and Sonic Sifter data; therefore a geometric mean of the two growth rates was used to compare results. The CSD plots did not use the average growth rate. The fines CSD is from Microtrac data and the product CSD is from Sonic Sifter data. The experimental growth rates listed in Table 5 are the averaged growth rates.

APPENDIX C

ALLEN-BRADLEY SONIC SIFTER DATA

Sieve Tray	Sieve Tray Size Range (microns)	Size Range Difference (microns)	Sieve Tray Average Size (microns)	Weight Distribution (grams)		
				Run 26	Run 27	Run 28
Residue	0- 63	-	-	-	0.05	0.02
21	63- 74	11	68	0.03	0.70	0.29
20	74- 88	14	81	0.04	0.64	0.27
19	88-106	18	96	0.19	0.85	0.64
18	106-125	19	115	0.28	0.85	0.71
17	125-149	24	136	1.34	1.98	2.15
16	149-177	28	162	2.60	1.89	6.59
15	177-210	33	193	2.33	1.60	3.74
14	210-250	40	229	1.39	0.46	2.11
13	250-297	47	273	0.37	0.25	0.49
12	297-354	57	324	0.02	0.36	0.05
11	354-420	66	386	0.01	0.29	0.01
10	420+	-	-	0.01	0.05	0.09

Sieve Tray	Sieve Tray Size Range (microns)	Size Range Difference (microns)	Sieve Tray Average Size (microns)	Weight Distribution (grams)	
				Run 29	Run 31
Residue	0- 63	-	-	0.22	0.40
21	63- 74	11	68	0.77	2.44
20	74- 88	14	81	0.36	1.61
19	88-106	18	96	0.53	1.72
18	106-125	19	115	0.48	1.41
17	125-149	24	136	1.06	1.49
16	149-177	28	162	1.20	1.02
15	177-210	33	193	0.81	0.88
14	210-250	40	229	0.64	0.88
13	250-297	47	273	0.46	0.68
12	297-354	57	324	0.07	0.35
11	354-420	66	386	0.02	0.08
10	420+	-	-	0.01	0.05

Sieve Tray	Sieve Tray Size Range (microns)	Size Range Difference (microns)	Sieve Tray Average Size (microns)	Weight Distribution (grams)	
				Run 32	Run 34
Residue	0- 63	-	-	0.02	0.66
21	63- 74	11	68	0.59	1.75
20	74- 88	14	81	0.51	0.72
19	88-106	18	96	0.66	0.40
18	106-125	19	115	0.67	0.14
17	125-149	24	136	1.21	0.25
16	149-177	28	162	1.25	0.33
15	177-210	33	193	1.49	0.48
14	210-250	40	229	0.96	0.76
13	250-297	47	273	0.93	0.84
12	297-354	57	324	0.59	0.97
11	354-420	66	386	0.05	0.40
10	420+	-	-	0.01	0.01

Sieve Tray	Sieve Tray Size Range (microns)	Size Range Difference (microns)	Sieve Tray Average Size (microns)	Weight Distribution (grams)
				Run 33
Residue	0- 42	-	-	0.81
23	42- 53	9	48	0.14
22	53- 63	10	57	0.17
21	63- 74	11	68	1.62
20	74- 88	14	81	0.22
19	88-106	18	96	0.22
18	106-125	19	115	0.20
17	125-149	24	136	0.78
16	149-177	28	162	1.37
15	177-210	33	193	0.72
14	210-250	40	229	0.08
13	250-297	47	273	0.02
12	297+	-	-	0.01

Run No	Sonic Sifter Sample (grams)	Slurry Density (g/L)	Crystal Density (g/mL)	Volume Shape Factor
26	8.62	39.54	2.32	0.5
27	10.00	30.58	2.32	0.5
28	17.22	44.96	2.32	0.5
29	6.63	41.44	2.32	0.5
31	13.24	16.29	2.32	0.5
32	9.03	46.55	2.32	0.5
33	6.39	30.43	2.32	0.5
34	7.77	39.05	2.32	0.5

APPENDIX D

CONVERTED SONIC SIFTER DATA

Particle Average Size (microns)	Run 26 ln (n)	Run 27 ln (n)	Run 28 ln (n)	Run 29 ln (n)	Run 31 ln (n)	Run 32 ln (n)	Run 33 ln (n)	Run 34 ln (n)
48	-	-	-	-	-	-	6.31	-
57	-	-	-	-	-	-	5.89	-
68	3.49	6.23	5.19	7.04	6.57	6.58	7.52*	7.65
81	3.01	5.38	4.36	5.52	5.39	5.67	4.75	5.99
96	3.81	4.90	4.46	5.14	4.69	5.17	3.99	4.64
115	3.60	4.30	3.97	4.45	3.90	4.59	3.30	3.00
136	4.43	4.41	4.34	4.50	3.22	4.44	3.92	2.84
162	4.41	3.69	4.78	3.95	2.16	3.80	3.81	2.44
193	3.61	2.83	3.52	2.87	1.32	3.28	2.48	2.12
229	2.39	0.88	2.25	1.92	0.62	2.14	-0.43	1.88
273	0.38	-0.42	0.10	0.91	0.33	1.42	-2.50	1.29
324	-3.25	-0.76	-2.89	-1.68	-1.70	0.26	-	0.73
386	-4.61	-1.65	-5.17	-3.61	-3.85	-2.88	-	-0.83

*Value not used in linear regression calculations.

APPENDIX E

MICROTRAC DATA

Average Size (microns)	ln (Population Density)*					
	Run 26 ln (n)	Run 27 ln (n)	Run 28 ln (n)	Run 31 ln (n)	Run 32 ln (n)	Run 33 ln (n)
2.3065	-	-	12.50	-	-	13.20
3.3045	12.63	-	11.39	13.50	-	-
4.6314	10.97	12.68	10.04	10.80	12.02	10.90
6.5498	9.95	11.48	8.94	10.10	10.44	10.32
9.2628	8.53	9.89	7.85	9.23	-	8.86
13.226	7.10	8.95	-	-	-	7.79
18.762	6.81	8.52	6.73	7.50	6.95	7.61
26.115	5.48	7.41	-	6.45	5.95	6.40
36.932	-	6.31	-	6.00	5.40	4.84

*Runs 29 and 34 are omitted because the Microtrac was not working during those runs. The blanks (-) are errors in Microtrac measurements that were omitted.

LIST OF REFERENCES

- Behrens, G. P. and O. W. Hargrove (prin. investigators), Evaluation of Chiyoda Thoroughbred 121 FGD Process and Gypsum Stacking Volume 1: Chiyoda Evaluation, EPRI (1980).
- Burton, W. K., N. Cabrera and F. C. Frank, Phil. Trans. Roy. Soc., London, A243, 299 (1951).
- Chereminsinoff, P. N. and R. A. Young (eds.), Air Pollution Control and Design Handbook Part 2, Marcel Dekker, Inc., New York, p. 891 (1977).
- Clontz, N. A. and W. L. McCabe, CEP Symp. Series, 67 (110), 6 (1971).
- Dean, J. A., Lange's Handbok of Chemistry 12th Ed., McGraw-Hill Book Co., p. 5-23 (1979).
- Etherton, D. L., Experimental Study of Calcium Sulfate (Gypsum) Crystallization from Stack-Gas Liquors, M.S. Thesis, University of Arizona, Tucson (1980).
- Larson, M. A., D. C. Timm and P. R. Wolff, AIChE J., 14, 448 (1968).
- Murray, D. C. and M. A. Larson, AIChE J., 11, 728 (1965).
- Randolph, A. D. and K. Rajagopal, I & EC Fund, 9, 165 (1970).
- Randolph, A. D. and M. A. Larson, AIChE J., 8 (5), 639 (1962).
- Randolph, A. D. and M. A. Larson, Theory of Particulate Processes, Academic Press, New York (1971).
- Sibert, W., Private communication.
- Skinner, D. G., The Fluidized Combustion of Coal, Mills & Boons Ltd., p. 47 (1971).
- Timm, D. C. and T. R. Cooper, AIChE J., 17, 285 (1971).
- Waters, A. and R. Whitaker (eds.), Coal: The R & D Pivot for New Energy Fuels, Cycles, and Storage, EPRI Journal, Jan/Feb, p. 8 (1977).

LIST OF REFERENCES

Anderson, G. V. and G. W. Barrows (eds). Insecticides.
Evaluation of Control Throughput and Use Problems
and Control Studies Volume I. Control Evaluation.
 EPA (1981).

Barton, M. E., K. Carter and W. C. Frank, Eds. Year Book
of Entomology, 1981, 28: 1-100.

Cartwright, E. H. and E. A. Young (eds.). Art Pollution
Control and Action Handbook Part 2. Manual Section.
 Int. Res. Conf. 8-11 (1977).

Chen, H. A. and W. L. L. Journal of Chemical Ecology, 8: 1-10.
 (1982).

Chen, J. A. Journal of Chemical Ecology 1981, 7: 1-10.
 (1981).

Chen, M. L., Experimental Study of Control Methods
(System) Crystallization from Steam-Sea Liquor.
 M.S. Thesis, University of Arizona, Tucson (1981).

Chen, M. A., D. C. Tim and P. A. Weiss, AIChE J., 28:
 448 (1982).

Chen, D. C. and M. A. Larson, AIChE J., 28: 179 (1982).

Chen, A. D. and M. A. Larson, AIChE J., 28: 182 (1982).

Chen, A. D. and M. A. Larson, AIChE J., 28: 187 (1982).

Chen, A. D. and M. A. Larson, Journal of Environmental
Engineering, 108: 1-10 (1981).

Chen, M. A., Private communication.

Chen, M. A., The Physical Chemistry of the Cell.
 Wiley, New York, 1981.

Chen, M. A. and J. K. Cheng, AIChE J., 28: 187 (1982).

Chen, M. A. and J. K. Cheng, AIChE J., 28: 187 (1982).

Chen, M. A. and J. K. Cheng, AIChE J., 28: 187 (1982).